

©2023 by Do Nguyen Hoang. All rights reserved.

Vietnamese – German University
Electrical Engineering and Information Technology Study Program

Frankfurt University of Applied Science
Faculty of Electrical Engineering

**DESIGN, IMPLEMENTATION, AND CHARACTERISATION
OF AN AUTONOMOUS WIRELESS AGROMETEOROLOGY STATION**

by

DO NGUYEN HOANG

Matriculation number: 1235052

First supervisor: Dr. Udo Klein

Second supervisor: M.Sc. Tran Quang Nhu

BACHELOR THESIS

Submitted in partial fulfillment of the requirements
for the degree of Bachelor Engineering in study program
Electrical Engineering and Information Technology,
Vietnamese – German University, 2023

Binh Duong, Vietnam, September 2023

**Design, Implementation, and Characterisation
of an Autonomous Wireless Agrometeorology Station**

Approved by

Dr. Udo Klein, First Supervisor

M.Sc. Tran Quang Nhu, Second Supervisor

Thesis Committee

DISCLAIMER

I declare that this thesis is the product of my work, unless otherwise referenced. All opinions, result, conclusions, and recommendations are my own to the best of my knowledge and may not represent the policies or opinions of the Vietnamese-German University.

Do Nguyen Hoang

ACKNOWLEDGEMENTS

First of all, I would like to express my gratitude toward my mentor and supervisor, Dr. Udo Klein, for being a role model of engineering passion for me to look up to every since my second year at Vietnamese – German University.

I would also like to thank Mr. Tran Quan Nhu, my second supervisor for all of his insights and helping me expand my skill set during my years of university.

I am grateful to Le Hoang Trong Minh – an enginner from the Fluid Lab at Vietnamese – German University, Pham Trung Hieu – a Master Student of class GPE2020, and Nguyen Khanh – a graduate from class ME2016, for coming to my aid when I struggled with the aspects of Mechanical Engineering in my thesis.

Finally, I am indebted to my family and friends for their support along the way; and I would like to pay a tribute to my late father and grandparents, whose love transcends even after all these year.

ABSTRACT

By applying technological advances to support, and even replace traditional methods of human observations and experience, precision agriculture could be realised for better productivity. Therefore, this project aims at the construction of a sensory unit that can help monitor the meteorology of a cultivation area with high consistency while keeping error to the lowest.

The design includes a set of sensors to sample targeted environmental parameters and allows the data to be accessed online, including the wind speed and direction, rainfall, ambient temperature at different heights, relative humidity, and barometric pressure.

The findings of this thesis suggest that the design for a such goal is viable, but not without some limitations. While the analogue sensors in this design require further studies into their nature, the digital sensors need to be properly calibrated. The microcontroller of choice also introduces some issues for which a workaround is to be considered.

TABLE OF CONTENTS

DISCLAIMER	i
ACKNOWLEDGEMENTS	ii
ABSTRACT.....	iii
TABLE OF CONTENTS.....	iv
LIST OF FIGURES	vi
LIST OF TABLES	viii
ABBREVIATIONS	ix
1. Introduction.....	1
1.1. Background	1
1.2. Objectives.....	1
1.3. Thesis structure.....	2
2. Module overview	3
2.1. STM32F103C8T6 Microcontroller	3
2.2. Sensor Units	4
2.2.1. Anemometer.....	4
2.2.2. Wind Vane	5
2.2.3. Rain Gauge.....	7
2.2.4. BME280.....	9
2.2.5. DS18B20.....	10
2.3. SX1278 for Wireless Communication	11
2.4. Other Modules.....	13
2.4.1. DS3231.....	13
2.4.2. microSD Card	14
2.4.3. Analogue Low-pass Filter (LPF)	15
2.5. System Powering.....	17
2.6. Server.....	17
3. Implementation	18
3.1. STM32F103C8T6 Microcontroller	18
3.2. Sensor units	23
3.2.1. Anemometer.....	23
3.2.2. Wind Vane	27
3.2.3. Rain Gauge.....	36
3.2.4. BME280	37

3.2.5. DS18B20.....	38
3.3. SX1278.....	43
3.4. Other Modules.....	47
3.4.1. DS3231SN	47
3.4.2. microSD Card	49
3.5. System Powering.....	51
3.6. Gateway and Server.....	52
4. Experimental Characterisation.....	60
4.1. Anemometer	60
4.2. Wind Vane.....	67
4.3. Rain Gauge	73
4.4. Temperature Sensors – Hygrometer – Barometer	74
4.5. LoRa Connectivity – ThingSpeak	78
4.6. LoRa Range Test	80
5. Conclusion and Further Development	84
APPENDIX A. HAL and DMA Configuration Functions for ADC	x
APPENDIX B. CA3140EZ Voltage Buffer Test Result.....	xiv
APPENDIX C. Op-Amp Pick-up Test for Voltage Buffer at 3.3-V Power Supply	xvii
APPENDIX D. Wind Vane Test Result for Circuitry of Figure 3-15	xx
APPENDIX E. Python Program on Raspberry Pi 4B	xxiv
APPENDIX F. LoRa Range Test – Node’s Log.....	xxvii
APPENDIX G. LoRa Range Test – Gateway’s Log	xxxii
APPENDIX H. Deployed Prototype.....	xxxvi
APPENDIX I. Encased Units – Printed Circuit Board	xxxvii
APPENDIX J. Turnitin Similarity Checking Report	xxxviii
REFERENCES.....	xliv

LIST OF FIGURES

Figure 2-1. The STM32F103C8T6-based Blue Pill board in the project	3
Figure 2-2. The counterfeit read as an STM32F103 Medium Density device with a 128-KB Flash memory	4
Figure 2-3. The three-cup anemometer	5
Figure 2-4. The internal reed switch of the anemometer	5
Figure 2-5. The wind vane	6
Figure 2-6. Electrical circuit of the wind vane.....	6
Figure 2-7. Examples of wind vane-reading circuits	7
Figure 2-8. The structure of the rain gauge	8
Figure 2-9. Rain gauge's reed switch on a PCB upon removal of base chassis cover cap	8
Figure 2-10. Orifice dimensions (in mm) of the funnel	8
Figure 2-11. BME280 module with header strip	9
Figure 2-12. DS18B20 hardware	10
Figure 2-13. Circuitry examples for communication with DS18B20	11
Figure 2-14. SX1278 LoRa module in test	13
Figure 2-15. DS3231SN pinout module	14
Figure 2-16. microSD card module from Thegioioic	15
Figure 2-17. Passive first-order RC LPF circuit	15
Figure 2-18. Frequency response of an example RC LPF with $R = 1\text{ k}\Omega$ and $C = 100\text{ nF}$ under simulation	16
Figure 2-19. The nodeMCU ESP8266 used at the server side of the project	17
Figure 3-1. The schematic of the STM32F103C8T6-housed Blue Pill board	19
Figure 3-2. Bus connections with the Blue Pill board	20
Figure 3-3. Block diagram of the current design for the Autonomous Wireless Agrometeorology Station.....	21
Figure 3-4. General software flow built for the Autonomous Wireless Agrometeorology Station ...	22
Figure 3-5. Circuitry for testing the anemometer in ideal conditions	23
Figure 3-6. An instance of noise spikes captured in an oscilloscope	24
Figure 3-7. Bypass capacitor test circuitry using the reed switch from the anemometer	25
Figure 3-8. Reed switch debounced by the 68-nF bypass capacitor	25
Figure 3-9. Circuitry for interfacing with the anemometer.....	25
Figure 3-10. Anemometer setup routine and interrupt service routine upon input event	26
Figure 3-11. Voltage divider circuitry with ADC module.....	27
Figure 3-12. Derivation of the Norton equivalent of the voltage divider	28
Figure 3-13. An instance of $R_{\text{external}} = 3.0\text{k}\Omega$ input to the voltage step-calculating sheet.....	29
Figure 3-14. A noise instance captured during a test on the wind vane	30
Figure 3-15. Circuitry for reading the wind vane	31
Figure 3-16. Frequency response of the active 11.587-kHz RC LPF	32
Figure 3-17. Step response of the active 11.587-kHz RC LPF.....	33
Figure 3-18. Circuitry for interfacing with the rain gauge.....	36
Figure 3-19. Anemometer setup routine and interrupt service routine upon input event	37
Figure 3-20. BME280 setup for the I ² C protocol.....	37
Figure 3-21. The concept of a DS18B20 powered via an external power supply V_P	39
Figure 3-22. Final circuitry for interfacing the DS18B20 with the microcontroller.....	40

Figure 3-23. Setup and reading routines for DS18B20.....	42
Figure 3-24. Hardware setup for SX1278 LoRa module	43
Figure 3-25. SX1278 software setup and message-handling routines	46
Figure 3-26. Hardware setup with the DS3231SN RTC module.....	47
Figure 3-27. Physical pin connections of the microSD card module with the microcontroller.....	50
Figure 3-28. Power supply input for the station and the voltage regulating unit.....	51
Figure 3-29. Observed output of the LM317 circuitry in Figure 3-28 with $V_{in} = +8.4V$	52
Figure 3-30. Hardware setup for the gateway	53
Figure 3-31. ThingSpeak channel’s “API Keys” tab	55
Figure 3-32. Gateway setup and loop routines	57
Figure 4-1. Axial Fan Module MFP107 by TecQuipment	60
Figure 4-2. Near-linear association between the anemometer’s and the Axial Fan Module’s wind speeds	62
Figure 4-3. Wind speed factors by the read wind speed from the anemometer.....	62
Figure 4-4. Curve Fitting result for $N = 1$	64
Figure 4-5. Curve Fitting result for $N = 2$	65
Figure 4-6. Curve Fitting result for $N = 3$	66
Figure 4-7. Number of correct and bad readings when sampling from the voltage divider	67
Figure 4-8. Number of correct and bad readings when sampling from the passive 11.587-kHz LPF	69
Figure 4-9. Op-Amp setup for the voltage buffer test.....	70
Figure 4-10. Number of correct and bad readings when sampling from an active 11.587-kHz LPF using a CA3140EZ Op-Amp	70
Figure 4-11. Number of correct and bad readings when sampling from an active 11.587-kHz LPF using a MCP6002-I/P Op-Amp	71
Figure 4-12. Final wind vane test result from the exact circuitry as Figure 3-15	72
Figure 4-13. The mini digital scale used in rain gauge test	73
Figure 4-14. Extech 445815 Humidity Alert II Hygro-Thermometer unit used as the reference, and an instance of environment parameters captured during the test	75
Figure 4-15. Temperature readings from the compound test.....	76
Figure 4-16. Humidity readings from the compound test	76
Figure 4-17. Barometric pressure readings from the compound test	77
Figure 4-18. Channel settings on ThingSpeak for LoRa connectivity and server test.....	78
Figure 4-19. Private view of the server test channel on ThingSpeak	79
Figure 4-20. Example of Chart Option window on ThingSpeak	80
Figure 4-21. LoRa Range Test – logged locations of LoRa transmissions by the node	81
Figure 4-22. RSSI and SNR of the gateway displayed on ThingSpeak.....	83

LIST OF TABLES

Table 2-1. Wind directions by resistor values	7
Table 2-3. BME280 setup parameters	9
Table 2-4. Comparison of different available wireless communication technologies for IoT in Vietnam	11
Table 3-1. Choosing bypass capacitor value based on available resistors from $30\text{k}\Omega$ to $50\text{k}\Omega$	24
Table 3-2. Voltage steps of the voltage divider by R_{external}	30
Table 3-3. A part of the component pick-up table for the passive LPF	31
Table 3-4. ADC functions for wind vane reading software	35
Table 3-5. Methods of the <code>OneWire</code> class used in the software for DS18B20	41
Table 3-6. ROM and function commands in use for the DS18B20	41
Table 4-1. Anewheel of timemometer test data with the Axial Fan Module MFP107	61
Table 4-2. Output by the microcontroller for the 270° direction in the test with the passive LPF	68
Table 4-3. Rain gauge test with a fixed amount of water	73
Table 4-4. Rain gauge test with different amounts of water	74
Table 4-5. LoRa range test result	82

ABBREVIATIONS

GDP	Gross Domestic Product
1-wire	One Wire
ADC	Analogue-to-Digital Converter
CSV	Comma-Separated Values
DMA	Direct Memory Access
ESR	Equivalent Serial Resistor
GPIO	General Purpose Input/Output
GPS	Global Positioning System
HAL	Hardware Abstract Layer
I ² C	Inter-Integrated Circuit
IC	Integrated Circuit
IDE	Integrated Development Environment
IoT	Internet of Things
LED	Light-Emitting Diode
LoRa	Long-Range
LoRaWAN	Long Range Wireless Area Network
LPF	Low-pass Filter
LSB	Least Significant Bit
MAC	Media Access Control
MOSFET	Metal-Oxide-Semiconductor Field-Effect Transistor
NFC	Near Field Communication
Op-Amp	Operational Amplifier
PCB	Printed Circuit Board
RFID	Radio-Frequency Identification
RSSI	Received Signal Strength Indicator
RTC	Real-time Clock
SD	Secure Digital
SDIO	Secure Digital Input Output
SNR	Signal-to-Noise Ratio
SPI	Serial Peripheral Interface
SWD	Serial Wire Debug
TCXO	Temperature-Compensated Crystal Oscillator
U(S)ART	Universal (Synchronous) Asynchronous Receiver-Transmitter
UART	Universal Asynchronous Receiver-Transmitter
URL	Uniform Resource Locator
USB	Universal Serial Bus
UTC	Coordinated Universal Time
UVC	USB Video Device Class
Wi-Fi	Wireless Fidelity

1. Introduction

1.1. Background

In Vietnam, agriculture provides work to over half the population [1] and accounts for 12.56% of the Gross Domestic Product (GDP) as of 2021 [2]. Despite experiencing a growth in agricultural productions [3], Vietnam still faces infrastructure limitations, particularly when it comes to applying technological advances. From 2019 to 2022, the number of installed agrometeorology station remained 29 across the 1,750 km long of land territory with no plans of addition [4], [5].

This project proposes a design of an Autonomous Wireless Agrometeorology Station to help improve the state of lacking domestic technologic product in the field of cultivation. Should the design be deemed viable, the stations could be installed at a low cost on any terrain and monitor the meteorological parameters of interest for remote access. This design also aims at harvesting Vietnam's natural resources of renewable energy for the expected outcome to be self-contained. As a result, the Autonomous Wireless Agrometeorology Station becomes a part of the Internet of Things (IoT) network, introducing Precision Agriculture to boost the productivity and partially relieve the stress of hard labour on the workforce.

1.2. Objectives

The main objective of this project is to develop a working design for an Autonomous Wireless Agrometeorology Station. Therefore, the viability of each included module needs evaluations.

In general, the Autonomous Wireless Agrometeorology Station should satisfy the following requirements:

- The station is automatic and operates off-grid.
- The station is able to monitor the following parameters and send the readings wirelessly to a server once every 5 minutes.
 - Temperature at ground level and 1 metre above the ground within the range of -50 °C to 70 °C at a resolution of 0.04 °C with an accuracy of at least 0.5 °C.
 - Barometric pressure within the range of 900 hPa to 1100 hPa at a resolution of 0.5 hPa with an accuracy of at least 4 hPa.
 - Humidity within the range of 0 %RH to 100 %RH at a resolution of 0.03 %RH with an accuracy of at least 3.5 %RH.
 - Wind direction by at least 8 principle directions, including the 4 basic cardinal directions of North, East, South, West, and the 4 ordinal directions Northeast, Southeast, Southwest, Northwest.
 - Wind speed with a maximum of 25 m/s and a relative accuracy of 1%
 - Precipitation data at the site of installation.
- The station is able in the Southeast Asia region.
- The station is small and simple enough to be deployed by 1 person with little to no experience.

Furthermore, since this project provides an opportunity, a side objective is set to be the evalution of the newly developed STM32duino firmware by STMicroelectronics in a real application.

1.3. Thesis structure

This thesis includes 5 main chapters listed as follows.

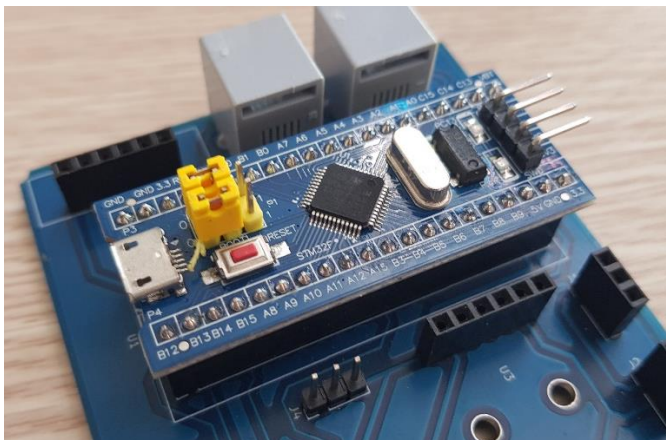
- Chapter 1: Introduction. This chapter explores the state-of-the-art of agrometeorology in Vietnam as the motivation for this thesis, as well as the requirements the project for this thesis must meet.
- Chapter 2: Module overview. This chapter goes over the modules included in the design for this thesis, including the theoretical aspects, the hardware, and for some part, why the modules are chosen for the design.
- Chapter 3. Implementation. This chapter focuses on the hardware and software design of the included modules.
- Chapter 4. Experimental characterisation. This chapter explores the characteristics and behaviours of the included modules when put into operation with the specific hardware and software design from Chapter 3.
- Chapter 5: Conclusion and further development. This chapter goes over the test results from Chapter 4 in general while proposing tasks to be done for an improved design.

2. Module overview

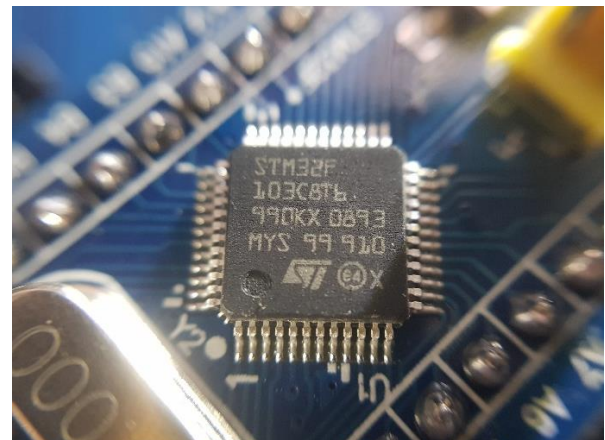
2.1. STM32F103C8T6 Microcontroller

There are numerous factors when it comes to choosing a microcontroller for a project, including the project requirements, physical and electrical characteristics of a microcontroller (size, architecture, built-in features, upgradability, etc.), development platforms, and supply chain factors (cost and availability) [6]–[10]. Based on the objectives of this thesis (Section 0) and the characteristics of other modules explored later in this chapter, it is determined that the microcontroller of choice must have at least 19 port pins that have the capability for handling GPIO, external interrupts, ADC, SPI, and I²C. Furthermore, since this thesis has a side objective of testing the STM32duino firmware, the options are limited to the STM32 family by STMicroelectronics.

All the devices belonging to the STM32 family run on a 2.0-3.6V power supply, which is relatively more power-efficient than higher-voltage microcontrollers (i.e., the 5-V AVR family) [11]. For testing and prototyping, one of the popular STM32 options in Vietnam that satisfies the port pin quantity requirement is the STM32F103C8T6 available on a Blue Pill board. However, upon purchased, the units appear to contain a counterfeit (Figure 2-1) which bears much similarities with an authentic STM32F103C8T6 apart from its doubled Flash memory size of 128 KB (Figure 2-2). For the sake of simplicity, this thesis shall still call the counterfeit an STM32F103C8T6 microcontroller.



(a) The Blue Pill board in testing and prototyping



(b) The counterfeit with the markings like an authentic STM32F103C8T6

Figure 2-1. The STM32F103C8T6-based Blue Pill board in the project

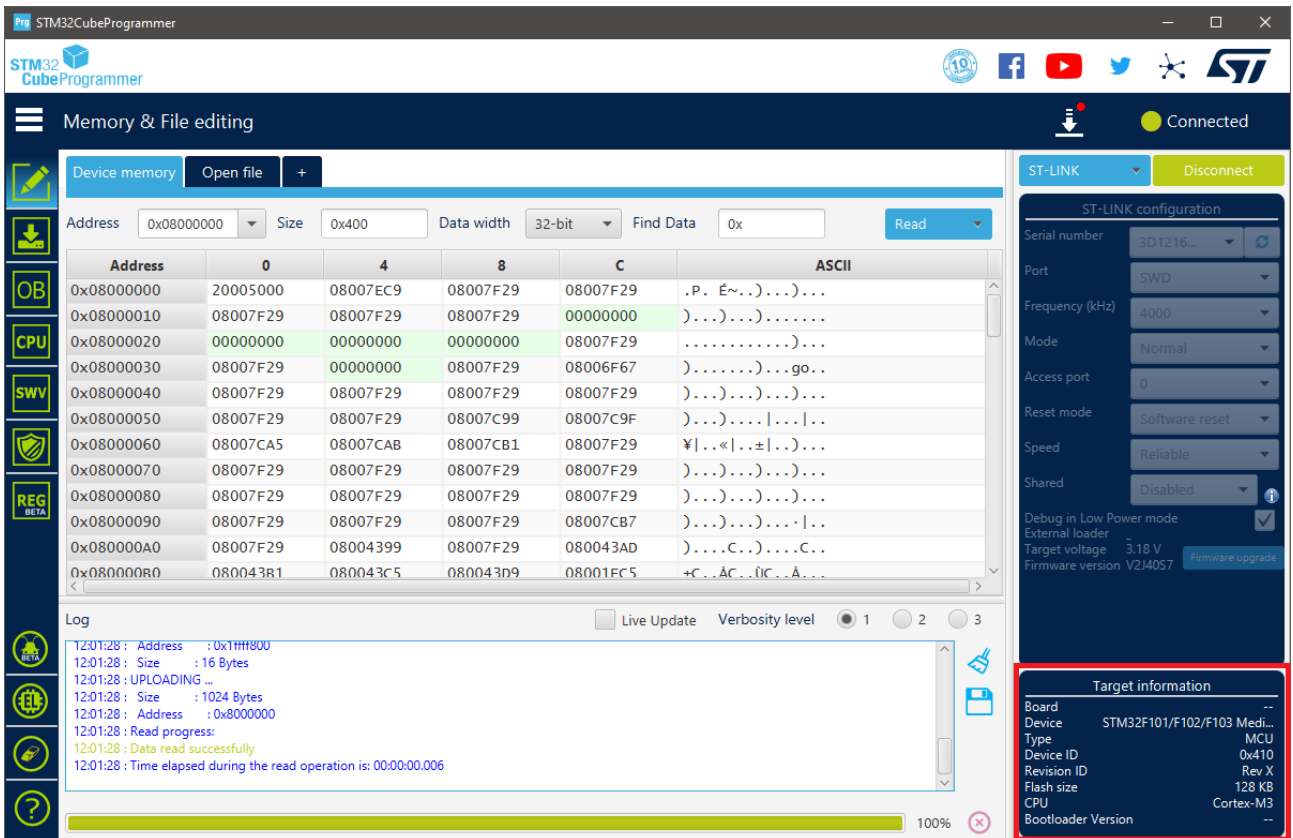


Figure 2-2. The counterfeit read as an STM32F103 Medium density device with a 128-KB Flash memory

Each Blue Pill board offers 32 input/output port pins available for use with interrupt capability, 18 of which are 5-V tolerant [12]–[14]. The STM32F103C8T6 microcontroller is built with 2 12-bit Analogue-to-Digital Converter (ADC) modules sharing 10 physical input pins (from PA0 to PA7, and PB0, PB1), 7 timers whose resolutions range from 16-bit to 24-bit, and remappable communication interfaces including I²C, U(S)ART, and SPI. As a result, the STM32F103C8T6 is determined to be able to handle communications with other devices used in this design.

2.2. Sensor Units

In agriculture, the weather factor plays a key role in the growth and development of plants, since it affects both the environment (e.g., soil, fungi, pests) and the plants themselves (e.g., the integrity of branches and leaves) [15]–[17]. By monitoring the corresponding meteorological parameters, agronomy helps to predict weather events and to plan suitable adjustments to an area for the maximised agric productivity. Some such qualities includes wind data, rainfall, temperature, humidity, and atmospheric pressure, which are to be monitored by the Autonomous Wireless Agrometeorology Station via a set of sensors which are looked into in this section.

2.2.1. Anemometer

The Autonomous Wireless Agrometeorology Station includes a sensor kit SP-WS02 for the Wireless Weather Station WH2081 by Misol Electronics. The kit consists of a thermo-hygrometer, an anemometer, a wind vane, and a rain gauge [18]. However, the temperature – humidity sensor is not used since it is of unknown type and encased along with the processing unit of Misol's Weather Station. Section 2.2 therefore explores the other 3 devices, first of which is the anemometer for reading wind speed.

The anemometer follows the standard design for 3-cup anemometers, which was built to replace the traditional 4-cup design due to its superior aerodynamic performance [19], with an addition of a magnet and a reed switch. The leads of the reed switch is further extended by an RJ11 cable to allow reading of the switch electrically with a suitable circuitry.

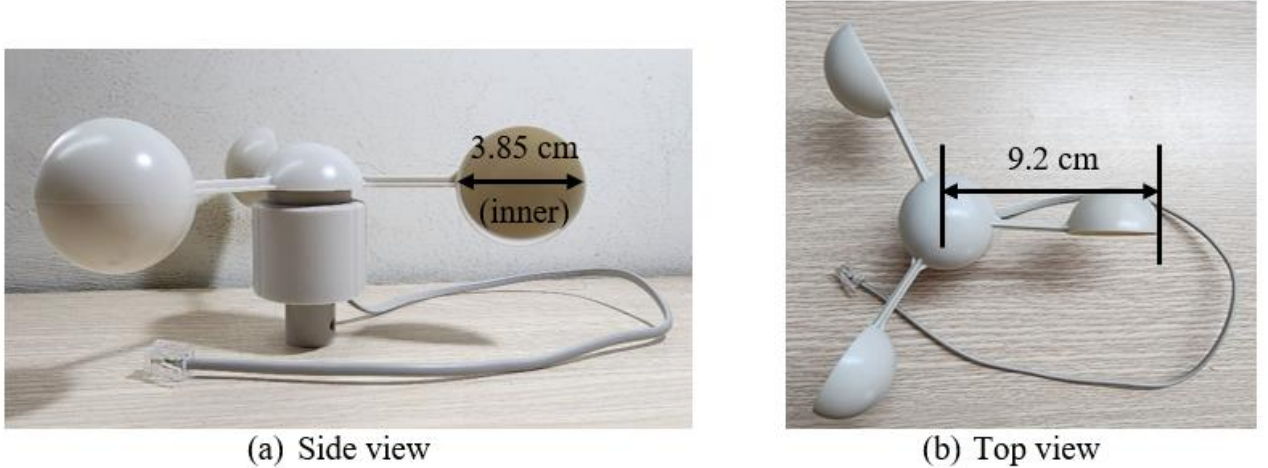


Figure 2-3. The three-cup anemometer

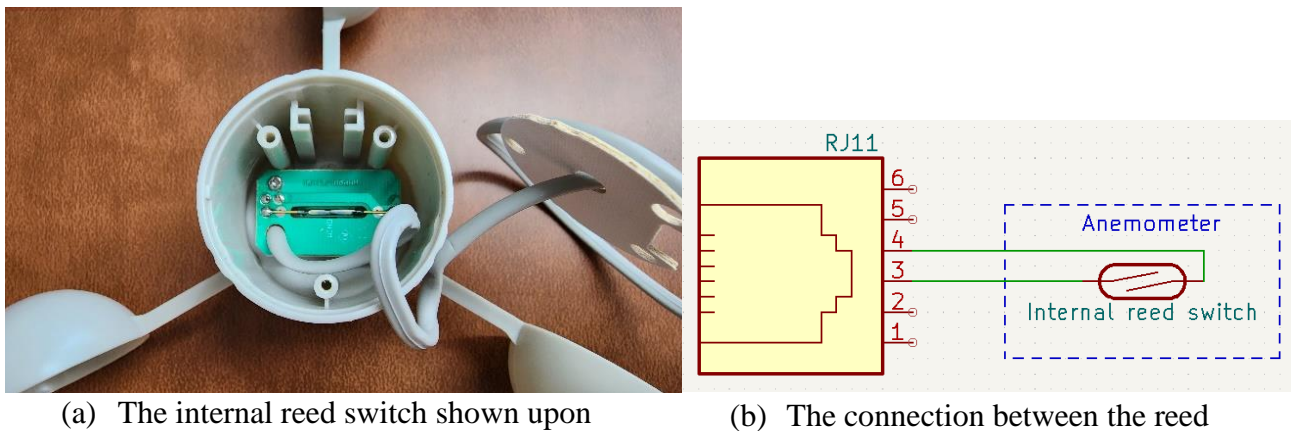


Figure 2-4. The internal reed switch of the anemometer

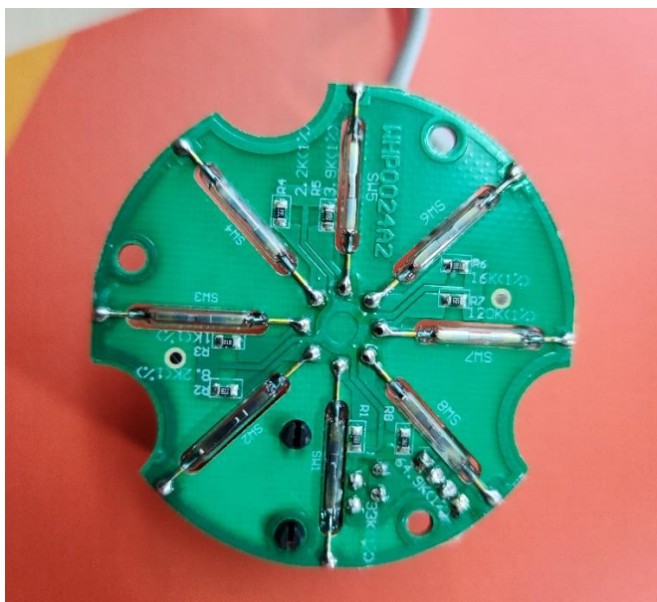
The reed switch is observed to be normally open upon removal of the PCB (Figure 2-4a) from the sensor body. When the magnet fixed under the rotor passes, the reed switch produces a click, based on which it is found to close twice per revolution of a cup.

2.2.2. Wind Vane

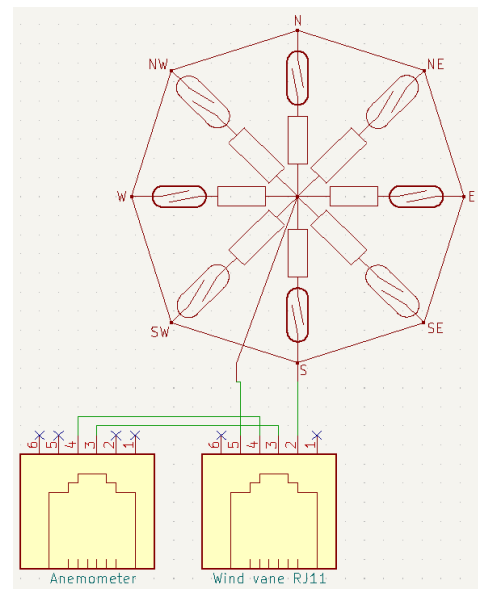
The second device from the sensor kit SP-WS02 is a wind vane for reading wind directions. Underneath the rotor of the wind vane is there a magnet which closes up to 2 out of 8 normally-open reed switches on the PCB inside the body of the sensor (Figure 2-6). Each reed switch is paired with a unique resistor whose value is read to determine the position of the rudder blade, thus the wind direction.



Figure 2-5. The wind vane



(a) Reed switches inside the wind vane



(b) Schematic of the wind vane's circuit from [20]

Figure 2-6. Electrical circuit of the wind vane

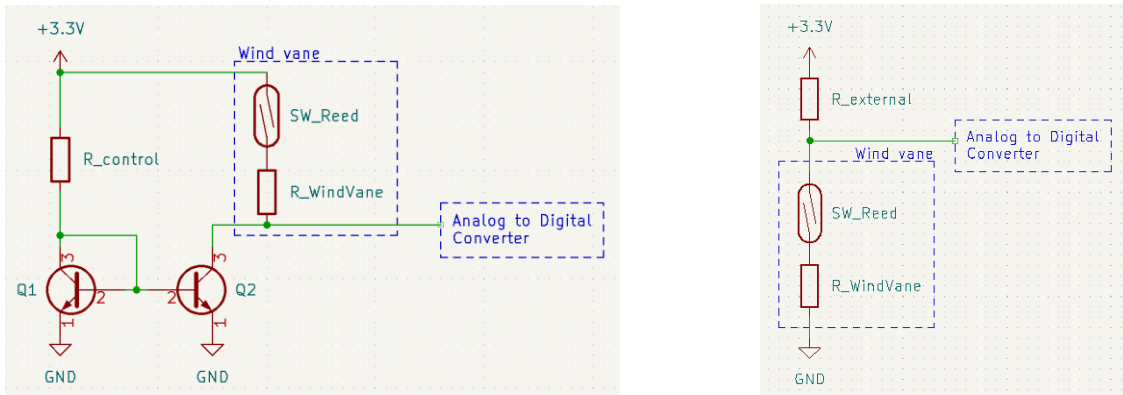
The wind vane has an RJ11 port for users to connect the anemometer and combine the 2 sensors into 1 output via the wind vane's RJ11 cable as illustrated in Figure 2-6b. When set up accordingly to the 4 directions marked on the sensor's body, the aforementioned resistors give the direction as shown in

Table 2-1. It has been pointed out that the magnet could close 2 reed switches simultaneously, thus parallel resistors formed and 8 additional wind directions to be read.

Table 2-1. Wind directions by resistor values [20]

Direction (single resistor)			R	Direction (parallel resistors)			R
Cardinal point		Azimuth degrees		Cardinal point		Azimuth degrees	
North	N	0°	33 KΩ	North-Northeast	NNE	22.5°	6.57 KΩ
Northeast	NE	45°	8.2 KΩ	East-Northeast	ENE	67.5°	891 Ω
East	E	90°	1 KΩ	East-Southeast	ESE	112.5°	688 Ω
Southeast	SE	135°	2.2 KΩ	South-Southeast	SSE	157.5°	1.41 KΩ
South	S	180°	3.9 KΩ	South-Southwest	SSW	202.5°	3.14 KΩ
Southwest	SW	225°	16 KΩ	West-Southwest	WSW	247.5°	14.12 KΩ
West	W	270°	120 KΩ	West-Northwest	WNW	292.5°	42.12 KΩ
Northwest	NW	315°	64.9 KΩ	North-Northwest	NNW	337.5°	21.88 KΩ

Table 2-1 data is given by Argent Data Systems and verified by the use of a multimeter. In a microcontroller-based system, reading resistor value, thus the wind direction, from the wind vane could be done by mimicking the behaviour of a multimeter in resistance measurement mode: injecting a constant current to get a voltage across the internal resistors [21]. Another approach is to use an external resistor to form a voltage divider [20]. Either way, the resistive value across the RJ11 inductors of the wind vane must be determined by an ADC module.



(a) Current mirror circuit as a constant current source

(b) Voltage divider with an external resistor

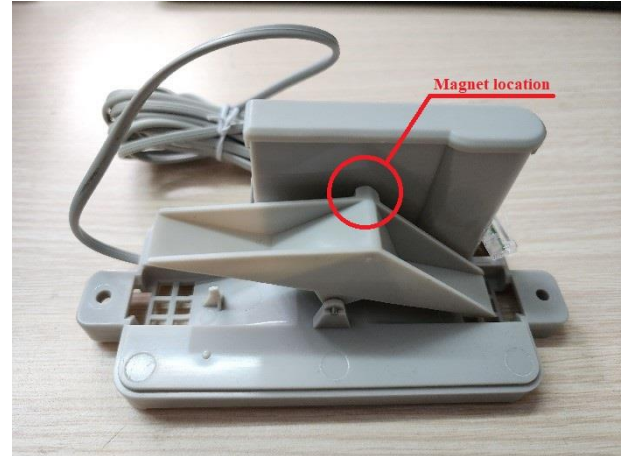
Figure 2-7. Examples of wind vane-reading circuits

2.2.3. Rain Gauge

The third device from the sensor kit SP-WS02 used in this project is a rain gauge as a self-emptying tipping bucket. It is comprised of 2 small buckets mounted on a fulcrum like a seesaw underneath a funnel (Figure 2-8). The design allows the buckets to tip over a side when one is full to be emptied through the openings on the base of the rain gauge, while the other in turn collects rain water. The magnet fixed to the bucket (Figure 2-8b), on the other hand, also moves pass the reed switch hidden inside the case on the rain gauge base and momentarily closes it. Since the reed switch leads are extended via an RJ11 cable, with a suitable circuitry, electrical pulses could be generated and read by the microcontroller.



(a) Top view: the orifice of the funnel



(b) Disassembly: the buckets on a pivot

Figure 2-8. The structure of the rain gauge [6]

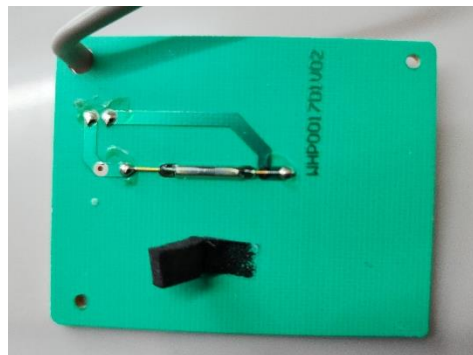


Figure 2-9. Rain gauge's reed switch on a PCB upon removal of base chassis cover cap [6]

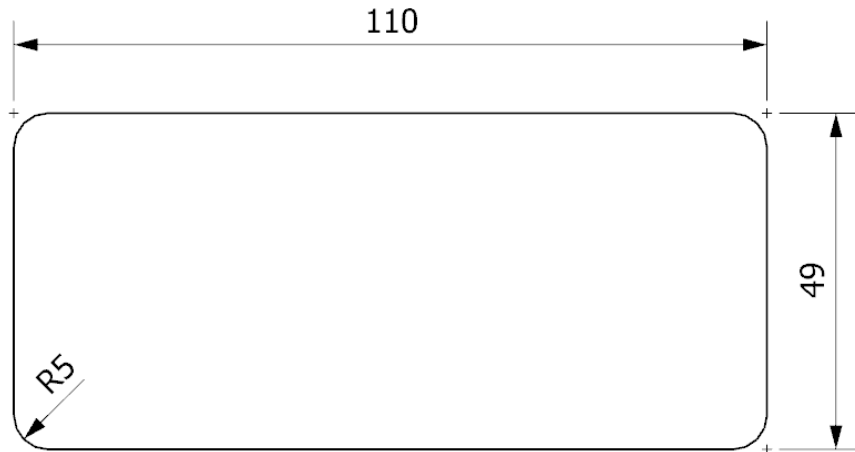
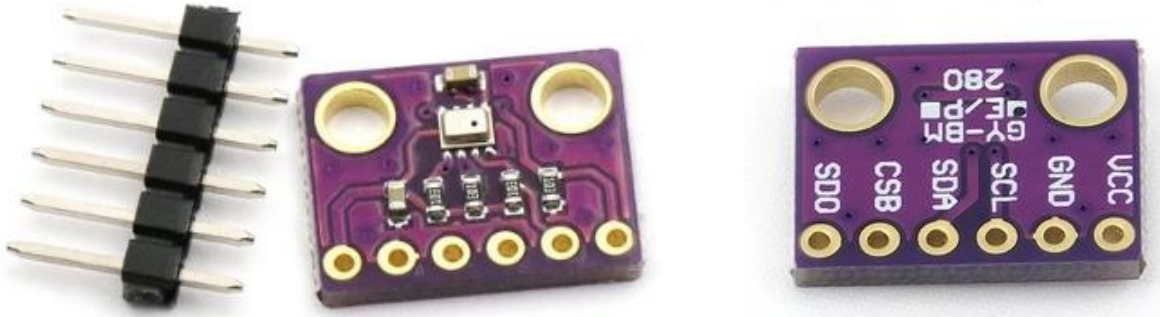


Figure 2-10. Orifice dimensions (in mm) of the funnel

Misol Electronics states that the rain gauge produces 1 pulse for every 0.3 mm of rain [22], while Argent Data System provides a value of 0.011", or 0.2794 mm [20]. However, since the resolution provided by the latter is converted from inches, the difference may be neglected, and the value of 0.3 mm rainfall per tip could later be used to construct the software for the Autonomous Wireless Agrometeorology Station.

2.2.4. BME280

BME280 is a self-calibrating environmental sensor by Bosch Sensortec GmbH. It is a combined digital sensor for barometric pressure, relative humidity, and ambient temperature, developed for multiple targets including mobile devices and wearables, thus the advantages of small size and low power consumption [23], [24]. The device in this design, arrives on a pinout board with a 2.54-mm single row header strip (Figure 2-11) for convenience in prototyping and testing.



(a) Top view

(b) Bottom view

Figure 2-11. BME280 module with header strip [25]

According to [24], the product specifications of the BME280 are as follows:

- Operational voltage: 1.71 V to 3.6 V
- Communicational voltage: 1.2 V to 3.6 V
- Typical current consumption: 0.1 μ A (sleep mode) to 714 μ A (pressure measurement)
- Communication interface: SPI and I²C
- Full-range output:
 - Temperature: -40 °C to +85 °C
 - Humidity: 0 %RH to 100 %RH
 - Pressure: 300 hPa to 1100 hPa
- Data resolution:
 - Temperature: 0.01 °C
 - Humidity: 0.008 %RH
 - Pressure: 0.18 hPa (minimum)
- Data accuracy:
 - Temperature: ± 0.5 °C (0 °C to 65 °C) up to ± 1.5 °C (-40 °C to -20 °C)
 - Humidity: ± 3 %RH
 - Pressure: ± 1 hPa

As an IC sensor, the BME280 is built with not only the sensing units but also mode control, data compensation, and noise reduction by oversampling and a digital filter. During software setup, the BME280 could be configured with the parameters shown in Table 2-2.

Table 2-2. BME280 setup parameters [24]

Parameter	Valid values
Sensor mode	Sleep mode, Normal mode, Forced mode
Pressure sampling rate	
Temperature sampling rate	None (sampling is turned off), x1, x2, x4, x8, x16
Humidity sampling rate	
IIR filter coefficient	Off (IIR filter is turned off), x2, x4, x8, x16
Standby time for normal mode (in milliseconds)	0.5, 10, 20, 62.5, 125, 250, 500, 1000

2.2.5. DS18B20

DS18B20 is a family of digital temperature sensors by Maxim Integrated that follows the design of DS1820, a predecessor introduced by Dallas Semiconductor in 1998 [26]. Although the DS18B20 sensors are offered in only 3 types of packages by the manufacturer [27], a waterproof version with a long cable built from the 3-pin TO-92 configuration DS18B20 is available and has had its application explored off a PCB in different environments (e.g., liquids) [26], [28]–[30]. Because of this version, the DS18B20 is chosen to monitor the ambient temperature at ground level for this project. Although there are other choices of sensors with long cables, they either need heavily calibrating (e.g., Resistance Temperature Detector PT100 [31]), or have higher price and unnecessary functions (e.g., the AM2315 temperature and humidity sensor priced at 830,000 VND compared to the 71,000-VND DS18B20 temperature sensor with 1-m long cable [32], [33]).



(a) TO-92 configuration

(b) Waterproof version with 1-m long cable

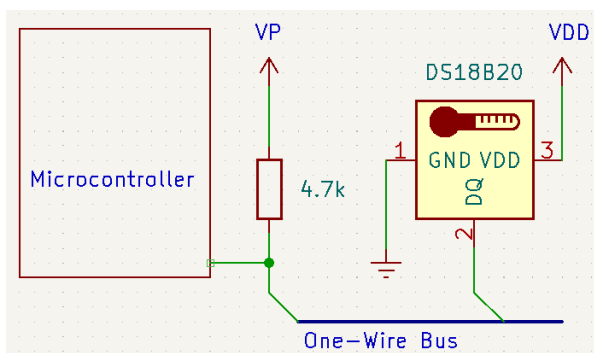
Figure 2-12. DS18B20 hardware

According to [2], the specifications of the sensor are as follows:

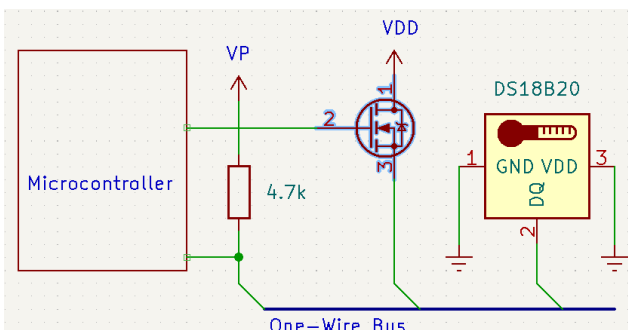
- Operating voltage: 3.0 V to 5.5 V
- Active current: typically, 1 mA ($V_{DD} = 5$ V)
- Standby current: typically, 750 nA
- Sink current: maximum, 4.0 mA
- Full-range temperature output: -55 °C to +125 °C
- Data resolution: programmable; 0.5 °C, 0.25 °C, 0.125 °C, and 0.0625 °C

- Minimum thermometer error: ± 0.5 °C (from -10 °C to +85 °C)

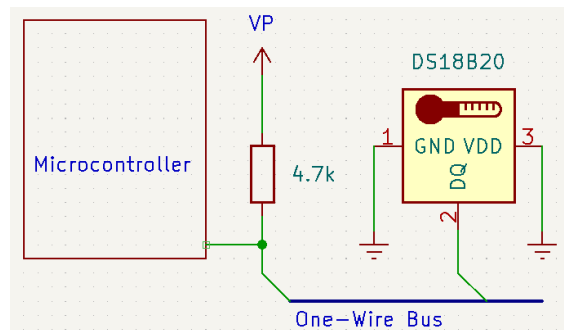
Communication with a DS18B20 is done asynchronously via the bi-directional One-Wire (1-Wire) protocol, which works under the principle of timing, digital input/output, and interchanging control of a single wire among masters (microcontrollers) and slaves (1-Wire devices). Although the standard communication speed is announced to be a maximum of 16.3 kbps, a high-speed mode “overdrive” of up to 90 kbps is available [34], [35]. The 1-Wire protocol allows a DS18B20 to operate not only on an external power supply but also in a parasite mode as depicted in Figure 2-13 for lower power consumption [27]. However, it is found that the circuitry in Figure 2-13b is only applicable if the microcontroller turns on the MOSFET before releasing the 1-Wire bus for the sensor when required. Alternatively, the MOSFET could be replaced by software (Figure 2-13c) when the microcontroller outputs “HIGH” on its digital pin of the 1-Wire bus as soon as releasing control.



(a) DS18B20 on an external power supply



(b) DS18B20 in parasite mode with a MOSFET



(c) DS18B20 in parasite mode
(software-controlled)

Figure 2-13. Circuitry examples for communication with DS18B20 [6], [27]

2.3. SX1278 for Wireless Communication

In the design of an Autonomous Wireless Agrometeorology Station, the wireless communication between the station and a server is done via LoRa. The choice for LoRa is done from the comparison below.

Table 2-3. Comparison of different available wireless communication technologies for IoT in Vietnam [36]–[40]

Technology	Highest data rate (uplink)	Maximum coverage	Power consumption
Wireless Fidelity (Wi-Fi)	93.38 Mbps	90 m	Medium to high
Bluetooth	1 – 3 Mbps	100 m	Low
Cellular network	18.27 Mbps	Several kilometres	Medium to high
LoRa	37.5 kbps	Several kilometres	Low
Zigbee	250 kbps	50 m	Low
Near Field Communication (NFC)	424 kbps	10 cm	Low
Radio-frequency Identification (RFID)	424 kbps	10 cm	Low

It could be observed that Wi-Fi provides the highest communication speed, while data-exchange is slowest via LoRa. The data collected and transmitted by the system are just sensor readings, so the data rate does not need to be high [41].

The next criterium to be taken into account is the range over which communications are performed. LoRa and Zigbee could be seen to allow data exchange range. Despite the maximum range of 90 m, Wi-Fi signals could typically reach a maximum of only 45 m [42], which should not be a problem for an agricultural application. The common Bluetooth modules HC-05 and HC-06 provide a connection up to 100 m [43], so Bluetooth remains an option. Only NFC and RFID technologies are invalid since they are applicable for only short-range communications.

In terms of power consumption, Wi-Fi and cellular network are not ideal for a self-contained off-grid design. Bluetooth, in spite of the low power consumption, is said to be more “power hungry” compared to LoRa [44]. That leaves LoRa and Zigbee the remaining choices for wireless communications.

For this project, LoRa and Zigbee are lastly compared over product prices. A major supplier in Ho Chi Minh City, Vietnam chosen for referencing is Thegioiic. The LoRa modules SX1278 are sold at around 100,000 VND, while prices for the Zigbee modules go from 183,000 VND [45], [46]. As a result, LoRa is the wireless communication technology chosen for this design, and 2 LoRa modules SX1278 are picked for the station and the server side. Each module is a PCB module with an 8-pin 2.54-mm dual row header strip for convenience in prototyping and testing.

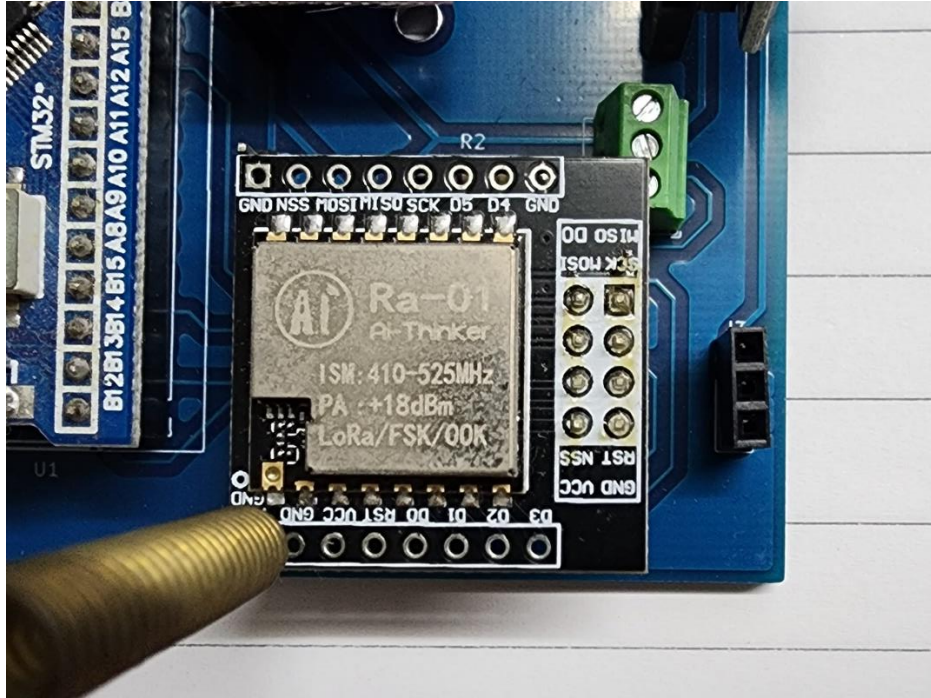


Figure 2-14. SX1278 LoRa module in test

The product specifications for LoRa mode from [47] are as follows:

- Operating voltage: 1.8 V to 3.7 V
- Current consumption: 0.2 μ A (sleep mode), up to 12 mA in receive mode or 120 mA during data transmissions
- Communication protocol: SPI
- Spreading factors: 6 to 12
- Cyclic coding rate: 4/5 to 4/8
- Signal bandwidth (in kHz): 7.8, 10.4, 15.6, 20.8, 31.2, 41.7, 62.5, 125, 250, and 500
- Package preamble length (in symbols): 6+4 to 65535+4
- User-defined package sync word: 8-bit sync word

2.4. Other Modules

2.4.1. DS3231

Time keeping is an extended feature for the Autonomous Wireless Agrometeorology Station. Although the STM32F103C8T6 microcontroller already has a built-in real-time clock (RTC), an external module is explored for higher precision of time data.

The DS3231SN is an RTC from the DS3231 product lines by Maxim Integrated, clocked at 32,768-Hz by an internal crystal. Another member from the DS3231 product lines is the DS3231M. A major difference between DS3231SN and DS3231M is that the former is built with a temperature-compensated crystal oscillator (TCXO) for the improved quality of time keeping [48], which could be checked via its 32K pin. As a result, the accuracy is proven to be much higher than that of the DS3231M [49]. For testing purposes, a DS3231SN pinout module (Figure 2-15) is in use.



Figure 2-15. DS3231SN pinout module

The key specifications of the DS3231SN from [50] are as follows:

- Operating voltage: 2.3 V to 5.5 V
- Battery voltage: 2.3 V to 5.5 V
- Maximum active current: 200 μ A at 3.63 V
- Maximum standby current: 110 μ A at 3.63 V
- Typical standby current from battery: 0.84 μ A
- Effective time keeping range: from 1970 to 2100
- Compensated base clock output on 32kHz pin
- Programmable square wave output or alarm on $\overline{\text{INT}}/\text{SQW}$ pin
- I²C communication interface at up to 400 kHz

2.4.2. microSD Card

In order to avoid the loss of data in case of dropped uplink connection from the Autonomous Wireless Agrometeorology Station to its designated server, a microSD card is included in its design. The microSD card module for this project is obtained from Thegioiic.com to be added as a module for easy prototyping and redesigning should anything goes wrong.

A microSD could be accessed via either the Secure Digital Input Output (SDIO) interface or SPI. Since the STM32F103C8T6 in this project is not designed with the SDIO interface, the microSD card module provides an SPI solution.

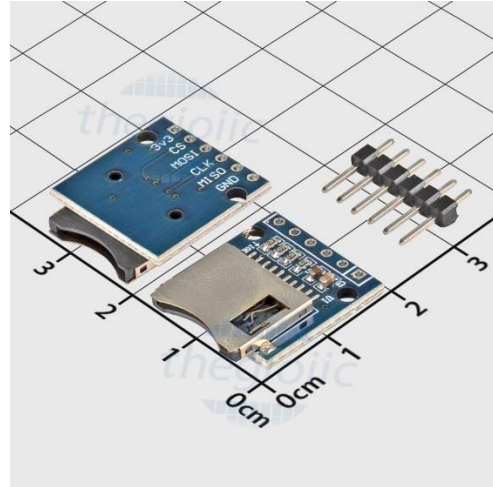


Figure 2-16. microSD card module from Thegioiic [51]

2.4.3. Analogue Low-pass Filter (LPF)

Any real-life systems are always faced with the noise problem which roots from various sources like external interference or the components of the system itself [52], [53]. Producing clean electrical signals to use in an application although is not possible, reducing the effects of noise to reach a such goal remains practical. Since noise are usually unwanted high frequency signals injected into the desired ones, the method of using analogue filters could be applied. The simplest form of LPFs against noise is a passive first-order RC LPF as demonstrated in Figure 2-17.

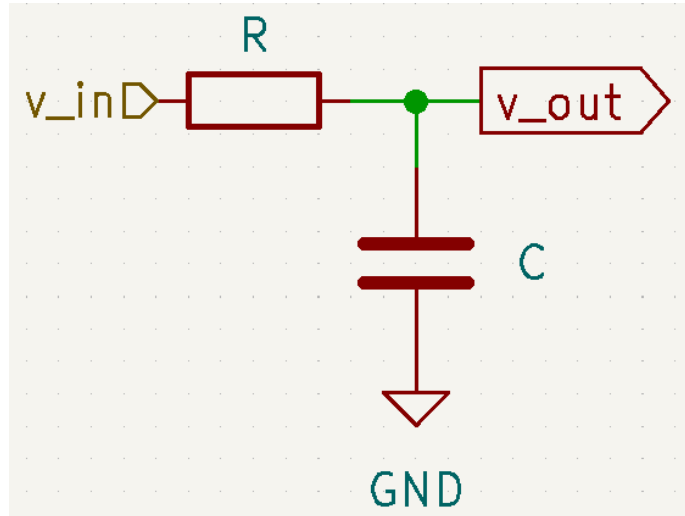


Figure 2-17. Passive first-order RC LPF circuit

The circuit above acts under the principle of a voltage divider:

$$\frac{v_{out}}{v_{in}} = \frac{Z_C}{Z} = \frac{Z_C}{\sqrt{R^2 + Z_C^2}}, \text{ where } Z_C = \frac{1}{2\pi f C} \text{ and } f \text{ is the frequency of the input signal } v_{in}.$$

The cut-off frequency f_c of a LPF is defined to be the frequency at which the voltage gain on the logarithmic scale of the output $A_V = 20 \times \log (\frac{v_{out}}{v_{in}})$ is -3 dB [54], or $\frac{v_{out}}{v_{in}} = \frac{1}{\sqrt{2}}$. As the result, the cut-off frequency of a passive RC LPF is $f_c = \frac{1}{2\pi R C}$. For example, a LPF with $R = 1 k\Omega$ and $C = 100 nF$ has the cut-off frequency $f_c = 1591.55 \text{ Hz}$.

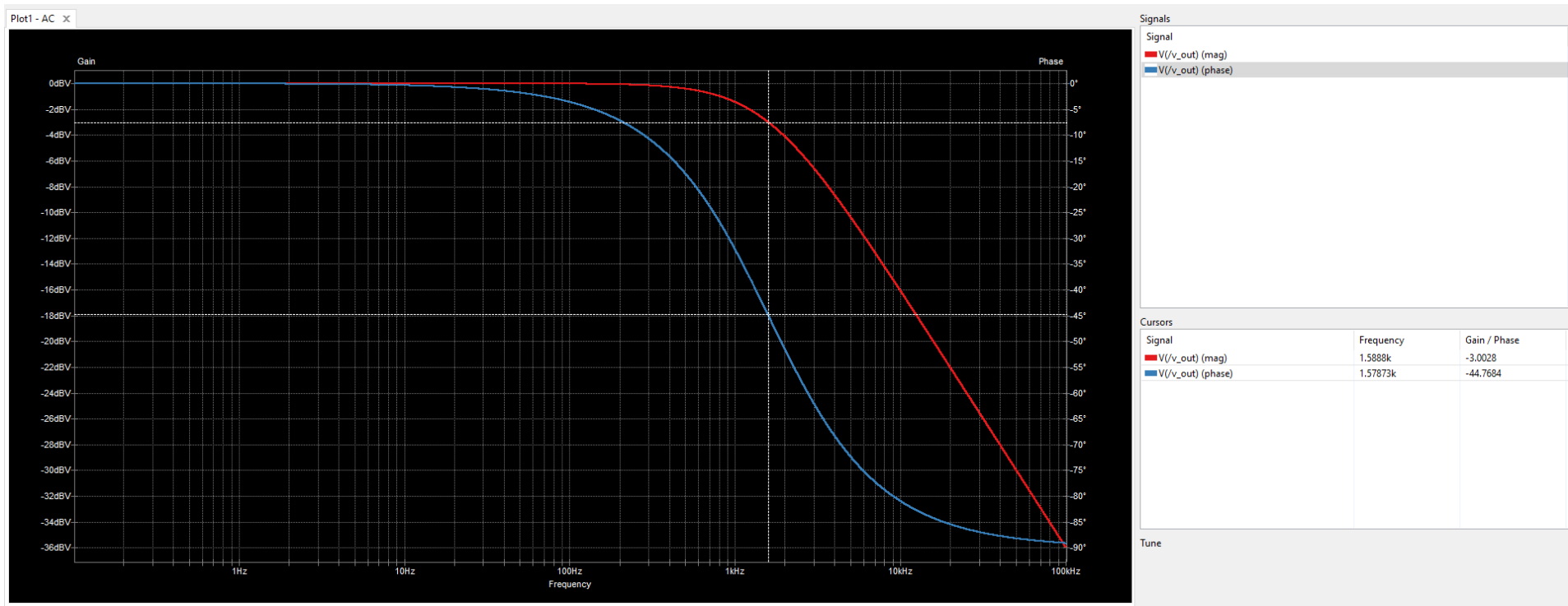


Figure 2-18. Frequency response of an example RC LPF with $R = 1\text{ k}\Omega$ and $C = 100\text{ nF}$ under simulation

2.5. System Powering

Since the Autonomous Wireless Agrometeorology Station is expected to operate off-grid, there requires an independent power source. By concept, a solar panel backed by Lithium-Ion batteries is to be included. However, due to the limitations of the project (i.e., the 12-week time limit for the thesis, and the shortage of supplies for desired hardware), it is decided that the power unit for the Station is to be left out to further developments. As a result, the current design of the Autonomous Wireless Agrometeorology Station takes in any voltage input up to +37V and regulates for +3.3V to power its main system.

2.6. Server

The server side for the Autonomous Wireless Agrometeorology Station consists of:

- A gateway that receives the sensor data wirelessly from the station via LoRa communication,
- And an online database which the gateway forwards the sensor data to and makes the data accessible for users.

The main idea is to involve another microcontroller to use with an SX1278 LoRa module as the gateway. The microcontroller should be able then to connect to the Internet to upload the received data to the online database of choice.

For the sake of simplicity, a nodeMCU ESP8266 is utilised because of its Wi-Fi connection capability and its availability, as well as the Arduino framework for software development. The online database of choice is ThingSpeak by The MathWorks Incorporation, on top of services like Microsoft Azure, Google Firebase, and InfluxDB.

Initially, InfluxDB was in use as the online database for the Autonomous Wireless Agrometeorology Station and proved to be intuitive [6]. However, it is discovered that this service only retains uploaded data for 30 days for free accounts, which makes it less ideal for a project of a bachelor thesis. Microsoft Azure and Google Firebase, on the other hand, offer decently free services, but the connection processes are quite complicated, thus ruled out. ThingSpeak is the remaining option whose service is free of charge while letting users accessing and handling data without a time limit. The only known downside of ThingSpeak is that each free account is only allowed 4 data channels, which is not an issue in testing and prototyping the Autonomous Wireless Agrometeorology Station.



Figure 2-19. The nodeMCU ESP8266 used at the server side of the project [6]

3. Implementation

3.1. STM32F103C8T6 Microcontroller

As mentioned in section 2.1, the STM32F103C8T6 microcontroller in test is shipped on a Blue Pill board (Figure 2-1) with all the necessary components for its peripherals. Therefore, the board is directly implemented with all the buses shown in Figure 3-2. In turn, the Agrometeorology Station is made up of the connections depicted in Figure 3-3, whose components are to be explored in this Chapter 3.

The software allowing the STM32F103C8T6 microcontroller to control all the connected devices is explored in Chapter 3 and constructed upon the STM32duino firmware for the Arduino framework. However, the STM32 core is not a built-in of the Arduino platform, thus board definitions required. By appending the following to the Additional Boards Manager URLs of the Arduino IDE, the STM32duino firmware could be installed via Boards Manager and used for programming in the later sections [55].

```
https://github.com/stm32duino/BoardManagerFiles/raw/main/  
package\_stmicroelectronics\_index.json
```

Since the microcontroller in use is an STM32F103C8T6 with a Flash memory size of 128 KB (Section 2.1), the Arduino IDE is set up as:

- Board: “Generic STM32F1 series”
- Board part number: “BluePill F103CB (or C8 with 128k)”
- U(S)ART support: “Enabled (generic ‘Serial’)”
- USB support (if available): “None”
- USB speed (if available): “Low/Full Speed”
- Optimize: “Smallest (-Os default)”
- Debug symbols and core logs: “None”
- C Runtime Library: “Newlib Nano + Float Printf”
- Upload method: “STM32CubeProgrammer (SWD)”

The software is built with the intention of debugging via UART, thus the U(S)ART support option being “Enabled (generic ‘Serial’)” to make use of the default `Serial` object of the Arduino framework. Furthermore, the “Newlib Nano + Float Printf” option is chosen for C Runtime Library to make use of the `printf(..)` method, which is ported from the C language to the C++ language of the Arduino framework exclusively for the STM32duino firmware.

Finally, the software for the Autonomous Wireless Agrometeorology Station makes use of the official STM32duino firmware by STMicroelectronics, so at the time of this thesis, the only known method of uploading to the STM32F103C8T6 microcontroller is via the Serial Wire Debug (SWD) interface with an ST-Link in-circuit debugger/programmer, and the driver for a such hardware is provided by the STM32CubeProgrammer application. Therefore, the Upload method option is chosen to be “STM32CubeProgrammer (SWD)”. For the rest of the tool settings on the Arduino IDE, the default options are left untouched.

After the microcontroller is properly set up, its software is built following Figure 3-4. All the software dependencies for the connected modules are written as depicted throughout Section 3.

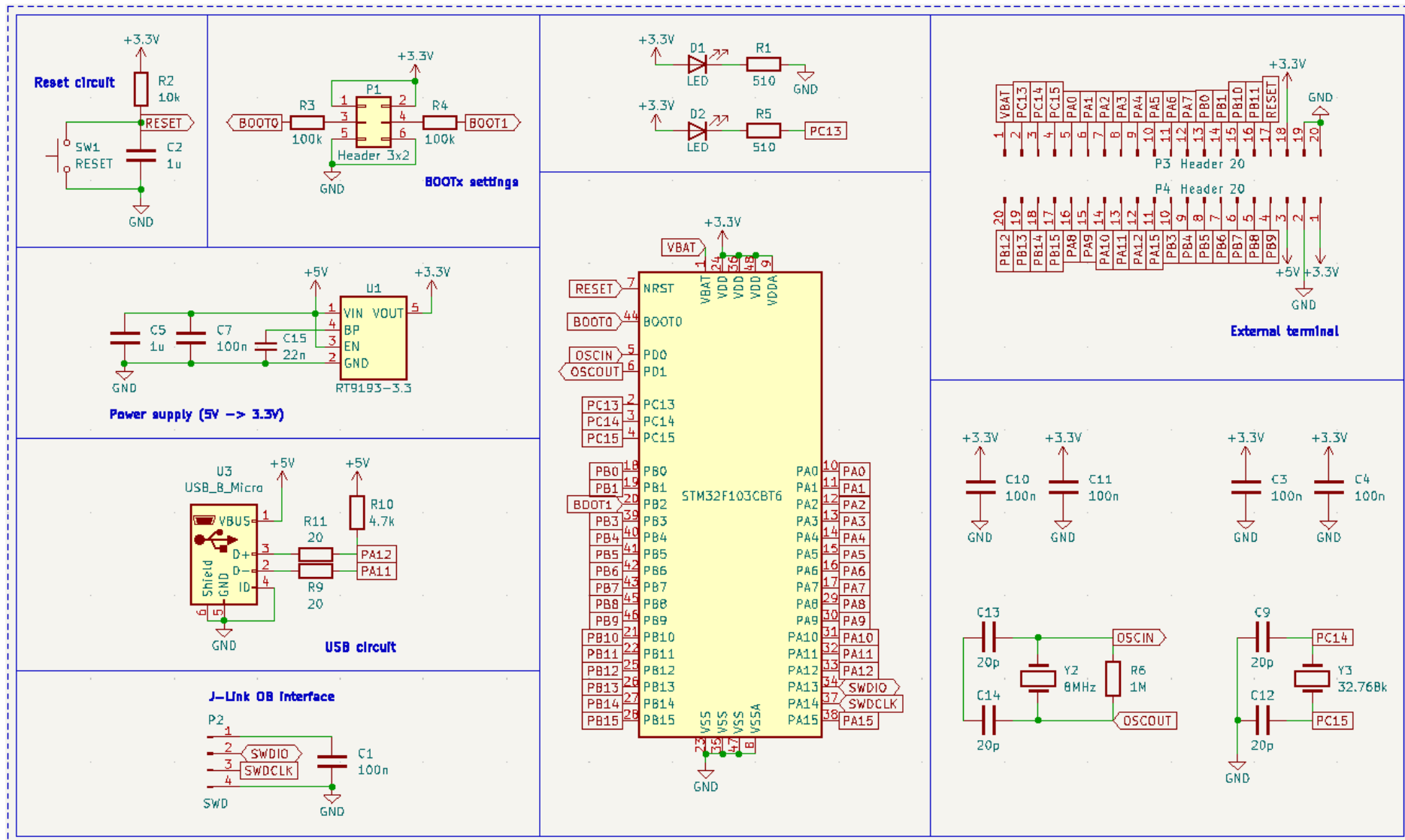


Figure 3-1. The schematic of the STM32F103C8T6-housed Blue Pill board [12]

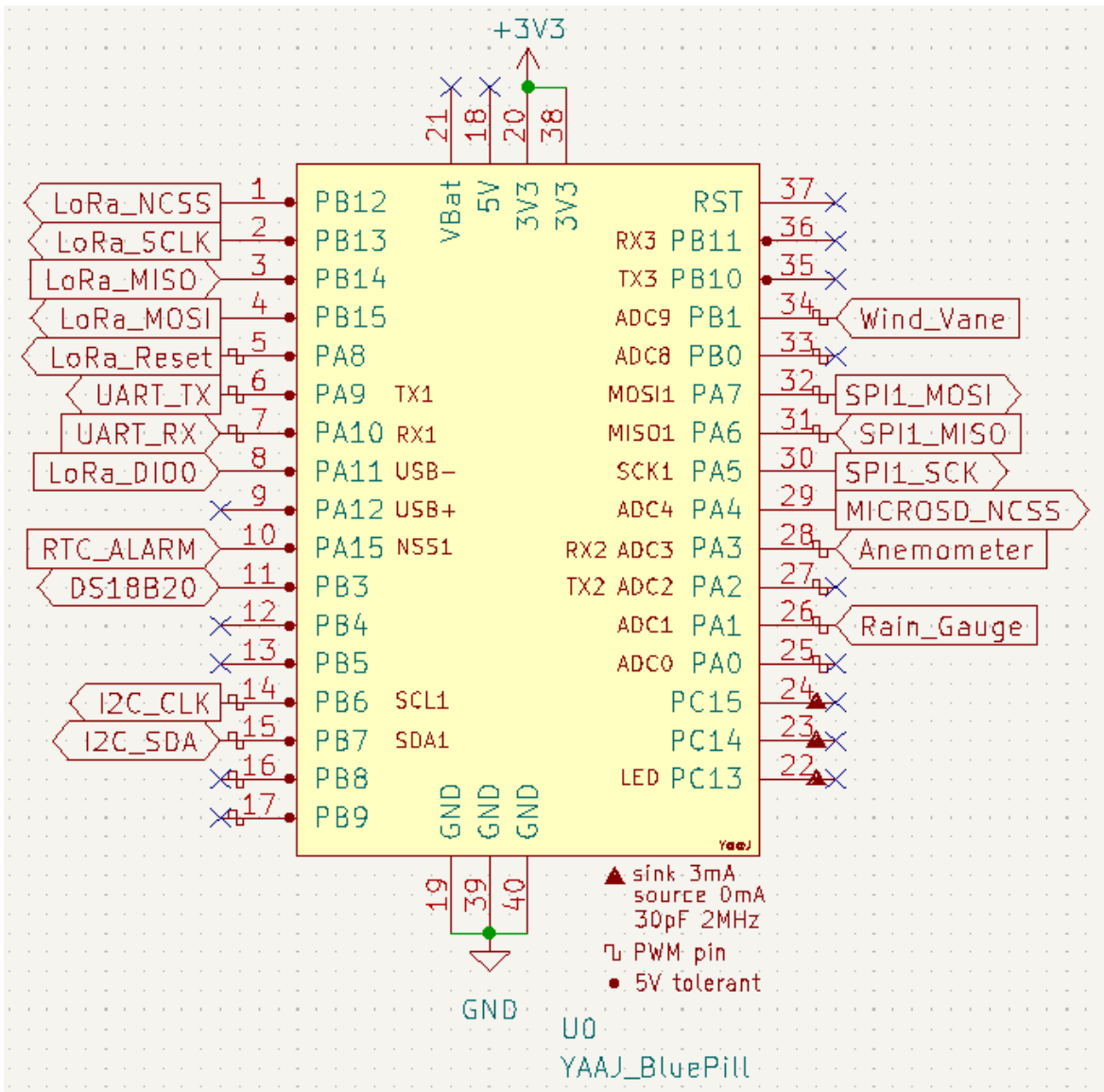


Figure 3-2. Bus connections with the Blue Pill board

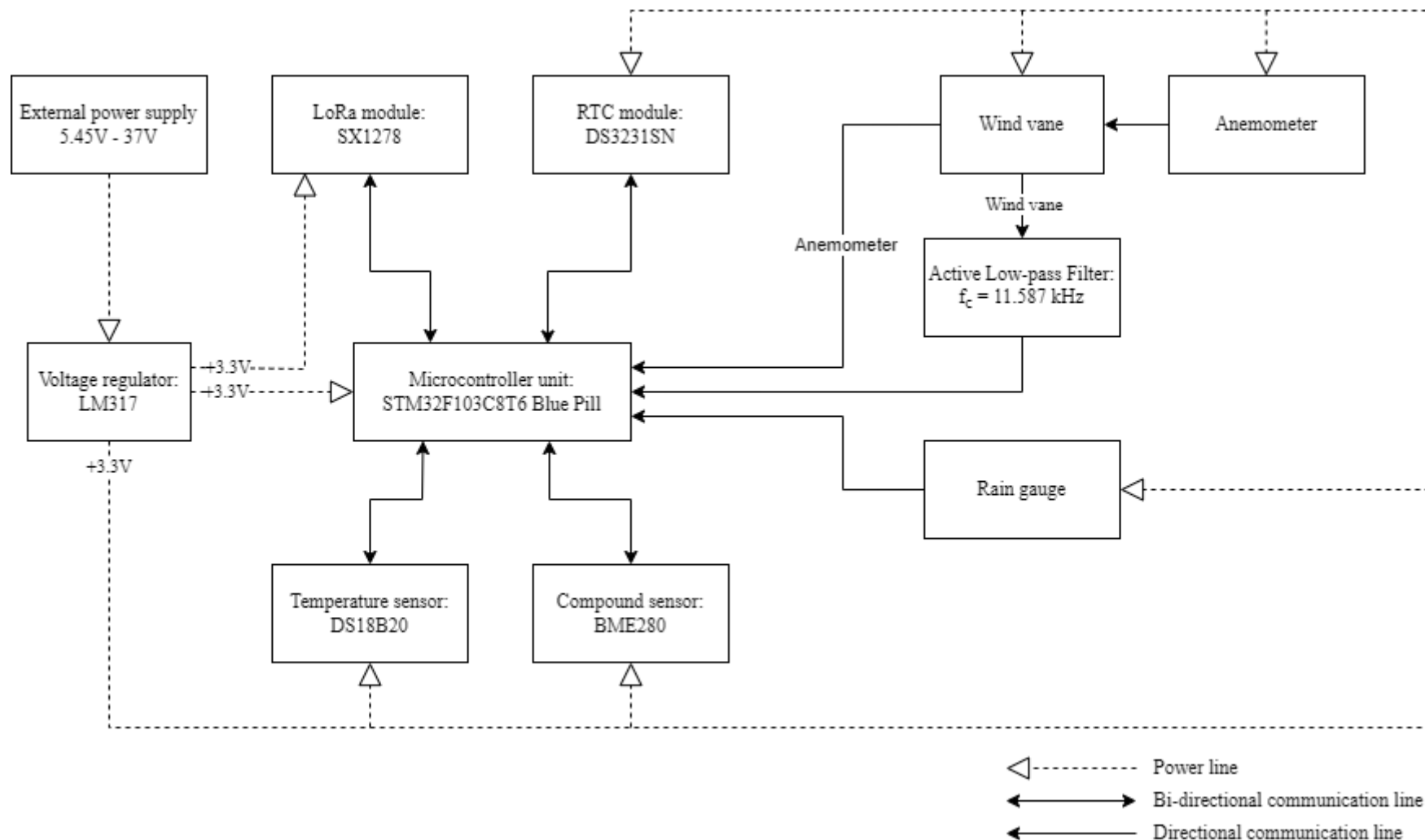


Figure 3-3. Block diagram of the current design for the Autonomous Wireless Agrometeorology Station

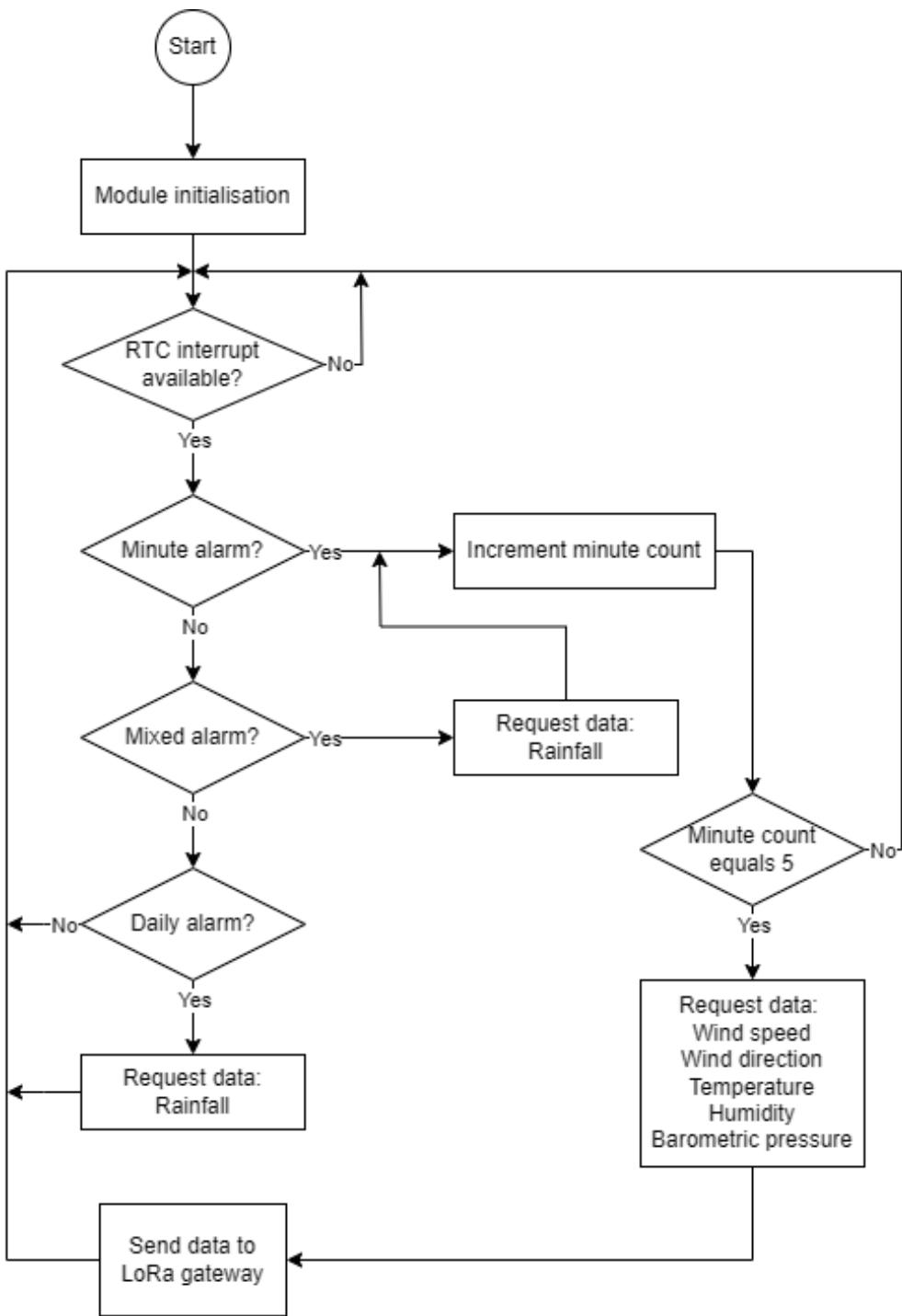


Figure 3-4. General software flow built for the Autonomous Wireless Agrometeorology Station

3.2. Sensor units

3.2.1. Anemometer

3.2.1.1. Hardware dependencies

Pull-up resistor

As mentioned in Section 2.2.1, the anemometer could be read through the inner 2 conductors of its RJ11 cable. If it is connected to the wind vane as shown in section 2.2.2, interfacing through the inner 2 conductors of wind vane's RJ11 cable is done instead. It is known that the electronic part of the anemometer is a mechanical device called the reed switch. As a standalone device, a reed switch does not create any electrical signals to be read, thus the use of a setup as simple as illustrated in Figure 3-5.

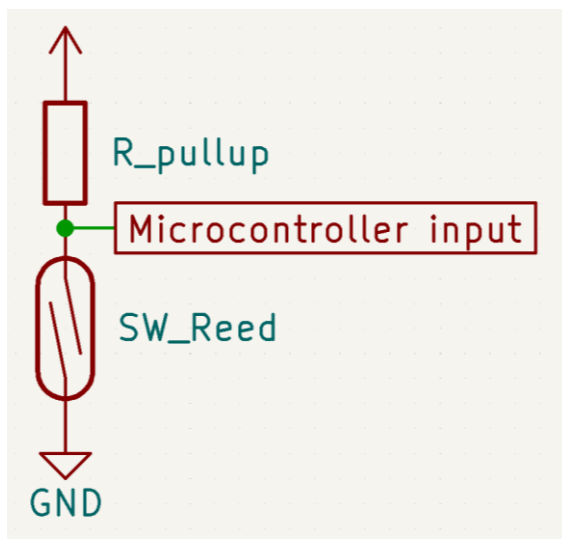


Figure 3-5. Circuitry for testing the anemometer in ideal conditions

The circuitry in Figure 3-5 generates active-LOW outputs by the use of the pull-up resistor, which means the microcontroller normally reads logic 1 and detects a logic 0 when the switch closes. Active-HIGH outputs could be achieved by switching the positions of the reed switch (SW_Reed) and the resistor (R_pullup); however, since there are potentially faults due to interference while the microcontroller detects logic 1 in that setup, active-HIGH signals are undesirable in this project.

The pull-up resistor value could be chosen for either strong or weak pull-up purpose. A resistor with a high value creates a weak pull-up which results in lower power consumption, and vice versa [56]. If the input impedance on the microcontroller pin is unknown, it is safe to choose a strong pull-up resistor (i.e. $4.7\text{k}\Omega$). However, [14] specifies that a resistor from $30\text{k}\Omega$ to $50\text{k}\Omega$ could be used to achieve a weak pull-up for an STM32F103CBT6 microcontroller, so the value of $33\text{k}\Omega$ is chosen in this project. As a result, the design would be more suitable as a battery-powered application.

Bypass capacitor

In [57], it is investigated that as a mechanical switch, a reed switch could produce noise spikes which yield wrong edge detections by a microcontroller, thus wrong data. For example, Figure 3-6 illustrates a noise instance which could make a microcontroller read 3 falling edges instead of an expected 1 edge within a window of $98.98\mu\text{s}$.

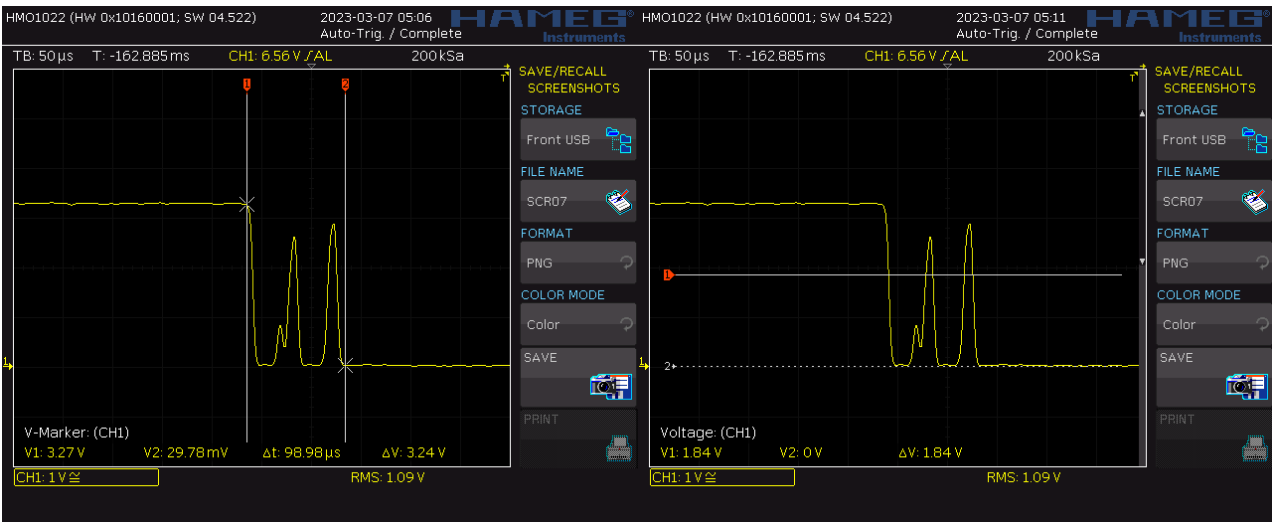


Figure 3-6. “An instance of noise spikes captured in an oscilloscope” [6]

The solution to a such problem is the implementation of either a LPF to filter out the noise [57] or just a bypass capacitor to debounce the switch. Due to lower edge rise and fall time, and less components involved, the latter is a more preferable method [6]. The choice for a such capacitor is to satisfy that the time constant of the pull-up resistor – bypass capacitor pair is about half of the debouncing time [58].

$$T = R \times C \text{ where } T \text{ (in seconds) is the time constant of the resistor – capacitor pair,}$$

$$R \text{ (in Ohms) is the value of the pull-up resistor of the switch circuit,}$$

$$C \text{ (in Farads) is the value of the decoupling capacitor.}$$

It is studied that reed switches have bounces up to 4.5ms. Moreover, the pull-up resistor for interfacing the anemometer with the microcontroller is chosen to be $33k\Omega$. Therefore, the value of the bypass capacitor is $C = \frac{T}{R} = \frac{4.5ms/2}{33k\Omega} = 68.18nF$. Since a such value does not exist in real life, the closest value of $68nF$ is chosen for the bypass capacitor instead.

Furthermore, the fact that the pull-up resistor is determined to be $33k\Omega$ relies on the calculation of the bypass capacitor in this part. The bypass capacitor value is derived from a list of manufactured resistor values, which should be available for both testing and prototyping when this thesis is conducted, and is picked from the closest real numbers for a capacitor. Table 3-1 shows that the resistor – capacitor pair of $33k\Omega$ – $68nF$ fits the theoretical calculation the most.

Table 3-1. Choosing bypass capacitor value based on available resistors from $30k\Omega$ to $50k\Omega$

Real resistor value	Calculated capacitor value	Closest real capacitor value
$30k\Omega$	75.00nF	82nF
$33k\Omega$	68.18nF	68nF
$36k\Omega$	62.50nF	68nF
$39k\Omega$	57.69nF	56nF
$47k\Omega$	47.87nF	47nF

In order to determine the practicability of the pull-up resistor and the bypass capacitor, a circuit illustrated in Figure 3-7 is put in use. The reed switch stays attached inside the anemometer and is read from the corresponding pins of the RJ11 connector. The smoothed-out transitions shown in Figure 3-8 are consistent with the findings in [6] and indicate that the setup is applicable in a real design.

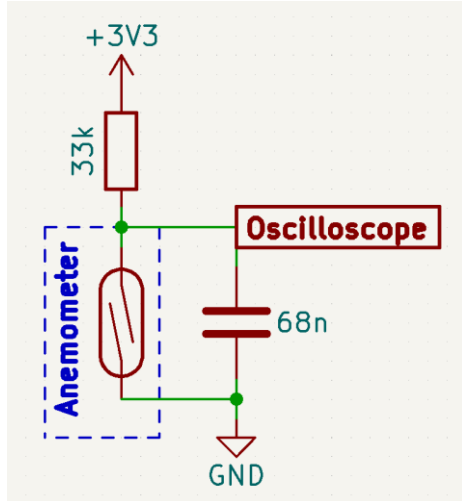


Figure 3-7. Bypass capacitor test circuitry using the reed switch from the anemometer

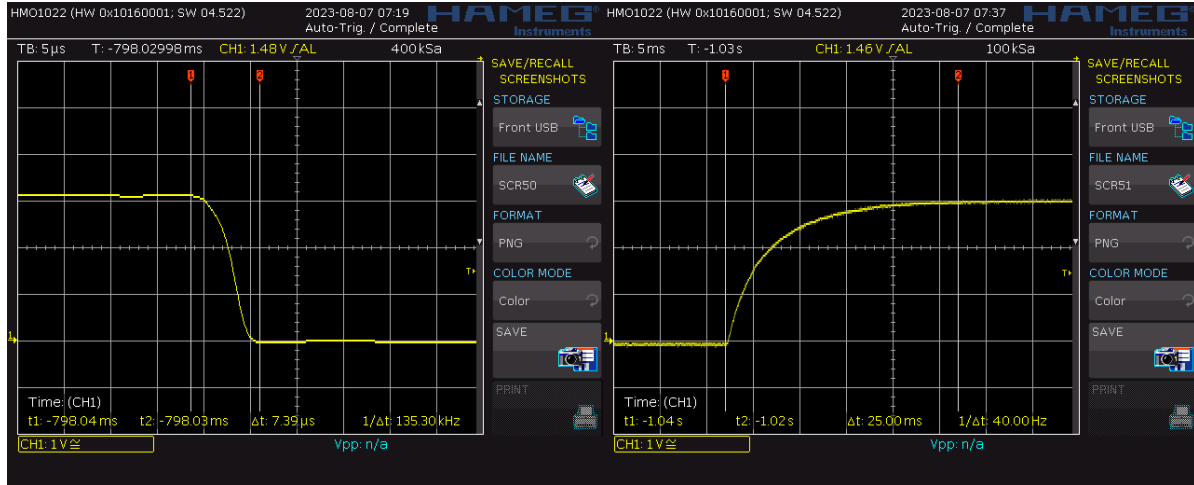


Figure 3-8. Reed switch debounced by the 68-nF bypass capacitor

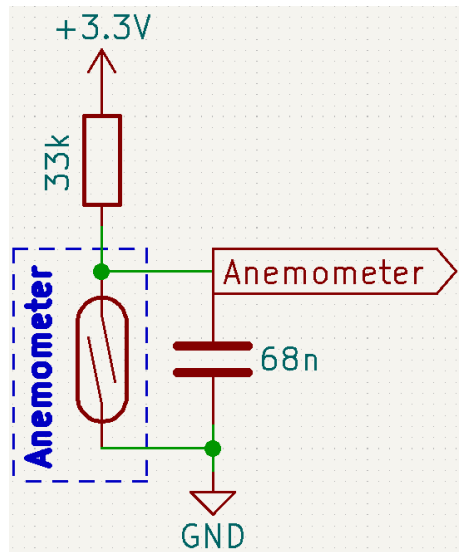


Figure 3-9. Circuitry for interfacing with the anemometer

3.2.1.2. Software design

It is determined that the average wind speed monitored via an anemometer is $\frac{n}{2} \times 2\pi R/T$, where n is the number of pulses over a period T detected from the anemometer by the microcontroller, and R is “the radius from the pivot to the edge of a cup” [6], [59]. However, a real anemometer always contain a parameter called the anemometer factor K as demonstrated by [19]. However, since the determination of the anemometer factor requires a deep study on the aerodynamic characteristics of the cup anemometer itself, the software design shall leave the anemometer factor $K = 1$ and test for the behaviours of the anemometer in Section 4.1.

Since monitoring wind speed is simply counting pulses from the anemometer, the software shall be interrupt-based to avoid blockage of other tasks while keeping the count constantly updated. All the necessary software parts for the anemometer are put into the one-time setup routine on microcontroller’s power-up.

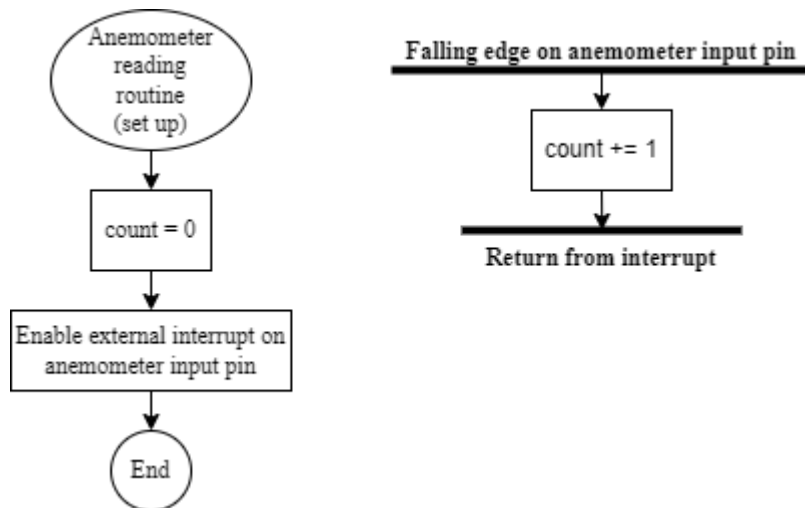


Figure 3-10. Anemometer setup routine and interrupt service routine upon input event

On the Arduino platform, enabling an external interrupt on the anemometer input pin is done via the built-in `attachInterrupt(..)` function. After the anemometer input pin is declared as `Anemometer_InputPin`, and the `count` variable is initialised with the value 0, since the hardware designs the anemometer input as active-LOW, the external interrupt is set to detect falling edges by

```
// Attach an interrupt on anemometer input pin for falling edge detection
pinMode(Anemometer_InputPin, INPUT);
attachInterrupt(digitalPinToInterrupt(Anemometer_InputPin),
               anemometerInput_Detected,
               FALLING);
```

Afterwards, whenever the anemometer rotates and produces a pulse, the interrupt service routine, namely `anemometerInput_Detected()`, is automatically called to increment the `count` variable. On the global scale, the software keeps track of the time and requests all sensor data, including the anemometer’s, once every 5 minutes. As soon as this global event happens, the value of the `count` variable is stored to a temporary variable, namely `count_temp`, and `count` is reset to 0; `count_temp` is used to converting the pulse count to wind speed to respond to the global data request, while `count` goes on a new counting cycle. By simplifying $\frac{n}{2} \times 2\pi R/T$ to $n \times \pi R/T$, the latest wind speed in metres per second is returned by a single line

```
return (count_temp * PI * 0.092 / 300);
```

where PI is a built-in macro for π on the Arduino platform, 0.092 is the radius in metres of the anemometer (Figure 2-3b), and 300 is the 5-minute window in seconds. The global sensor data request occurs every 5 minutes because this is the chosen sampling duration for the anemometer to minimise the effects of wind gusts [60].

3.2.2. Wind Vane

3.2.2.1. Hardware dependencies

Voltage divider

In section 2.2.2, it is illustrated that there are 2 circuitries that could be used for the wind vane: a current mirror and a voltage divider. For simplicity, the latter is utilised in this project.

In order to form a voltage divider, an external resistor as shown in Figure 2-7b is required. The value of a such component in turn needs to satisfy that:

- Current output at the voltage divider is enough for the ADC module to charge its internal capacitor C_{ADC} for each conversion.
- Voltage step of the voltage divider values generated by all the wind vane positions is large enough for the microcontroller to distinguish.

Figure 3-11 illustrates the voltage divider circuit when integrated with the microcontroller's ADC module. It is assumed that at the beginning of each conversion cycle, the internal capacitor C_{ADC} has been fully discharged and the switch ("SW") is then closed.

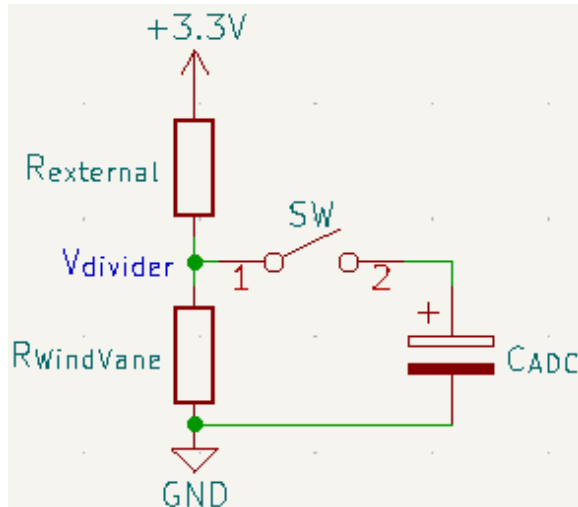


Figure 3-11. Voltage divider circuitry with ADC module

By applying the source transformation technique, the voltage divider could be changed into a first order RC charging circuit as shown in Figure 3-12. The Norton equivalent circuit is produced by deriving a Thévenin equivalent circuit of the $+3.3V$ voltage source in series with the resistor R_{external} , which yields:

$$I_S = \frac{+3.3V}{R_{\text{external}}} \quad (1)$$

The resulted circuitry is then further simplified by combining the parallel resistors into a single value:

$$R_{equivalent} = \frac{R_{external} \times R_{WindVane}}{R_{external} + R_{WindVane}}$$

At this point, the step response of an RC circuit as given by [61] could be applied:

$$v_{C_{ADC}} = I_S \times R_{equivalent} + (V_0 - I_S \times R_{equivalent}) \times e^{-t/T}, \quad t \geq 0 \quad (2)$$

or, based on previously made assumption, and by substituting (3) into (2):

$$v_{C_{ADC}} = I_S \times R_{equivalent} \times (1 - e^{-t/T}), \quad t \geq 0$$

where $T = R_{equivalent} \times C_{ADC}$ is the time constant for the RC circuit. It is worth noticing that the voltage up to which the capacitor C_{ADC} is charged is:

$$V_{divider} = I_S \times R_{equivalent} = 3.3V \times \frac{R_{WindVane}}{R_{external} + R_{WindVane}}$$

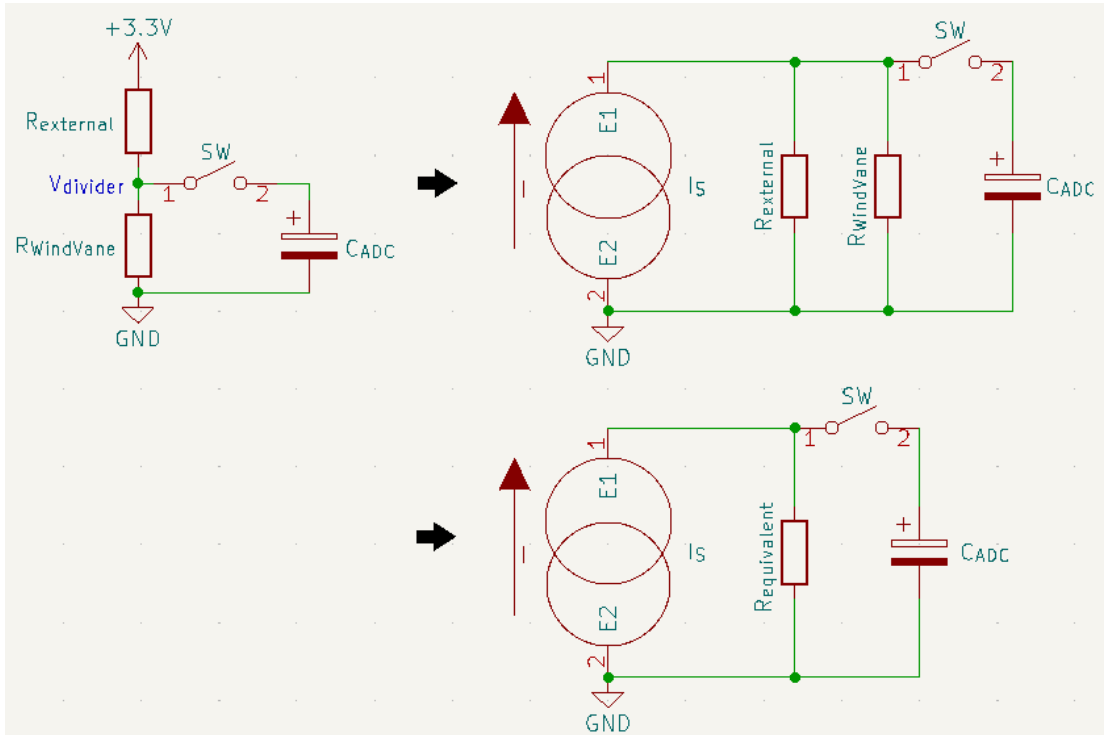


Figure 3-12. Derivation of the Norton equivalent of the voltage divider

According to the capacitor charging voltage curve shown in [62], C_{ADC} would reach its steady state within $4T$ after the switch is closed, and become fully charged at $t = 5T$. It is desirable that the ADC internal capacitor C_{ADC} is fully charged during the sampling window of the ADC module. Since the lowest sample rate of the STM32F103C8T6 microcontroller is 1.5 ADC clock cycles [13], there holds a condition for $R_{external}$:

$$5T \leq \frac{1.5}{f_{ADC}}$$

$$\Rightarrow 5 \times R_{equivalent} \times C_{ADC} \leq \frac{1.5}{f_{ADC}}$$

$$\Rightarrow 5 \times \frac{R_{external} \times R_{WindVane}}{R_{external} + R_{WindVane}} \times C_{ADC} \leq \frac{1.5}{f_{ADC}}$$

This project uses an STM32F103CBT6 microcontroller on the official Arduino core by STMicroelectronics, so the ADC clock frequency could be derived to be 12MHz from the core project on Github [55]. Furthermore, [14] specifies that the internal sample and hold capacitor of the ADC module is guaranteed to be 8pF by design. By substituting the wind vane internal resistance values from Table 2-1, the condition of $R_{external} \leq 3.208k\Omega$ is obtained. Afterward, all the manufactured resistor values which meet that condition are put into an Excel sheet to calculate the corresponding voltage step of the voltage divider with a fixed value of +3.3V power supply.

The screenshot shows an Excel spreadsheet with the following structure:

- Row 1:** A, B, C, D, E, F, G. Cell E contains the formula $V_{cc} = 3.3$.
- Row 2:** A, B, C, D, E, F, G. Cell E contains the formula $R = 3.0K$.
- Row 3:** A header row for the main data table. Columns: Direction (fixed), $R_{WindVane}$, $V_{divider}$, Direction (mixed), $R_{WindVane}$, $V_{divider}$.
- Rows 4-11:** Data table for various wind vane directions. The data is as follows:

Direction (fixed)	$R_{WindVane}$	$V_{divider}$	Direction (mixed)	$R_{WindVane}$	$V_{divider}$
0	33.00K	2.997500	22.5	6.57K	2.244703
45	8.20K	2.394107	67.5	0.89K	0.748994
90	1.00K	0.817500	112.5	0.69K	0.609661
135	2.20K	1.383462	157.5	1.41K	1.043772
180	3.90K	1.848261	202.5	3.14K	1.671155
225	16.00K	2.753684	247.5	14.12K	2.696907
270	120.00K	3.190244	292.5	42.12K	3.052580
315	64.90K	3.125523	337.5	21.88K	2.875650

- Row 12:** A blank row.
- Row 13:** A header row for the summary table. Column: $V_{divider}$ handler.
- Row 14:** A header row for the sorted data table. Columns: $V_{divider}$ (sorted), Step.
- Rows 15-20:** Summary statistics for the sorted data. The data is as follows:

$V_{divider}$ (sorted)	Step
3.190244	$\max(V_{divider})$
3.125523	$\min(V_{divider})$
3.052580	$\text{mean}(step)$
2.997500	$\max(step)$
2.875650	$\min(step)$
2.753684	0.055080

- Row 21:** A blank row.
- Row 22:** A blank row.
- Row 23:** A blank row.
- Row 24:** A blank row.
- Row 25:** A blank row.
- Row 26:** A blank row.
- Row 27:** A blank row.
- Row 28:** A blank row.
- Row 29:** A blank row.
- Row 30:** A blank row.
- Row 31:** A blank row.

Note: All the voltage values are measured in Volts.

Figure 3-13. An instance of $R_{external} = 3.0k\Omega$ input to the voltage step-calculating sheet

Table 3-2 records all the minimum voltage steps of the voltage divider for all the resistor values under $3.208k\Omega$. Since the STM32F103C8T6 microcontroller has 12-bit ADC modules, in theory, it could detect analogue input changes as low as $\frac{3.3V}{2^{12}} = 805.7\mu V$. Therefore, all voltage steps in Table 3-2 is detectable. However, in practice, there are a number of factors like ADC offset errors, input noise, imprecise analogue reference, etc. that could cause unpredictable behaviours and/or unusable data if an ADC module were applied in ideal conditions. As a result, the largest voltage step by design for an ADC module to detect is always desired, which is 0.0555854V for $R_{external} = 3.0k\Omega$.

Table 3-2. Voltage steps of the voltage divider by R_{external}

R_{external} (in Ohms)	Voltage step (in volts)
510	0.010647
560	0.0116597
680	0.0140682
820	0.0168393
910	0.0185989
1.0K	0.02
1.2K	0.02
1.5K	0.0297257
1.8K	0.0351217
2.0K	0.0386253
2.2K	0.0420557
2.4K	0.0454148
2.7K	0.0503233
3.0K	0.0555854

Low-pass filter

It has been mentioned that ADC readings could be different from expected due to input noise, which is inevitable. However, the effects of those unwanted fluctuations could first be reduced by the use of an analogue filter. Since noise is usually high frequency signals, the use of an analogue LPF is desired.

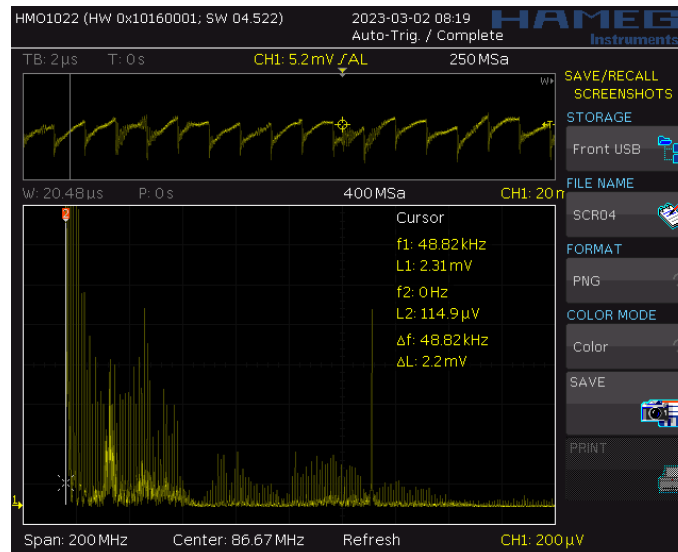


Figure 3-14. A noise instance captured during a test on the wind vane

Designing a LPF firstly requires the cut-off frequency. In order to achieve the best possible ADC accuracy, it is predetermined that the software for reading the wind vane shall utilise the ADC module at the highest sampling time of 239.5 ADC clock cycles [13]. The reviewed STM32duino firmware for the STM32F103C8T6 microcontroller, combined with the reference manual [13] and the STM32CubeMX, gives the ADC clock of 12 MHz and the sampling frequency for the 239.5-cycle sampling time of $\frac{12\text{MHz}}{(235.9+12.5)\text{cycles}} = 47.619\text{ kHz}$ [55]. Furthermore, [63] states that the sampling frequency should range from 2 to 5 times the frequency limit of the input signal, which results in the

cut-off frequency by the LPF to be between 9.524 kHz and 23.810 kHz. The such frequency band is then narrowed down to 9.524 kHz – 12.62 kHz since the latter was observed to be the lowest noise signal when the test for Figure 3-14 was conducted. A table, a part of which is Table 3-3, is then constructed with the known manufactured resistor and capacitor values; each LPF option contains only 1 resistor R_{filter} , while there could be up to 4 capacitors in parallel for higher capacitance and lower equivalent series resistance (ESR). The final cut-off frequency is chosen based on 2 criteria:

- The theoretical cut-off frequency must be between 9.524 kHz and 12.62 kHz.
- The resistor value must be low to avoid unwanted signal attenuation caused by insufficient input current.

As a result, the LPF option with $f_{-3\text{dB}} = 11.587$ kHz is chosen to be included in the hardware design for the wind vane.

Table 3-3. A part of the component pick-up table for the passive LPF

R_{filter}	C_1	C_2	C_3	C_4	$f_{-3\text{dB}}$
680 Ω	10 nF	4.7 nF	1 nF		14.908 kHz
	10 nF	3.3 nF	1 nF		16.367 kHz
	10 nF	4.7 nF	3.3 nF	1 nF	12.318 kHz
	10 nF	4.7 nF	3.3 nF	2.2 nF	11.587 kHz
820 Ω	10 nF	4.7 nF	1 nF		12.363 kHz
	10 nF	4.7 nF	2.2 nF		11.485 kHz
	10 nF	4.7 nF	3.3 nF		10.783 kHz
1 k Ω	10 nF	4.7 nF	1 nF		10.137 kHz
	10 nF	3.3 nF	1 nF		10.130 kHz
	10 nF	2.2 nF	1 nF		12.057 kHz

Although the construction of the LPF takes into account the attenuation caused by insufficient current at the ADC input side, the hardware design for the wind vane takes another precaution to avoid any further issues by adding a voltage buffer to make the LPF an active one. Finally, a pull-down resistor is put in parallel with the ADC input of the microcontroller to avoid floating output of the active LPF, completing the hardware design for the wind vane as shown in Figure 3-15. The choices of the MCP6002-I/P as the operational amplifier (Op-Amp) and the 3.3-k Ω pull-down resistor R_{pulldown} are based upon the experimental characterisation of the set of options explored in section 4.2.

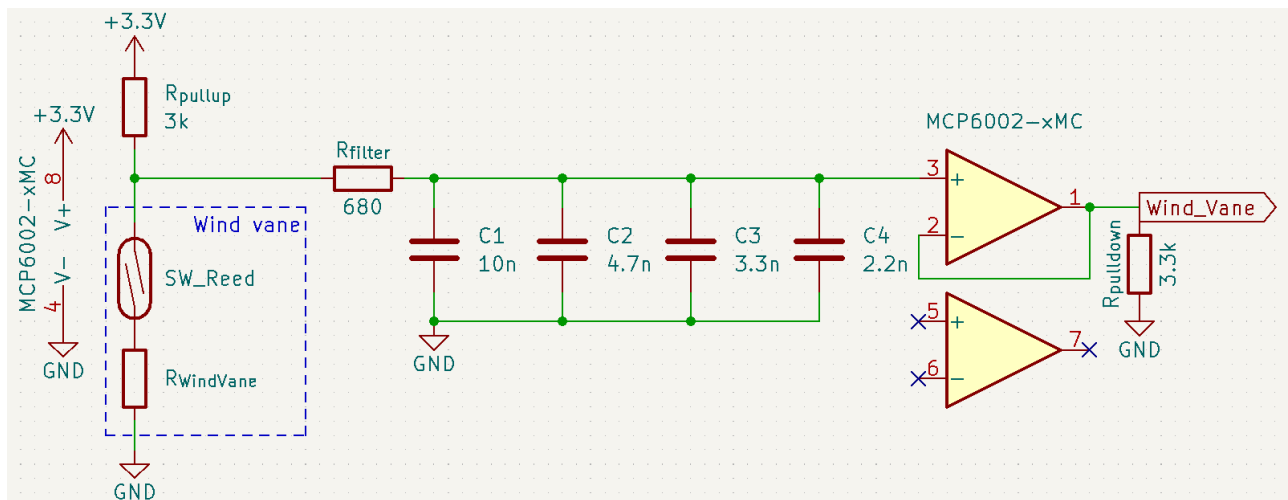


Figure 3-15. Circuitry for reading the wind vane

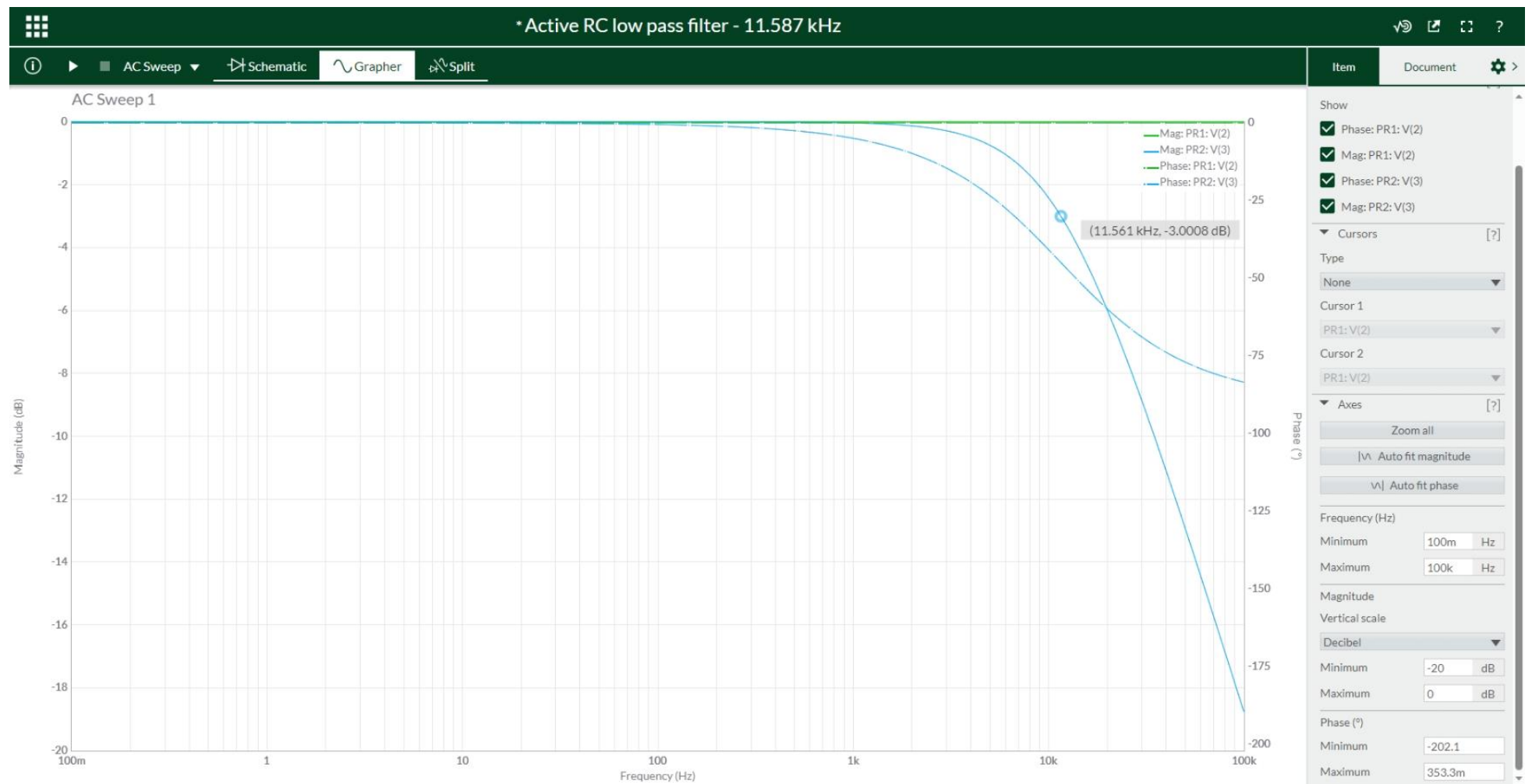


Figure 3-16. Frequency response of the active 11.587-kHz RC LPF



Figure 3-17. Step response of the active 11.587-kHz RC LPF

3.2.2.2. Software design

Reading the wind direction from the wind vane mostly involves determining the resistive value returned by the sensor, which is done directly via the built-in ADC functionality of the STM32F103C8T6 microcontroller.

Since the wind vane is hooked on the same +3.3V power supply as the microcontroller (Figure 3-3 and Figure 3-15), and the STM32F103C8T6 microcontroller uses its power supply as analogue reference [13], at the beginning of each sampling cycle, the apparent value of the +3.3V is checked by the ADC internal reference channel and stored in a temporary variable V_{cc} to overcome the issue of any instabilities on the power supply. Afterwards, the microcontroller continuously samples 21 ADC values from the input by the wind vane, then discards the first entry and takes the mean value ADC_{mean} of the remaining 20 data points. Since the signal from the analogue circuitry of the wind vane is essentially a step response, the raw ADC values are expected to remain stable after the settling time, thus the discarded first value.

By applying the formula for the voltage divider, the momentary internal resistor of the wind vane is estimated

$$R_{WindVane} = (3k\Omega) \times \frac{v_{ADC_input}}{V_{cc} - v_{ADC_input}}$$

where

$$v_{ADC_input} = V_{cc} \times \frac{ADC_{mean}}{2^{12} - 1}$$

Finally, the value of $R_{WindVane}$ is compared with the given values in Table 2-1. The corresponding Azimuth degree of the given resistor value which $R_{WindVane}$ is closest to is determined to be the wind direction.

One major part of the software design for the wind vane is the use of the Hardware Abstract Layer (HAL) for ADC and the Direct Memory Access (DMA) controller instead of the simple built-in *readAnalog()* function of the Arduino framework. The DMA controller allows ADC sampling in non-blocking mode, which means the microcontroller could perform other tasks while the sampling operation takes place, and writes the conversion results directly to a pre-defined buffer. The respective functions for HAL and DMA configurations as shown in Appendix A are generated in C language by the STM32CubeMX software and modified to be used in the native C++ language of the Arduino platform. Furthermore, in order for the HAL module to be initialised for ADC during compilation, there must exist a header file named ***hal_conf_extra.h*** whose content is a single definition line:

```
#define HAL_ADC_MODULE_ONLY
```

The header file ***hal_conf_extra.h*** is then included in the main Arduino source file (namely ***Main_Code.ino*** in this project), following the official instructions from STMicroelectronics [55].

On each wind vane reading cycle, the necessary ADC functions by the STM32duino firmware are shown in Table 3-4. Upon powered, the microcontroller needs to call the functions in the order of 0-3-1 to initialise the DMA controller and perform a calibration of the ADC module as described in [13]. On each sampling cycle, the function order 2-4-6-7-6-7 is called to read the analogue reference V_{cc} , then 3-4-6-7 for a dummy reading (discarded value). Finally, the main conversion routine takes place by the function order 3-5.

Table 3-4. ADC functions for wind vane reading software

Function number	Function	Return type	Purpose
0	<code>MX_DMA_Init();</code>	None	Initialising the DMA controller for HAL ADC module
1	<code>HAL_ADCEx_Calibration_Start(&hadc1);</code>	None	Perform a calibration of the ADC module
2	<code>MX_ADC1_Init(INTERNAL_REFERENCE_VOLTAGE);</code>	None	Switching ADC to internal channel
3	<code>MX_ADC1_Init(EXTERNAL_INPUT_SIGNAL);</code>	None	Switching ADC to external channel
4	<code>HAL_ADC_Start(&hadc1);</code>	None	Initiating a single ADC sampling in blocking mode (used for internal channel when reading analogue reference voltage, and external channel when sampling the then-discarded value)
5	<code>HAL_ADC_Start_DMA(&hadc1, (uint32_t*)storage, (uint32_t)storage_size);</code>	None	Initiating ADC sampling with the DMA controller. The number of ADC samples (20, in this design) is declared by the <code>storage_size</code> input parameter.
6	<code>HAL_ADC_PollForConversion(&hadc1, 10);</code>	None	Halting the system for 10 ms to wait for the conversion called by <code>HAL_ADC_Start(&hadc1);</code> to finish. The delay time could be changed accordingly to the sampling time.
7	<code>HAL_ADC_GetValue(&hadc1);</code>	uint32_t	Reading the raw ADC result in blocking mode. This function is called after <code>HAL_ADC_PollForConversion(..);</code>

3.2.3. Rain Gauge

3.2.3.1. Hardware design

Since the electrical parts of the rain gauge and the anemometer are essentially the same, the exact circuitry for the anemometer could be used for the rain gauge.

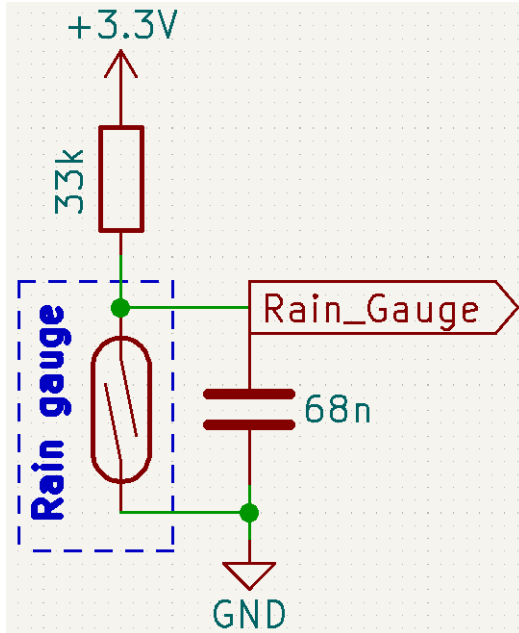


Figure 3-18. Circuitry for interfacing with the rain gauge

3.2.3.2. Software design

In terms of software, it could be considered that the rain gauge is the anemometer on a bigger scale, since the principle of monitoring rainfall via the tipping bucket is also to count the number of pulses produced over a fixed period of time, only that this period is longer. The typical duration is typically 24, 48, or 72 hours, depending on the site where the observation is done. In this project, the rainfall data is updated daily at 9:00 in the morning.

The software for the rain gauge is also interrupt-based. The setup routine for the rain gauge is called once on microcontroller's power-up.

```
// Attach an interrupt on rain gauge input pin for falling edge detection
pinMode(RainGauge_InputPin, INPUT);
attachInterrupt(digitalPinToInterrupt(RainGauge_InputPin),
               raingaugeInput_Detected,
               FALLING);
```

The interrupt service routine for the rain gauge input, namely `raingaugeInput_Detected()`, increments the local variable `count` on a falling edge event on the input pin `RainGauge_InputPin`. When the rainfall data is requested, the value of the `count` variable is stored to a temporary holder `count_temp`, then reset to 0. Since the buckets tip once per 0.3 mm of rainfall [22], the rainfall data is returned by

```
return (0.3 * count_temp);
```

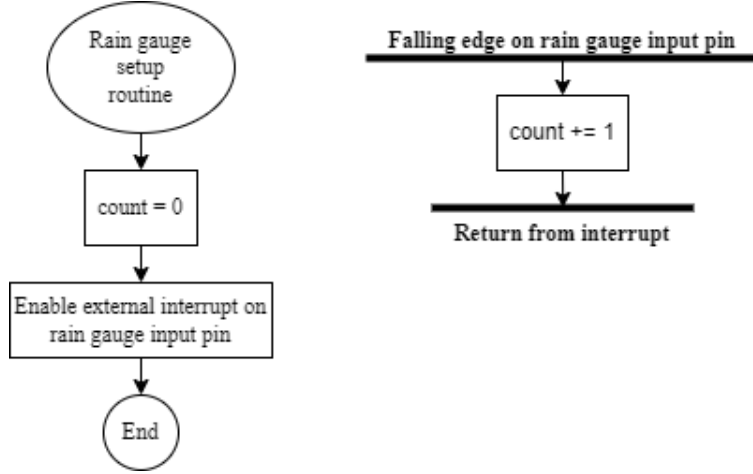


Figure 3-19. Anemometer setup routine and interrupt service routine upon input event

Unlike other sensors, the software part of the rain gauge does not respond to the 5-minute global sensor data request. Instead, the microcontroller requests for its data specifically as the time keeper announces a daily alarm at 9:00 in the morning to the microcontroller, which is later explored in Section 3.4.1.

3.2.4. BME280

3.2.4.1. Hardware design

The BME280 is designed with 2 communication interfaces, SPI and I²C, configurable via the shared 4 pins, CSB, SDI, SCK, and SDO [24]. Although the STM32F103C8T6 microcontroller has 2 SPIs, both are reserved for other modules. Moreover, while the number of slaves on each SPI bus is limited by only the number of GPIO pins as SS pins, having multiple devices on the same bus introduces higher current consumption, thus lower communication effectiveness, particularly in low-power applications. The increased power consumption issue by more slaves also exists for I²C buses, but it would be much lower since this interface addresses the slaves by software [64]. As a result, the I²C interface is utilised for BME280 in this thesis.

According to [24], the BME280 is put into I²C mode by keeping the CSB pin “HIGH” at VDDIO; while the SDO pin is pulled either “HIGH” or “LOW” by direct wirings to VDDIO or GND respectively to set the I²C address to 0x77 or 0x76. Since the Arduino library for BME280 chooses 0x76 as the default I²C address for the sensor [65], this thesis designs the hardware as such.

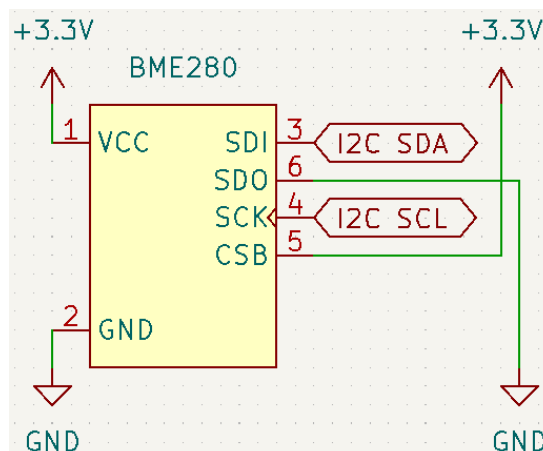


Figure 3-20. BME280 setup for the I²C protocol

3.2.4.2. Software design

On the Arduino platform, the software handling all the communications with the BME280 sensor could be built upon the “Adafruit BME280 Library”, written by Limor Fried [65] and available both on Github and via the Library Manager of the Arduino IDE.

Before the initialisation of the BME280 sensor, an instance of the class `Adafruit_BME280` must be created. Since the microcontroller communicates with the sensor via I²C, no input parameter is passed in order to call the default constructor of the class:

```
Adafruit_BME280 bme280;      // Create an instance to use libraries for BME280
```

Then, the initialisation of the sensor is done with the `begin()` method, followed by `setSampling()`. Since the Autonomous Wireless Agrometeorology Station is to be put outdoor, the suggested settings for weather monitoring by [24] is applied.

```
// Initialise the BME280 on the I2C bus with the default address  
  
bme280.begin();  
  
// Set up the BME280 for weather monitoring  
bme280.setSampling(  
    Adafruit_BME280::MODE_FORCED,           // Forced mode  
    Adafruit_BME280::SAMPLING_X1,            // Temperature sampling rate x1  
    Adafruit_BME280::SAMPLING_X1,            // Pressure sampling rate x1  
    Adafruit_BME280::SAMPLING_X1,            // Humidity sampling rate x1  
    Adafruit_BME280::FILTER_OFF);           // IIR filter is turned off  
);
```

Following the anemometer, the BME280 is expected to return the latest readings when there is a global request every 5 minutes. This duration is of no problem since [24] specifies that the weather monitoring mode has the data rate of 1/60 Hz, which means the minimum duration between 2 data sampling by the BME280 is 1 minute. When a request is issued, the microcontroller forces the BME280 sensor to sample the environment parameters, and pulls back the results instantly as soon as the sensor responds with the availability of the readings.

```
// Issue a data conversion to sensor in forced mode  
bme280_instance->takeForcedMeasurement();  
  
// Fetch the latest sensor readings  
temperature = bme280.readTemperature();          // Read temperature in °C  
pressure   = bme280.readPressure() / 100.0F;       // Read pressure data in hPa  
humidity   = bme280.readHumidity();                // Read humidity data in %RH
```

3.2.5. DS18B20

3.2.5.1. Hardware design

In Section 2.2.5, it is shown that a DS18B20 could operate in 2 modes: parasite and local power modes. Due to potential issues caused by software timing and/or electrical delays [6], in this thesis, the implemented DS18B20 temperature sensor shall be powered with an external supply.

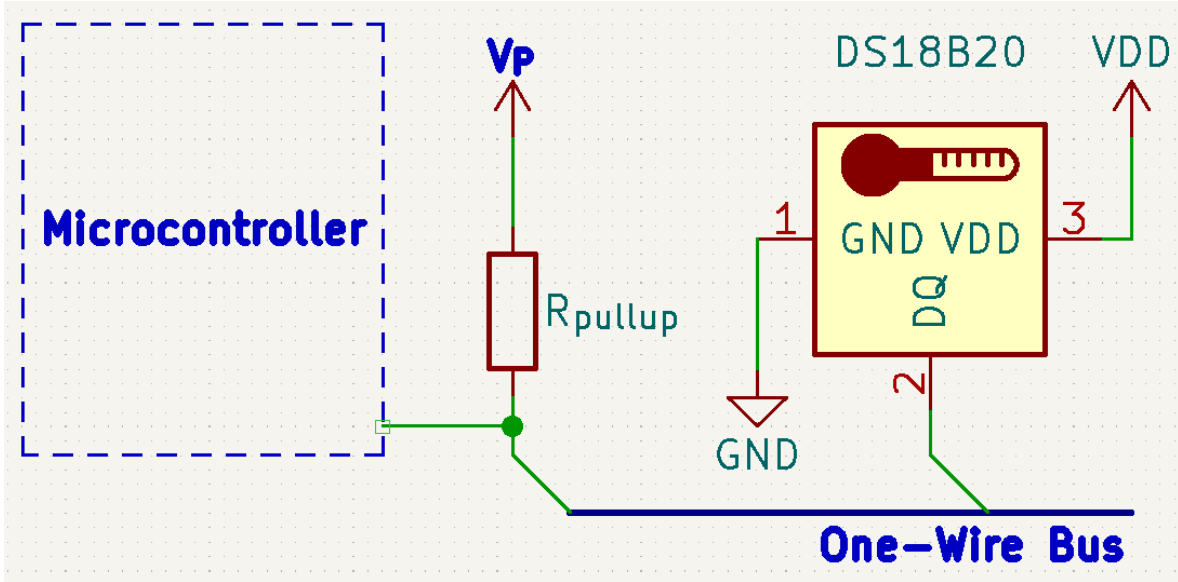


Figure 3-21. The concept of a DS18B20 powered via an external power supply V_p

Given that the DS18B20 communicates via 1-wire protocol, [66] provides the formula to calculate the available current on the bus as

$$I_{avail} = \frac{V_{pullup} - V_{pullup_min}}{R_{pullup}}$$

thus the value for the pull-up resistor for the 1-wire bus

$$R_{pullup} = \frac{V_{pullup} - V_{pullup_min}}{I_{avail}}$$

Since the DS18B20 is externally powered, the active current I_D is provided directly in the V_{dd} pin, which leaves the “extra power demand” dependent on the input current of the data pin DQ [66]. Maxim Integrated specifies the DQ input current I_{DQ} to be typically $5\mu A$, and the minimum pullup supply voltage to be $3V$ [27]. The power supply for the DS18B20 is also the $3.3-V$ supply for the station, which yields the pull-up resistor to be

$$R_{pullup} = \frac{V_{pullup} - V_{pullup_min}}{I_{avail}} = \frac{3.3V - 3V}{5\mu A} = 60k\Omega$$

It is worth noticing that the given DQ input current is the necessary amount for data exchange to be successful, so it could go higher than $5\mu A$ but not lower. As a result, the calculated $60-k\Omega$ pullup resistor is the maximum value to achieve 1-wire communication between the microcontroller and the DS18B20 temperature sensor. Since there shall be no other 1-wire devices included in this design, and the active current I_D does not contributes in local power mode, the suggested value of $4.7 k\Omega$ for the pullup resistor could be used freely, thus implemented in the design for the Autonomous Wireless Meteorology Station.

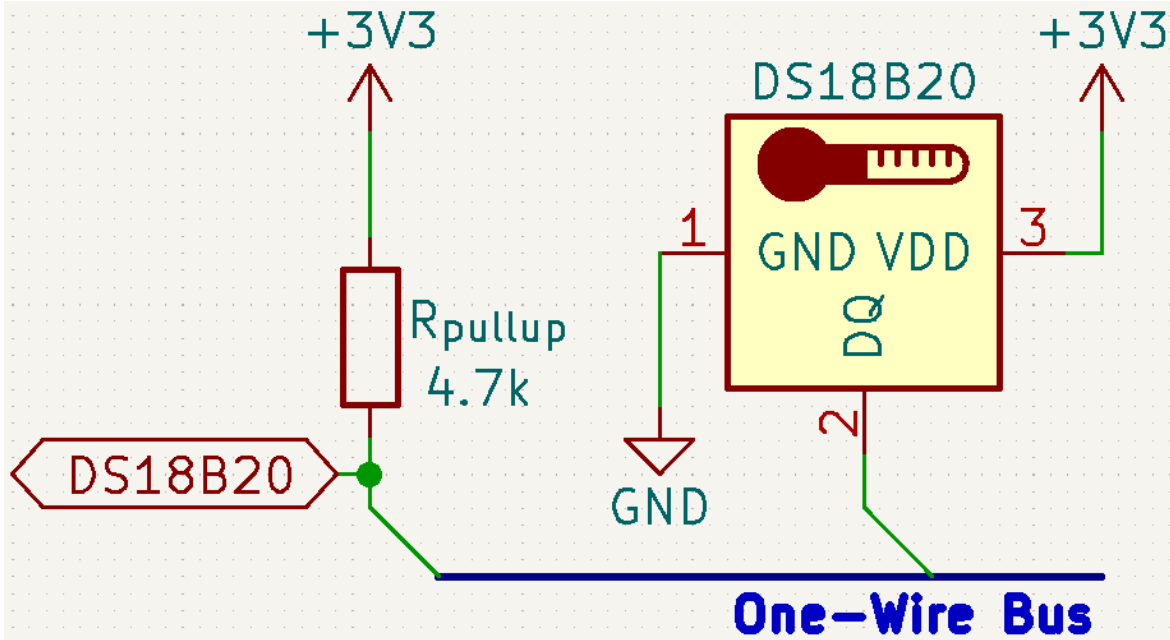


Figure 3-22. Final circuitry for interfacing the DS18B20 with the microcontroller

3.2.5.2. Software design

There exists multiple Arduino libraries for the DS18B20 sensor, yet this design only uses the “OneWire” library by Paul Stoffregen to handle the 1-wire bus in general. Although it is relatively simple to construct from scratch the firmware for the 1-wire protocol, which is not a built-in of the Arduino platform, a library helps avoid excessive coding.

Like the BME280, the DS18B20 only needs to read the temperature and return its latest data when there is a global request. The software piece contains 2 hard-coded operation procedures as depicted in Figure 3-23. The setup routine is called once on power-up, while the reading routine is in response to the global sensor data requests. Both routines start with a declaration of a `OneWire` instance, which is done with a pre-defined GPIO pin `DS18B20_InputPin` as the physical pin of the 1-wire bus.

```
// Declare a OneWire instance on the bus DS18B20_InputPin
OneWire ds(DS18B20_InputPin);
```

Since one of the requirements for the Autonomous Wireless Agrometeorology Station is the temperature at ground level with a resolution of 0.04 °C, the only thermometer setting that could give the closest values is the 12-bit resolution for 0.0625 °C [27]. Therefore, in the setup routine, there is a byte of 0x7F sent to the DS18B20 by the microcontroller.

In the reading routine, there is no software delay since the microcontroller actively reads 1 bit in a `while (..)` loop from the sensor after issuing the “Convert T” command. The microcontroller reads 2 bytes from the DS18B20 device to a 2-element byte array `data[2]`. This is because, out of the 9 bytes of the scratchpad, only the first 2 bytes contain the raw temperature data, all 16 bits of which are used to calculate the temperature in degree Celsius because of the 12-bit thermometer resolution [27]. The temperature is then obtained and returned as response to the global request by

```
// Obtain the 16-bit raw temperature data
int16_t raw = (data[1] << 8) + data[0];

// Convert from 2's complement to floating-point value
float temperature = (float)raw / 16.0;
```

```
// Return the temperature as response to global request
return temperature;
```

Throughout the procedures of setup and reading routines, the following methods of the `OneWire` class are used:

Table 3-5. Methods of the `OneWire` class used in the software for DS18B20

Method	Example of use	Function
<code>.reset()</code>	<code>byte present = ds.reset();</code>	Performs a reset on the 1-wire bus and returns the presence indicator of 1-wire device(s) on the bus.
<code>.write(command)</code>	<code>ds.write(0x44);</code>	Writes a command to the 1-wire device.
<code>.read()</code>	<code>byte data = ds.read();</code>	Reads a single byte from a 1-wire device.

Since the `.write(..)` method requires a suitable command as the input parameter, Table 3-6 dives into the ROM and function commands necessary for the software part for the DS18B20 sensor. Although [27] gives a total of 11 commands, this project utilises only 4.

Table 3-6. ROM and function commands in use for the DS18B20

Command	Value	Description
Skip ROM	0xCC	Addressing all 1-wire slaves on the bus. Since there exists only 1 device, the DS18B20, “Skip ROM” command makes it faster for data exchange.
Read scratchpad	0xBE	Requesting the content of the sensor’s scratchpad. The data is then transferred from byte 0 in the LSB order every time the master calls a read method. Since the scratchpad contains 9 bytes, the master could only call the read method up to 9 times.
Write scratchpad	0x4E	Overwriting the existing temperature alarm thresholds and thermometer resolution configurations of the DS18B20. Every time the “Write scratchpad” command is issued, the master must write exactly 3 corresponding bytes; otherwise corruption of data may occur.
Convert T	0x44	Initiating a temperature conversion by the DS18B20 sensor.

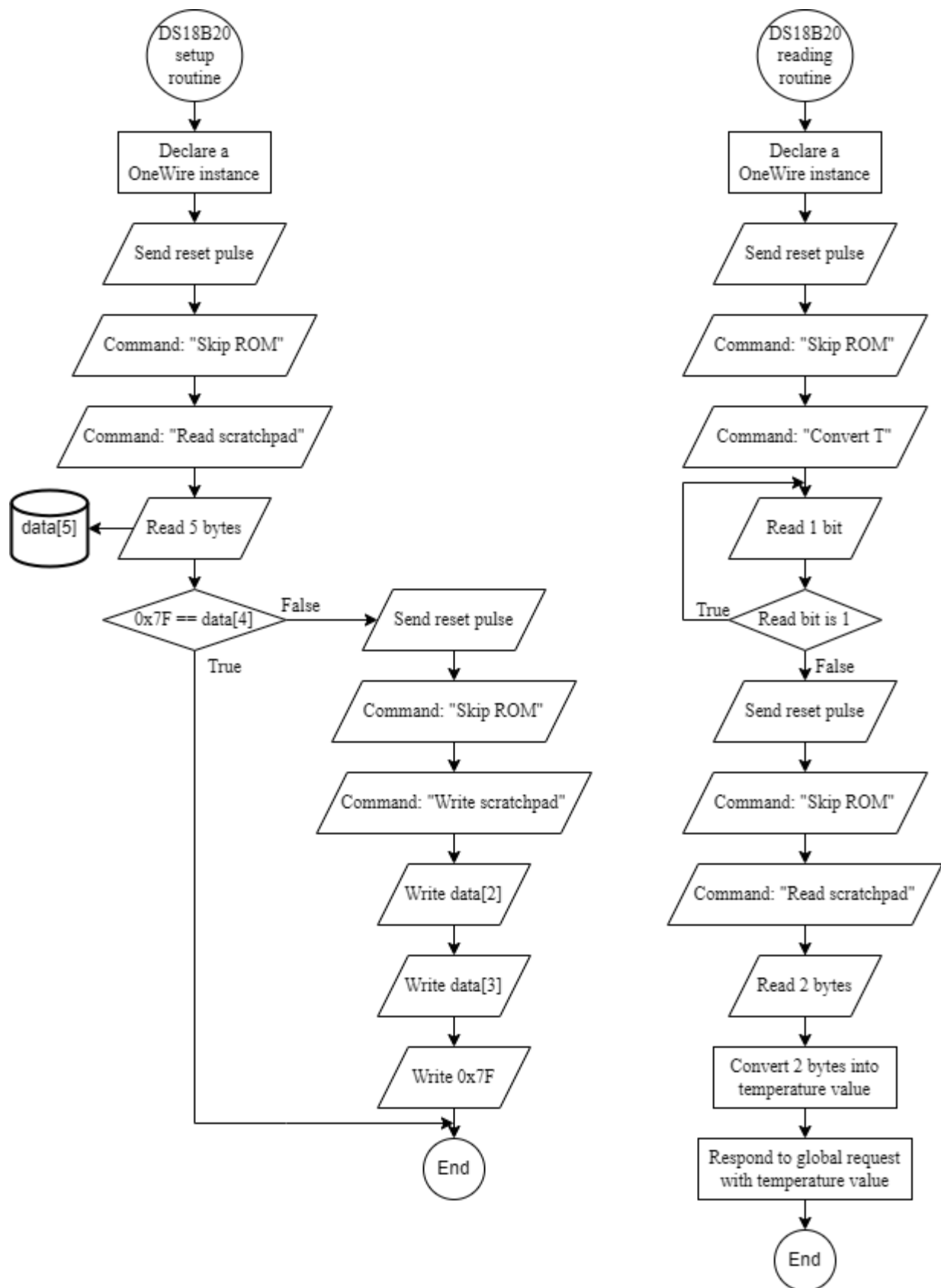


Figure 3-23. Setup and reading routines for DS18B20

3.3. SX1278

Hardware design

Since this design makes use of SX1278 pinout module, further circuitries are not necessary to establish hardware connections. In the design of the Autonomous Wireless Agrometeorology Station, all the communication and control pins of the LoRa module could be connected directly to the corresponding pins of the STM32F103C8T6 microcontroller because of the similar 3.3-V logic level. If the microcontroller and the LoRa module share a voltage regulator as power source, there may be occasions when the latter puts stress on the regulator by drawing too much current during a transmission, resulting in unexpected behaviours like sudden voltage drops and undesired resets, or even damages to other components and devices. In order to prevent such issues, a separate voltage regulator is setup for the SX1278 LoRa module.

Apart from the SPI connections, the SX1278 LoRa module requires 2 more pins from the microcontroller for interrupts and resets. The interrupt pin is controlled by the module to inform the microcontroller of incoming data communication, while the LoRa_Reset signal line is required and controlled by software.

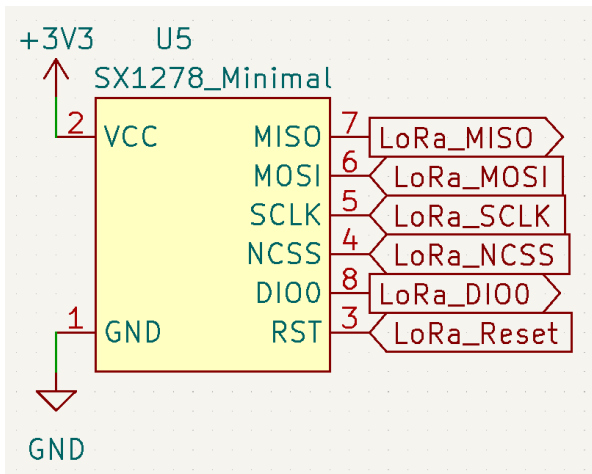


Figure 3-24. Hardware setup for SX1278 LoRa module

Software design

LoRa and LoRaWAN are 2 separate concepts. LoRa refers to the technology of wireless modulation, thus the physical layer of the LoRa Network [67]. LoRaWAN, on the other hand, is a set of protocols developed on top of the LoRa physical layer, also known as the Media Access Control (MAC) layer [67]–[69]. An SX1278 module allows a system to join a LoRa network as a node for transmission of data; however, data exchange could only be done between a node and a gateway as illustrated in [39], [69] because of the star topology by LoRaWAN [67], [70].

In this design, 2 SX1278 modules are supposed to establish communications between the sensor station and a server. Without a LoRa gateway, a such task is unachievable. However, a workaround could be done by mimicking some behaviours of a LoRa gateway at the server side by software.

The software is built on the Arduino library “arduino-LoRa” by Sandeep Mistry. At the initialisation step, the LoRa frequency band on which communication is established must be chosen. Not all the frequency bands of LoRa are available to use due to the Regional Parameters of LoRaWAN [71]. According to [72], [73], the frequency plan in Vietnam is AS923-925 (“AS2”), which ranges from

923.2 MHz to 924.8 MHz [74] and is to be avoided since permission to use is not available. [69] states that the 433 MHz frequency band could be used without a license in Vietnam, so it is put in software setup at both the server side and the sensor station.

Upon choosing the LoRa frequency, the LoRa module is ready to be used in the software design. After the **LoRa** library is included, the setup parameters for the SX1278 LoRa module is defined. The spreading factor, signal bandwidth, and coding rate are chosen to be 12, 500 kHz, and 4/8 respectively for the maximum data transfer rate. The sync word is picked randomly to be **0x92**.

```
#include <SPI.h>      // Built-in SPI library for LoRa
#include <LoRa.h>     // LoRa library handling SX1278

// LoRa setup parameters
const long frequency = 433E6;    // LoRa frequency

int spreadingFactor = 12;        // LoRa spreading factor
long signalBandwidth = 500E3;   // LoRa signal bandwidth
int codingRate4 = 8;            // Denominator for LoRa coding rate
int syncWord = 0x92;             // Sync word for LoRa communication
```

Since the LoRa module introduces some more physical connections with the microcontroller, those pins must also be defined to use used in software.

```
// LoRa module hardware dependencies
const int csPin = PB12;    // SPI NCSS for LoRa
const int resetPin = PA8;  // LoRa reset
const int irqPin = PA11;   // Interrupt by LoRa
```

It could be seen from the hardware design with the SX1278 LoRa module that the SPI2 port on the STM32F103C8T6 microcontroller is utilised for LoRa. However, the SPI2 is not defined by the STM32duino firmware [55], so it must be user-defined. Firstly, the physical pins of the SPI2 port are to be declared.

```
uint32_t SPI2_MOSI_Pin = PB15; // SPI2 MOSI pin
uint32_t SPI2_MISO_Pin = PB14; // SPI2 MISO pin
uint32_t SPI2_SCLK_Pin = PB13; // SPI2 SCLK pin
```

The **LoRa** library initiates a **LoRaClass** instance by design, so the **LoRa** name of the instance could be used directly. After the declaration of parameters and functional pins comes the software setup routine as shown in Figure 3-25. Before the initialisation of the LoRa module, the **LoRa** object must know which SPI port it is going to use and what the physical pins between the LoRa module and the microcontroller is, thus the assignments:

```
// Create an SPI object on the SPI2 pins
SPIClass* NewSPI = new SPIClass(SPI2_MOSI_Pin, SPI2_MISO_Pin, SPI2_SCLK_Pin);

// Assign the newly created SPI object to LoRa object
LoRa.setSPI(*NewSPI);

// Assign LoRa pins
LoRa.setPins(csPin, resetPin, irqPin);
```

after which comes the first attempt to initialise the physical LoRa module, where `LoRa_InitStatus` is a pre-defined variable of `int` type storing the initialisation result of the LoRa itself.

```
LoRa_InitStatus = LoRa.begin(frequency);
```

From this point, the `LoRa_InitStatus` variable is used with an `if` clause to guard the software, in case the initialisation fails. For example, within the “Initialise LoRa module at 433MHz” step, at the stage of pushing LoRa setup parameters to the LoRa module, the following operations are done with `LoRa_InitStatus` guard:

```
if (LoRa_InitStatus) {
    LoRa.setSpreadingFactor(spreadingFactor);
    LoRa.setSignalBandwidth(signalBandwidth);
    LoRa.setCodingRate4(codingRate4);
    LoRa.setSyncWord(syncWord);
} else {
    // Make another initialisation attempt
    LoRa_InitStatus = LoRa.begin(frequency);
}
```

Then, excluding the guard, the LoRa driver requires external definitions for `.onReceive()` and `.onTxDone(onTxDone)` routines by

```
LoRa.onReceive(onReceive);
LoRa.onTxDone(onTxDone);
```

where the 2 functions `onReceive()` and `onTxDone()` must be written separately at the end of the source code of the software for station:

```
void onReceive(int packetSize) {
    String rx_message = "";
    while (LoRa.available()) {
        rx_message += (char)LoRa.read();
    }
}

void onTxDone() {
    Serial.println("TxDone\n");
    LoRa_rxMode();
}
```

Since the Autonomous Wireless Agrometeorology Station is designed to only send data uplink to a server via a gateway, the `onReceive(..)` function does not handle any notifications or received messages to the main program. The `rx_message` variable is put in the software merely to help clear the LoRa buffer should any messages arrive somehow.

Although the station is only designed to send sensor data, there requires 2 additional functions to be defined, 1 to set the LoRa module in receive mode, and the other to set the LoRa module in transmit mode:

```
// Set LoRa in receive mode
void LoRa_rxMode() {
    LoRa.enableInvertIQ();           // active invert I and Q signals
```

```

    LoRa.receive();           // set receive mode
}

// Set LoRa in transmit mode
void LoRa_txMode() {
    LoRa.idle();           // set standby mode
    LoRa.disableInvertIQ(); // normal mode
}

```

Like `onReceive()` and `onTxDone()`, these 2 functions must be put at the end of the source code for the station. Since the SX1278 allows setting LoRa I and Q signals [47], the behaviours of a simple LoRa node could be mimicked, and the functions `LoRa_rxMode()` and `LoRa_txMode()` must handle the I and Q signals of the LoRa modules. For the node, the I and Q signals follows [75]:

- Transmit mode: Normal I and Q signals (`.disableInvertIQ()`)
- Receive mode: Inverted I and Q signals (`.enableInvertIQ()`)

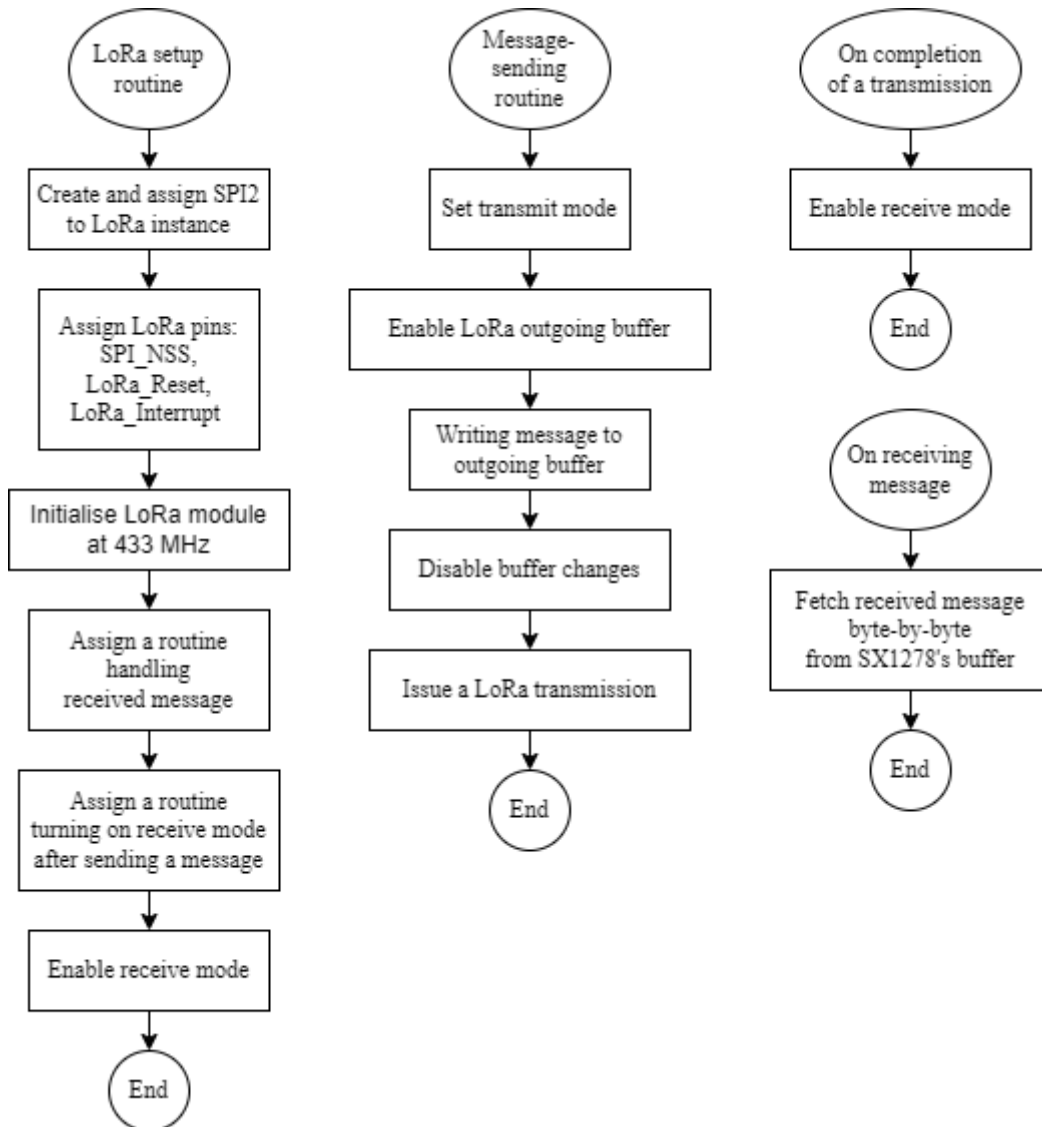


Figure 3-25. SX1278 software setup and message-handling routines

3.4. Other Modules

3.4.1. DS3231SN

3.4.1.1. Hardware design

Since the DS3231SN pinout module contains all the necessary components for the RTC IC, there is no need for further circuitries. It does not matter whether the DS3231SN is powered at 3.3 V or 5 V, since the I²C pins of the STM32F103C8T6 microcontroller are 5-V tolerant [14]. However, if the RTC module is powered at 5 V, the minimum logic “HIGH” input is $0.7 \times (5\text{ V}) = 3.5\text{ V}$, which is higher than the logic level of the microcontroller. Furthermore, sharing the I²C bus is another device with the maximum input/output voltage of 3.6 V, the BME280 sensor [24], 5-V power supply is not ideal for integrating the DS3231SN with the system. Therefore, the RTC module is to be powered at 3.3 V, and the backup battery is chosen to be a non-rechargeable CR2032. The removal of either the 1N4148 or the 200- Ω resistor is not necessary in this setup since the difference between power supply and the battery voltage $|3.3\text{ V} - 3\text{ V}| = 0.3\text{ V}$ is not enough for the diode to conduct and damage the battery.

The SQW of the RTC module is connected to an interrupt input of the microcontroller under a signal named *RTC_Alarm* to provide the microcontroller with any RTC alarm events, while the 32K pin is wired to a header to allow checking the compensated 32768-Hz clock of the RTC device.

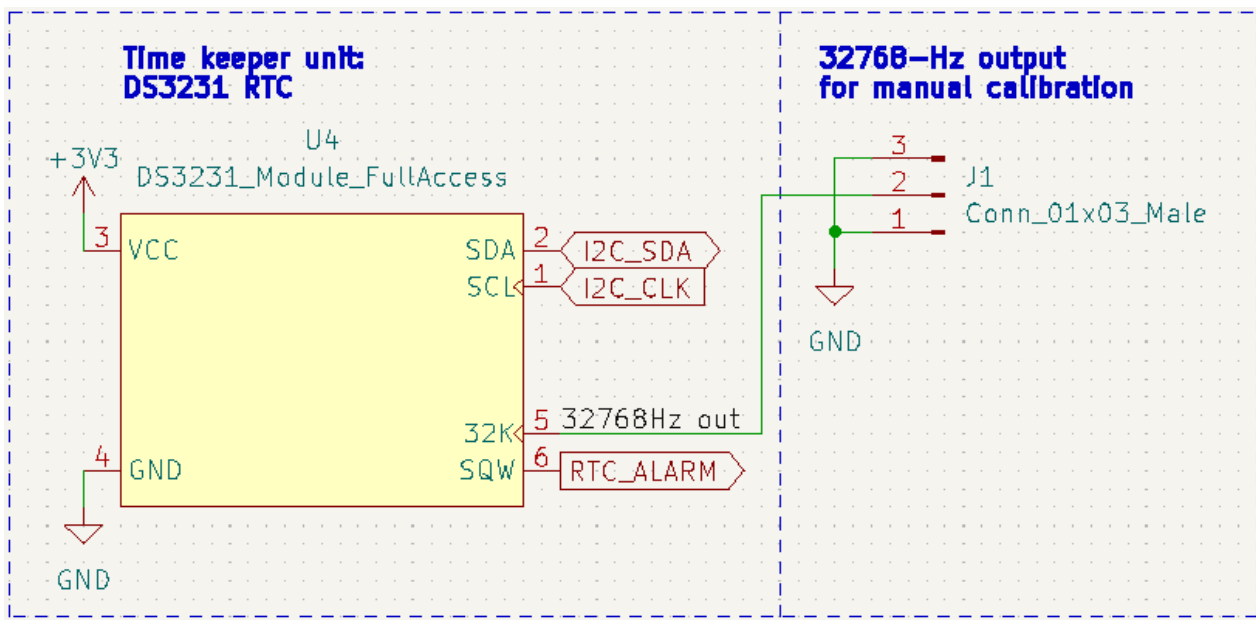


Figure 3-26. Hardware setup with the DS3231SN RTC module

3.4.1.2. Software design

On the Arduino platform, communications with the DS3231 RTC module could be handled with the “DS3231” library by Andrew Wickert. The library itself is not a built-in, but could be installed via Library Manager of the Arduino IDE.

In order to use the library, it first needs to be included in the software:

```
#include "DS3231.h"
```

The library provides 2 classes, `DS3231` to handle the settings of the DS3231 module, and `DateTime` to access date and time data. The objects for the 2 classes could be initialised before the set-up routine of the main software, or they could be temporarily called to access the RTC module. This software design follows the latter.

The first functionality of the library to be explored is setting the DS3231 up with a specific date and time. For example, if the date and time are desired to be 11 September 2023 at 9 sharp in the morning, the software calls:

```
DS3231 clock;      // Initiate a DS3231 object

clock.setClockMode(false); // Set clock mode to 24h

clock.setYear(2023);      // Set year: 2023
clock.setMonth(9);        // Set month: September
clock.setDate(11);        // Set date: 11th

clock.setHours(9);        // Set hour: 9
clock.setMinute(0);       // Set minute: 0
clock.setSecond(0);       // Set second: 0
```

After the `clock` object of the class `DS3231` is initiated, any setting method could be called to set a specific field to the DS3231 chip without the need to call all the other setting methods.

In the software design for the Autonomous Wireless Agrometeorology Station, the system is expected to issue a global sensor data request once every 5 minutes, which could be helped by the DS3231 module. The alarm 2 of the RTC is to be initialised during the setup routine on the global scale, which goes off every minute, and the microcontroller then recognise the 5-minute windows every 5 falling edges on the `RTC_Alarm` pin.

```
pinMode(RTC_Alarm, INPUT_PULLUP);

DS3231 clock;
clock.turnOffAlarm(2);
clock.setA2Time(0, 0, 0, 0x70, false, false, false); // Alarm every minute
clock.turnOnAlarm(2);
clock.checkIfAlarm(2);

// Enable interrupt from alarm 2
attachInterrupt(digitalPinToInterrupt(RTC_Alarm), Alarm_Callback, FALLING);
```

Moreover, there is a specific device, the rain gauge, that needs to return data daily at 9 in the morning. Therefore, the alarm 1 of the RTC is dedicated for this purpose.

```
DS3231 clock;
clock.turnOffAlarm(1); // Disable alarms
clock.setA1Time(1, 9, 0, 0, 0x8, false, false, false); // Set up daily
// alarm at 9am
clock.turnOnAlarm(1); // Enable alarms
clock.checkIfAlarm(1); // Make sure there are no alarms present initially
```

The previously set-up alarm 2 already initiate the interrupt function of the RTC_Alarm pin, so the function `attachInterrupt()` does not need to be called again. If the alarm settings for alarms 1 and 2 are put in the same scope, the line `DS3231 clock;` is to be omitted.

For requesting date and time data from the RTC, the procedure involves initiations of a `DS3231` object, then a `DateTime` object. Afterward, each date time field is to be read separately.

```
RTClib myRTC;
DateTime now = myRTC.now();

int dayValue = now.day();           // Day of month
int monthValue = now.month();       // Month
int yearValue = now.year();         // Year

int hourValue = now.hour();          // Hour
int minuteValue = now.minute();      // Minute
int secondValue = now.second();      // Second
```

Earlier, it is mentioned that the alarms produce falling edges as external interrupt signals on the `RTC_Alarm` pin, so an ISR must be defined at the end of the source code to handle these alarms. The custom function `Alarm_Callback` acts as the ISR which checks the alarm type from the RTC for suitable global actions, by first initiating a `DS3231` object

```
DS3231 alarm;
```

then check the alarms of the `DS3231` module one by one with `alarm.checkIfAlarm(1)` and `alarm.checkIfAlarm(2)`. These 2 lines return the conditional parameter `true` or `false`, which could be used with `if` clauses; and upon calling each line, the corresponding alarm is cleared for the `DS3231` module.

3.4.2. microSD Card

3.4.2.1. Hardware design

Since the microSD card is interfaced with the STM32F103C8T6 microcontroller via a microSD card module, no further circuitry is required apart from the direction pin connections.

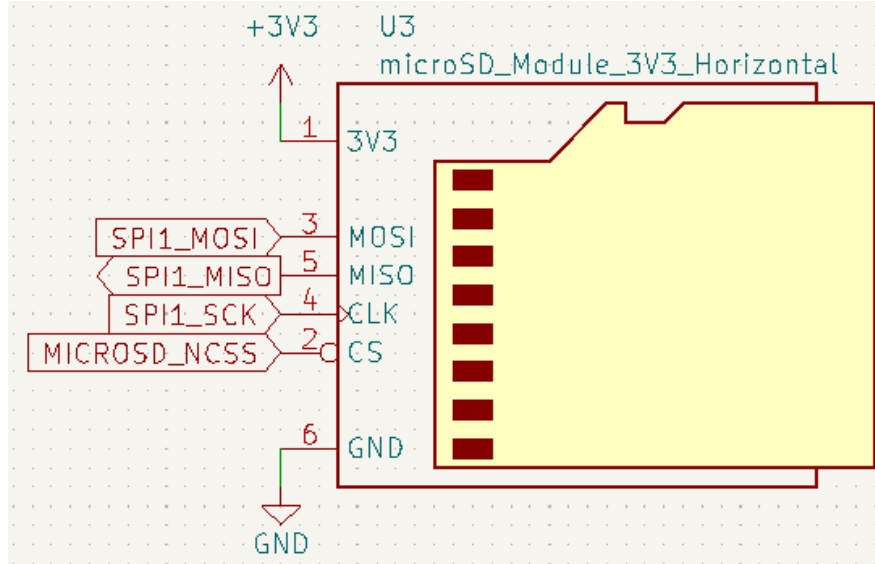


Figure 3-27. Physical pin connections of the microSD card module with the microcontroller

3.4.2.2. Software design

On the Arduino framework, there is a built-in library `SD.h` that allows accessing and managing files on any type of Secure Digital (SD) card, including microSD cards. Therefore, no external library needs installing before the software piece for the microSD card module is constructed. On the global scale, after including the library declaring the slave select pin for the micro SD card, and initialising an file-managing object, the library is ready to be used.

```
// Include the built-in SD library
#include <SD.h>

// Declare slave select pin for SPI
uint32_t CSPin = PA4;

// Initialise a file-handling object
File cardData;
```

Everytime the log file (namely `STATION_LOG.CSV`) is to receive a new data line entry, the microcontroller simply attempts to open the microSD card and write the content of entry to the designated log file `STATION_LOG.CSV`. If the file named `STATION_LOG.CSV` does not exist, the `.open(..)` method creates a file that file by default. In case the microSD card cannot be accessed, or if there is a problem with the designated file to be written, the `File` class provides a mechanism which passes the value `0` to `cardData` and prevents any further complications

```
cardData = SD.open("STATION_LOG.CSV", FILE_WRITE);
if (cardData) {
    cardData.println(entry);
    cardData.close();
} else {
    // For debugging only
    Serial.println("Error accessing microSD card.");
}
```

3.5. System Powering

As mentioned in section 2.5, this thesis leaves out the powering system for the Agrometeorology Station; instead, it receives a single power supply externally and regulates to +3.3V for the main system. The input voltage is fed through a 5.5-mm barrel jack and regulated to +3.3V by an LM317 adjustable voltage regulator as depicted in Figure 3-28. The circuitry with the LM317 is taken directly out of the device datasheet [76], with an addition of the bypass capacitors C7 and C8 to stabilise the input voltage V_{in} as well as the output +3.3V.

The +3.3V output from the LM317 is determined by the 2 resistors R7 and R8 following the output voltage formula given by the device datasheet [76]:

$$V_{out} = V_{ref} \times \left(1 + \frac{R8}{R7} \right) + I_{ADJ} \times R8$$

where $V_{ref} = 1.25V$, $I_{ADJ} = 50\mu A$ (typically), and the value for R7 is recommended to be 240Ω . With the output voltage desired to be +3.3V, the value of R8 is calculated to be 389.86Ω . The manufactured resistor that is the closest to this value is 390Ω , which yields a highly acceptable output of $V_{out} = 3.28V$. A quick test on the such circuitry later on agrees with this theoretical aspect of the voltage regulator LM317, with little observed ripples on the output (Figure 3-29).

The use of LM317, however, contains some limitations. The most notable one for this design is the condition by which the LM317 maintains the regulation. Although the datasheet [76] specifies the line regulation to be $\Delta V_{out} = V_{in} - V_{out} \in [3V, 40V]$, which means $V_{in} \in [6.3V, 37V]$ in this design, it is found that the lower limit for the input voltage V_{in} only needs to be about +5.45V to maintain the adjustment pin current and the reference voltage at the ADJ pin for the desired +3.3V output.

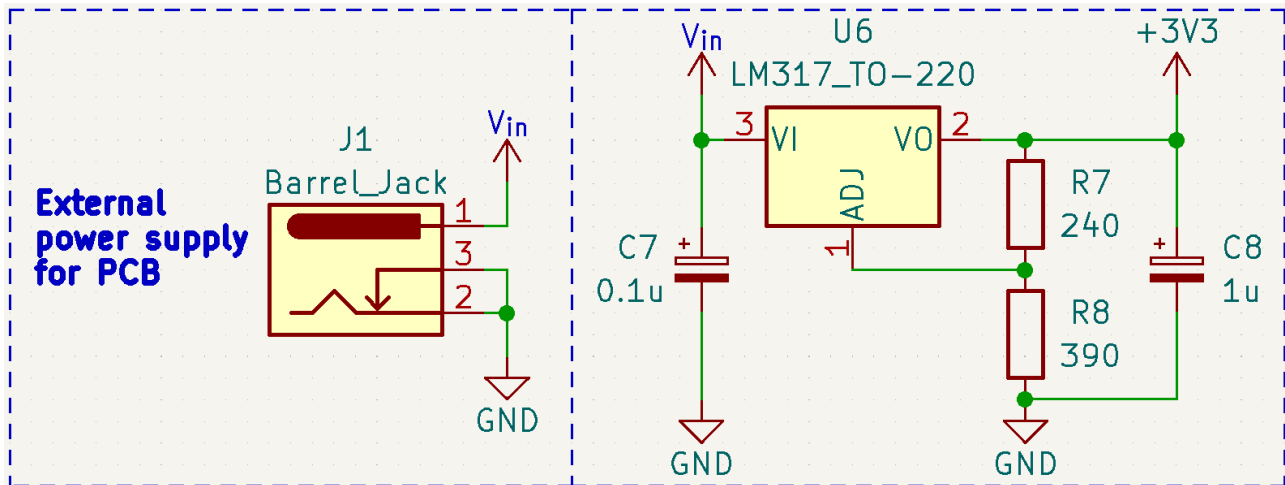


Figure 3-28. Power supply input for the station and the voltage regulating unit

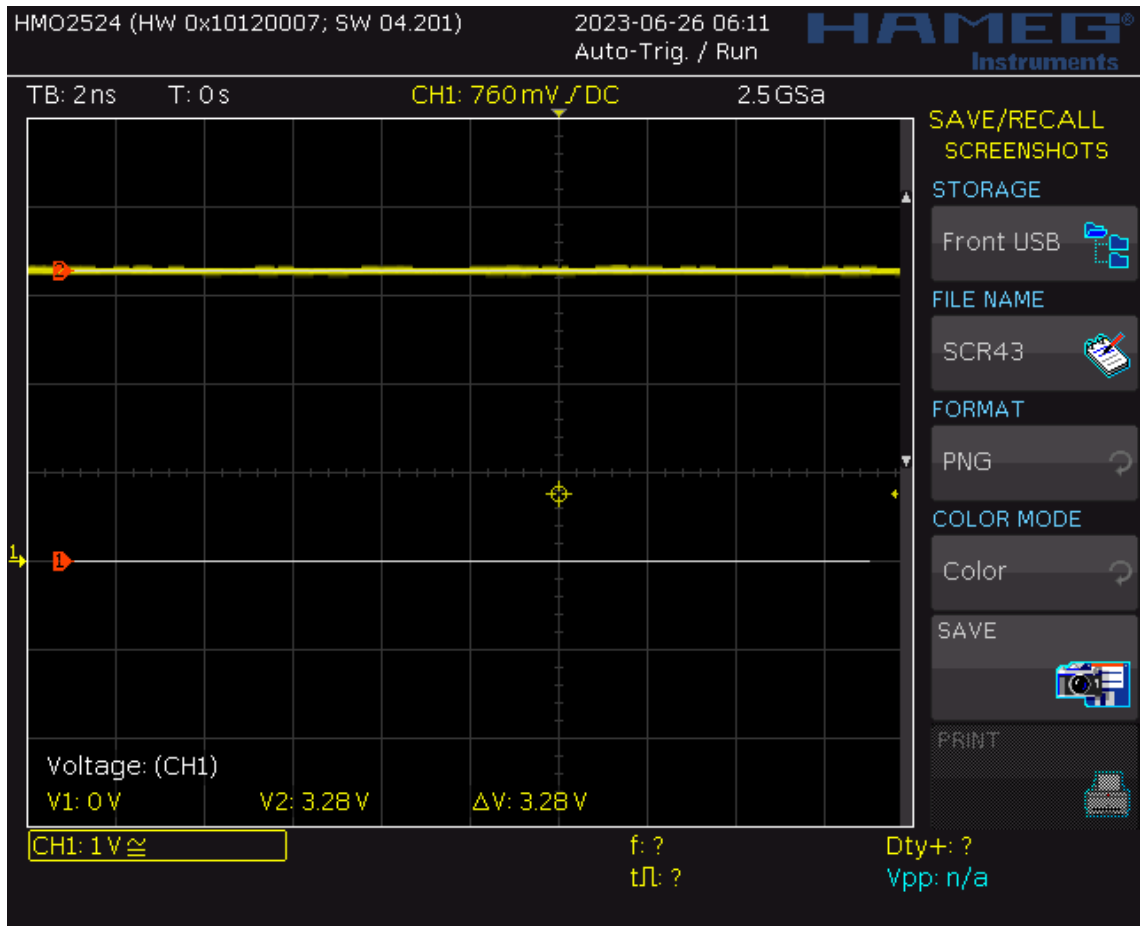


Figure 3-29. Observed output of the LM317 circuitry in Figure 3-28 with $V_{in} = +8.4V$

3.6. Gateway and Server

Hardware design

As mentioned in Section 2.6, a LoRa gateway is built upon a nodeMCU to push the read sensor data to an online database, ThingSpeak. In this project, there is no indepth hardware design for the gateway since it does not contain multiple parts other than the nodeMCU ESP8266 and a LoRa module SX1278. Since it is expected to positioned indoor near a Wi-Fi source, the gateway is to be powered by a 9-V wall adapter. The nodeMCU ESP8266 has an on-board voltage regulator for 3.3V, so the 9-V supply is fed directly to its V_{in} pin. The LoRa module, on the other hand, is powered via an LM317 circuit demonstrated in Section 3.5 for the station. The physical connections are depicted in Figure 3-30. There have been attempts to try switching the LoRa_RST and LoRa_DIO0 pins to D3 and D4 pins on the nodeMCU, but these physical pins take part in the boot process of the ESP8266 microcontroller [77] and could not work on any test for LoRa.

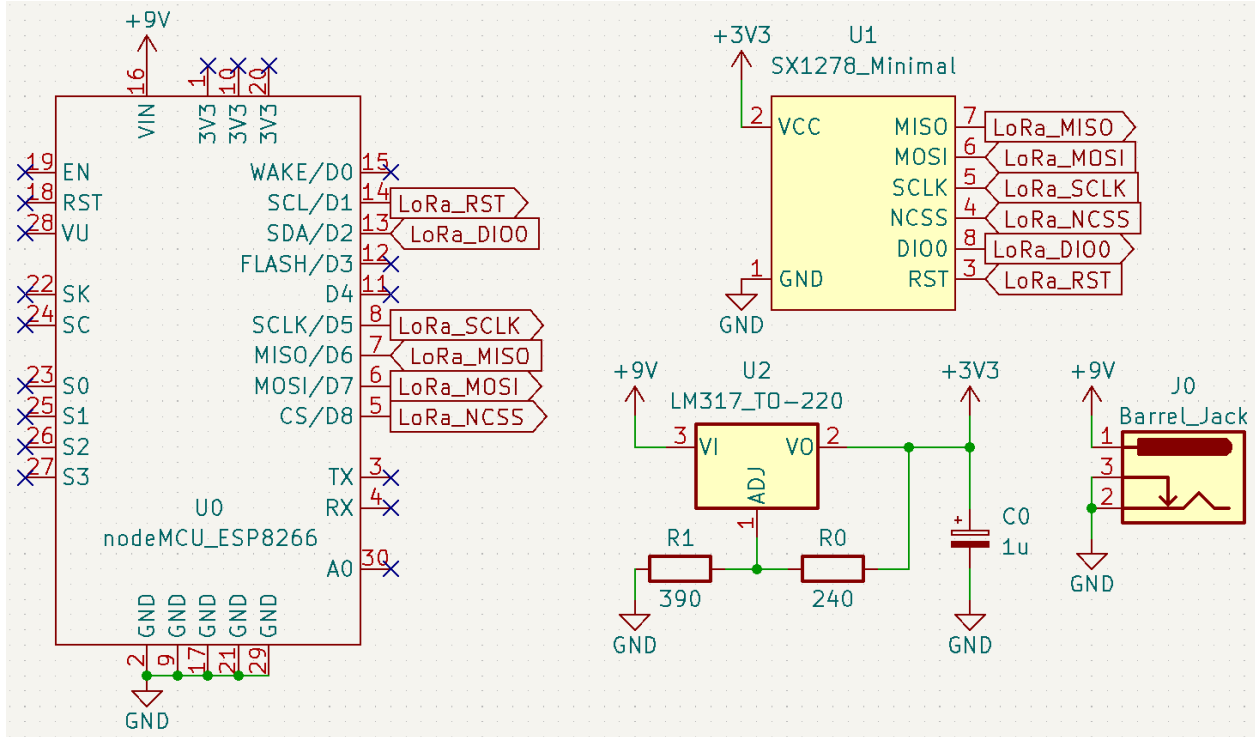


Figure 3-30. Hardware setup for the gateway

Software design

Like the Autonomous Wireless Agrometeorology Station, the software for the gateway is developed on the Arduino platform. Although the ESP8266 is not an officially supported microcontroller, the board definitions could be added by appending the following to the Additional Boards Manager URLs in the Arduino IDE, then installing “esp8266” by ESP8266 Community from Boards Manager [78]:

https://arduino.esp8266.com/stable/package_esp8266com_index.json

On the Arduino IDE, after the board is chosen to be “NodeMCU 1.0 (ESP-12E Module)” (due to the “ESP8266MOD” marking and the built-in LED as shown in Figure 2-19), the rest of the tool settings are left at default. The software for the ESP8266 as the gateway is then constructed upon the [ESP8266WiFi](#) library, which is shipped with the board definitions and firmware of the ESP8266 microcontroller line, and the [ThingSpeak](#) library, which could be found in the Library Manager as “ThingSpeak” by MathWorks. The [LoRa](#) library, which is installed to be used for the software of the station (node), is then imported for the gateway’s software as well.

```
#include <ESP8266WiFi.h> // Wi-Fi connection handling library
#include "ThingSpeak.h" // Library providing APIs for ThingSpeak access

#include <SPI.h> // Built-in SPI library, used for LoRa
#include <LoRa.h> // LoRa library handling SX1278
```

After the library come the setup parameters. The Wi-Fi network credentials must match the Wi-Fi router’s in order for the ESP8266 microcontroller to establish a connection. The `channelNumber` and `writeAPIKey` parameters could be found directly on the “API Keys” tab of the ThingSpeak channel for the project as “Channel ID” and on the “Key” box under “Write API Key” header respectively (Figure 3-31). The hardware dependencies for LoRa module are just the necessary physical pins declaration accordingly to the hardware setup (Figure 3-30). The LoRa setup parameters are initiated

accordingly to the node's; a side note to which is that only the frequency and syncWord need to match the node's counterparts.

```
// Wi-Fi network credentials
const char* ssid = "Station - test network";      // SSID
const char* password = "testnetwork";                // Password

// ThingSpeak - Channel feed access parameters
unsigned long channelNumber = 2103173;
const char* writeAPIKey = "TKJB5M4KKRH868E4";

// LoRa module hardware dependencies
const int csPin = D8;          // SPI NCSS pin for LoRa
const int resetPin = D1;        // LoRa reset
const int irqPin = D2;          // Interrupt by LoRa

// LoRa setup parameters
const long frequency = 433E6;    // LoRa frequency

int spreadingFactor = 12;        // LoRa spreading factor
long signalBandwidth = 500E3;    // LoRa signal bandwidth
int codingRate4 = 8;             // Denominator for LoRa coding rate
int syncWord = 0x92;              // Sync word for LoRa communication
```

Finally, in the software preparation, a WiFiClient instance must be declared for the WiFi object of [ESP8266WiFi](#) to initialise the Wi-Fi connection for [ThingSpeak](#) client.

```
// Initiate a WiFiClient instance
WiFiClient client;
```

Figure 3-31. ThingSpeak channel’s “API Keys” tab

The setup routine follows the flow and contains the functions shown in Figure 3-32. It could be seen that if the initialisation of the LoRa module is successful, the ESP8266 is supposed to push the LoRa settings to the SX1278 module. This could be done by calling a user-defined function containing

```
LoRa.setSpreadingFactor(spreadingFactor);
LoRa.setSignalBandwidth(signalBandwidth);
LoRa.setCodingRate4(codingRate4);
LoRa.setSyncWord(syncWord);
```

Then, the LoRa driver requires external definitions for `.onReceive()` and `.onTxDone(onTxDone)` routines by

```
LoRa.onReceive(onReceive);
LoRa.onTxDone(onTxDone);
```

where the 2 functions `onReceive()` and `onTxDone()` must be written separately at the end of the source code of the software for gateway:

```
void onReceive(int packetSize) {
    rx_message = "";

    while (LoRa.available()) {
        rx_message += (char)LoRa.read();
    }

    nodeMessageAvailable = true;
}

void onTxDone() {
```

```

    Serial.println("TxDone\n");
    LoRa_rxMode();
}

```

Within the `onReceive()` function, there is a global variable of the `bool` type, `nodeMessageAvailable`, which lets the microcontroller know when data is received from the node and perform suitable tasks in the `loop()` scope. There exists another global variable of `String` type, `rx_message`, where the message from the node is stored upon arrival and to be processed by the ESP8266 microcontroller.

Although the gateway is only designed to receive sensor data from the node, there requires 2 additional functions to be defined, 1 to set the LoRa module in receive mode, and the other to set the LoRa module in transmit mode:

```

// Set LoRa in receive mode
void LoRa_rxMode() {
    LoRa.disableInvertIQ();    // normal mode
    LoRa.receive();           // set receive mode
}

// Set LoRa in transmit mode
void LoRa_txMode() {
    LoRa.idle();              // set standby mode
    LoRa.enableInvertIQ();    // active invert I and Q signals
}

```

Like `onReceive()` and `onTxDone()`, these 2 functions must be put at the end of the source code for the gateway. As mentioned in Section 3.3, the SX1278 LoRa modules does not turn the connected microcontrollers into real LoRaWAN nodes and gateways, but mimics the behaviours as simple ones, so the functions `LoRa_rxMode()` and `LoRa_txMode()` must handle the I and Q signals of the LoRa modules. For the gateway, the I and Q signals are the opposite of those for the node:

- Transmit mode: Inverted I and Q signals (`.enableInvertIQ()`)
- Receive mode: Normal I and Q signals (`.disableInvertIQ()`)

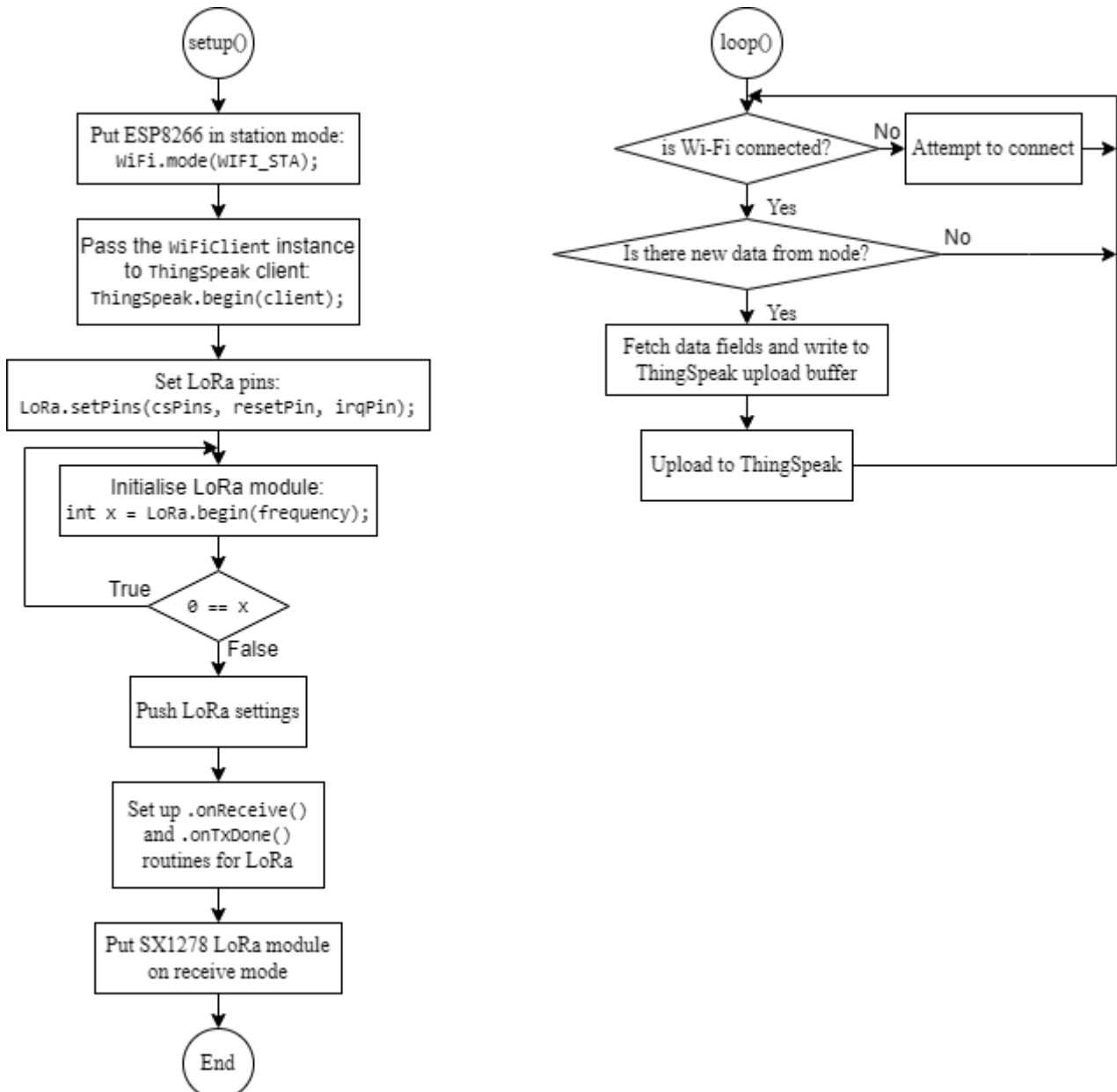


Figure 3-32. Gateway setup and loop routines

After the setup routine, the software design for the gateway of the Autonomous Wireless Agrometeorology Station puts the ESP8266 microcontroller in a loops as depicted in Figure 3-32. On each loop run, the ESP8266 microcontroller always check is its Wi-Fi connection to the router remains; if it is disconnected, the operation `WiFi.status() != WL_CONNECTED` returns `true` and it shall make attempts to reconnect to the Wi-Fi network, since data cannot be pushed to ThingSpeak server without an Internet connection:

```

while (WiFi.status() != WL_CONNECTED) {
    WiFi.begin(ssid, password);
    delay(5000);
}

```

Then, if the aforementioned variable `nodeMessageAvailable` is `true`, since the data is always transmitted as `String` via LoRa, the `nodeMessageAvailable` variable is cleared and the `String` methods are used to extract data for each field of the ThingSpeak upload buffer. A side note is that

the gateway shall always assume the node transmits data correctly if the transmission operation is successful, and the received data is a String in the format of:

YYYY-MM-DD HH:MM:SS+07,[1],[2],[3],[4],[5],[6],[7]

where

- YYYY is the year,
- MM is the month,
- DD is the day of month,
- “+07” is the timezone of Vietnam, UTC+07,
- [1] is the wind speed,
- [2] is the wind direction,
- [3] is the temperature at ground level read by the DS18B20,
- [4] is the temperature at 1 m above the ground read by the BME280,
- [5] is the barometric pressure read by the BME280,
- [6] is the relative humidity read by the BME280,
- and [7] is the rainfall data,

with “,” is the delimiter of the data fields. For example,

“2023-09-11 09:00:00+07,4.44,22.5,29.1,28.8,1001.4,75,6.604” means:

- The date is 11 September 2023 at 9 in the morning, UTC+07 time.
- The wind speed is 4.44 m/s, blowing from the 22.5° direction.
- The temperature at the ground level read by the DS18B20 sensor is 29.1 °C.
- The temperature at 1 m above the ground read by the BME280 sensor is 28.8 °C.
- The barometric pressure measured is 1001.4 hPa.
- The relative humidity is estimated to be 75 %RH.
- The rainfall amount of the previous day is 6.604 mm.

On the point of view of ThingSpeak, there are a total of 7 data fields and a timestamp. Therefore, the timestamp is to be extracted and written to the ThingSpeak upload buffer first:

```
int delimiterIndex = rx_message.indexOf(',');
ThingSpeak.setCreatedAt(rx_message.substring(0, delimiterIndex));
```

Then, a `for` loop runs 7 times to extract the entries sequentially and write to the respective buffer fields. Unlike the C++ programming language of the Arduino framework, ThingSpeak manages its database from index 1 for each entry, so the `for` loop runs with the `fieldIndex` parameter taking the initial value of 1, not 0, and the stop condition being `fieldIndex <= 7` instead of `fieldIndex < 7`.

```
for (int fieldIndex = 1; fieldIndex <= 7; fieldIndex += 1) {
    float fieldValue;

    int startPoint = delimiterIndex + 1;
    if (fieldIndex < 7) {
        delimiterIndex = rx_message.indexOf(',', startPoint);
        fieldValue = rx_message.substring(startPoint, delimiterIndex).toFloat();
    } else {
        fieldValue = rx_message.substring(startPoint).toFloat();
    }
}
```

```
    ThingSpeak.setField(fieldIndex, fieldValue);  
}
```

Finally, the upload buffer is pushed to ThingSpeak by a single line below, and the main loop routine starts over.

```
ThingSpeak.writeFields(channelNumber, writeAPIKey);
```

The **ThingSpeak** library provides the APIs with return codes, for example, a code of **int** type for the **.setField(..)** method. These return codes allow the determination of the status of each called operation for/with ThingSpeak and suitable subsequent actions to be taken if necessary on the software level. However, since the focus of this project is the sensor station, the gateway shall assume no issues further than the Wi-Fi connection availability and take no measures against failed communications with ThingSpeak. The such subject, on the other hand, does not remain overlooked and is reserved for further developments of this project.

4. Experimental Characterisation

In this thesis, there shall not be a full integration test for the Autonomous Wireless Agrometeorology Station. Instead, the sensors from the SF-WS02 kit are tested separately since the reading methodologies are merely either interrupt-based or software-controlled activation of the microcontroller's ADC module. The LoRa module has its own experiments as well for connectivity and range, while giving some insights into how integration with ThingSpeak performs. Finally, there is a test for the accuracy of BME280 and DS18B20 sensors, along with the determination if all the communication interfaces could be utilised in a single firmware for the STM32F103C8T6 microcontroller.

4.1. Anemometer

The test for the 3-cup anemometer behaviour involves an MFP107 Axial Fan Module by TecQuipment. The fan module has protective grilles at both ends of the duct, so the anemometer is set up just outside the duct to catch the exiting air whose flow is assumed to be uniform. The slide-valve is opened to 100% for maximum air flow. The fan speed is increased manually via the control panel by a step of 200 revolutions per minute; the volume metric flow rate is measured by the fan module and recorded via software once per second. For each fan speed value, the STM32F103C8T6 microcontroller counts the number of pulses from the anemometer for 20 seconds and displays on the Serial Monitor at the end of each sampling window. The mean volume metric flow rate of the fan module and the pulse count by the microcontroller are then recorded manually to a spreadsheet to be processed later.



Figure 4-1. Axial Fan Module MFP107 by TecQuipment [79]

Although the MFP107 Axial Fan Module does not monitor the air speed through the duct directly, its built-in sensors still read the volume metric flow rate, which could still be used to calculate the air

speed by dividing it by the cross-section of the duct, whose diameter is 40cm. The test run result is as follows.

Table 4-1. Anewheel of timemometer test data with the Axial Fan Module MFP107

Duct diameter	D = 40 cm		R = 9.2 cm	T = 20 s
Mean flow rate f_{mean} , (m ³ /s)	Machine wind speed V_m , (m/s)	Pulse count n	Read wind speed V_s , (m/s)	Factor = V_m/V_s
0.85	6.764085081	30	0.433539786	15.60199386
0.91	7.241549911	55	0.794822941	9.110896948
0.958	7.623521774	92	1.329522011	5.734032014
1.022	8.132817592	135	1.950929038	4.168689601
1.14	9.071831756	176	2.543433412	3.566765976
1.33	10.58380372	254	3.670636856	2.88336987
1.44	11.4591559	289	4.176433274	2.743766068
1.56	12.41408556	329	4.754486322	2.611025613
1.65	13.13028281	370	5.346990696	2.455639733
1.78	14.16478994	383	5.534857937	2.559196658
1.9	15.11971959	437	6.315229552	2.394167855
2.03	16.15422672	505	7.297919734	2.213538558
2.15	17.10915638	538	7.774813499	2.200587369

Although there appears to be a linear association between the read wind speed by the anemometer, this relationship remains inapplicable since the test is limited by the highest fan speed of the Axial Fan Module. However, the wind speed factors between the machine's and sensor's values by the read wind speed from the anemometer pose a more practical trend.

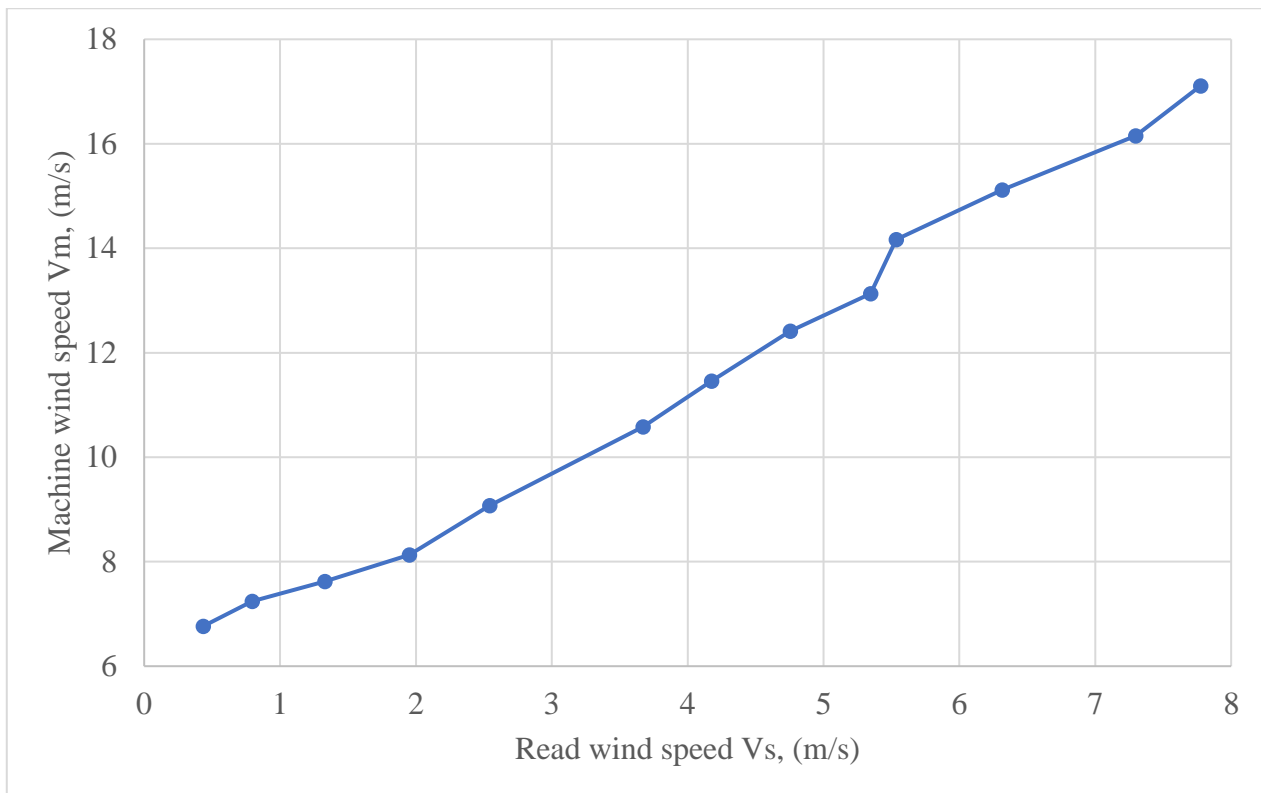


Figure 4-2. Near-linear association
between the anemometer's and the Axial Fan Module's wind speeds

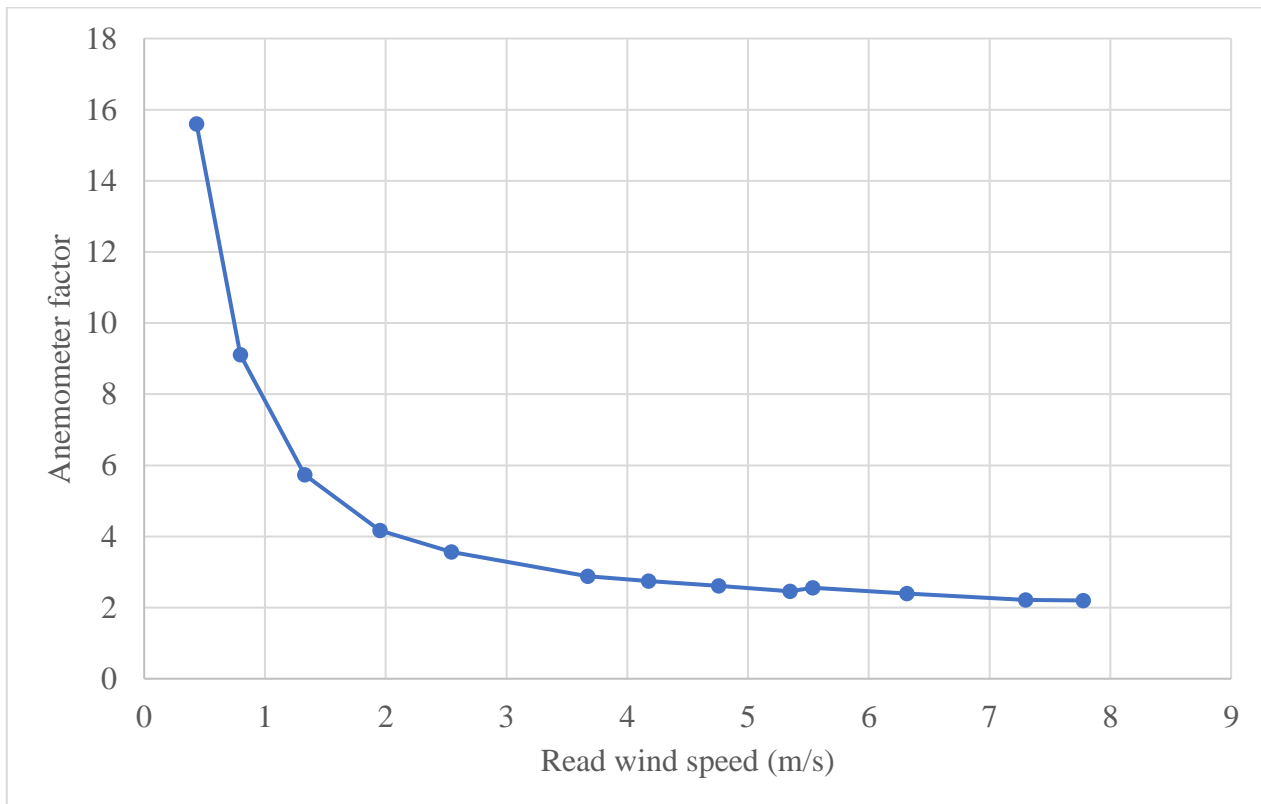


Figure 4-3. Wind speed factors by the read wind speed from the anemometer

It could be observed that at stronger wind, the wind speed factor approaches a certain value. Although the such value appears to be 2 from Figure 4-3, without the exact model based on aerodynamics, it is

uncertain how the anemometer factor really behaves. On the other hand, by the use of Curve Fitting Tool in Matlab, the mathematic model could be estimated. For the time being, the wind speed V_m by the Axial Fan Module is considered the absolute value, and the wind speed read by the anemometer V_s is derived by a factor F following $V_m = V_s \times F$, or $V_m = V_s \times f(V_s)$ if the factor $F = f(V_s)$ is considered a function of V_s .

To keep it simple, the function $F = f(V_s)$ is determined to be a rational function of the same degree on the numerator and the denominator:

$$F = f(V_s) = \sum_{i=0}^N \frac{p_i \times V_s^{N-i}}{q_i \times V_s^{N-i}}, N \geq 1$$

For $N = 1$, the Curve Fitting Tool gives

$$F = f(V_s) = \frac{1.393 \times V_s + 5.675}{V_s - 0.03219}$$

This function, however, is undesirable because it produces a negative factor F as wind speed V_s approaches 0 from $+\infty$, resulting in a negative value for speed, a non-negative quantity.

$$\lim_{V_s \rightarrow 0} F = \lim_{V_s \rightarrow 0} f(V_s) = \frac{1.393 \times 0 + 5.675}{0 - 0.03219} \approx -176.297 \Rightarrow \lim_{V_s \rightarrow 0} V_m = V_s \times \lim_{V_s \rightarrow 0} F < 0$$

For $N = 2$, the Curve Fitting Tool gives

$$F = f(V_s) = \frac{1.698 \times V_s^2 + 3.797 \times V_s + 2.632}{V_s^2 - 0.002605 \times V_s + 0.1079} \quad (3)$$

As the wind speed V_s approaches 0 from $+\infty$, the anemometer factor F remains positive, thus a valid value for the real wind speed V_m .

$$\lim_{V_s \rightarrow 0} F = \lim_{V_s \rightarrow 0} f(V_s) = \frac{1.698 \times 0^2 + 3.797 \times 0 + 2.632}{0^2 - 0.002605 \times 0 + 0.1079} \approx 24.393 \Rightarrow \lim_{V_s \rightarrow 0} V_m = V_s \times \lim_{V_s \rightarrow 0} F > 0$$

For higher values of N , the Curve Fitting result starts to show fluctuations (Figure 4-6). The such issue could be avoided by using a rational function model whose numerator degree is different from the denominator degree. However, this solution complicates the software, and potentially introduces computational errors, so the model (3) is the most suitable function for the anemometer F to fix the anemometer behaviour as shown in Table 4-1.

Last but not least, it is worth noticing that the rational function suggested as the model for the anemometer function is not absolute. [19] digs into the aerodynamics of the cup anemometer and gives a much more detailed, yet complex, model of the anemometer factor. In order to avoid complexity which is out of scope of this thesis, the only model built with the Curve Fitting Tool in Matlab is presented.

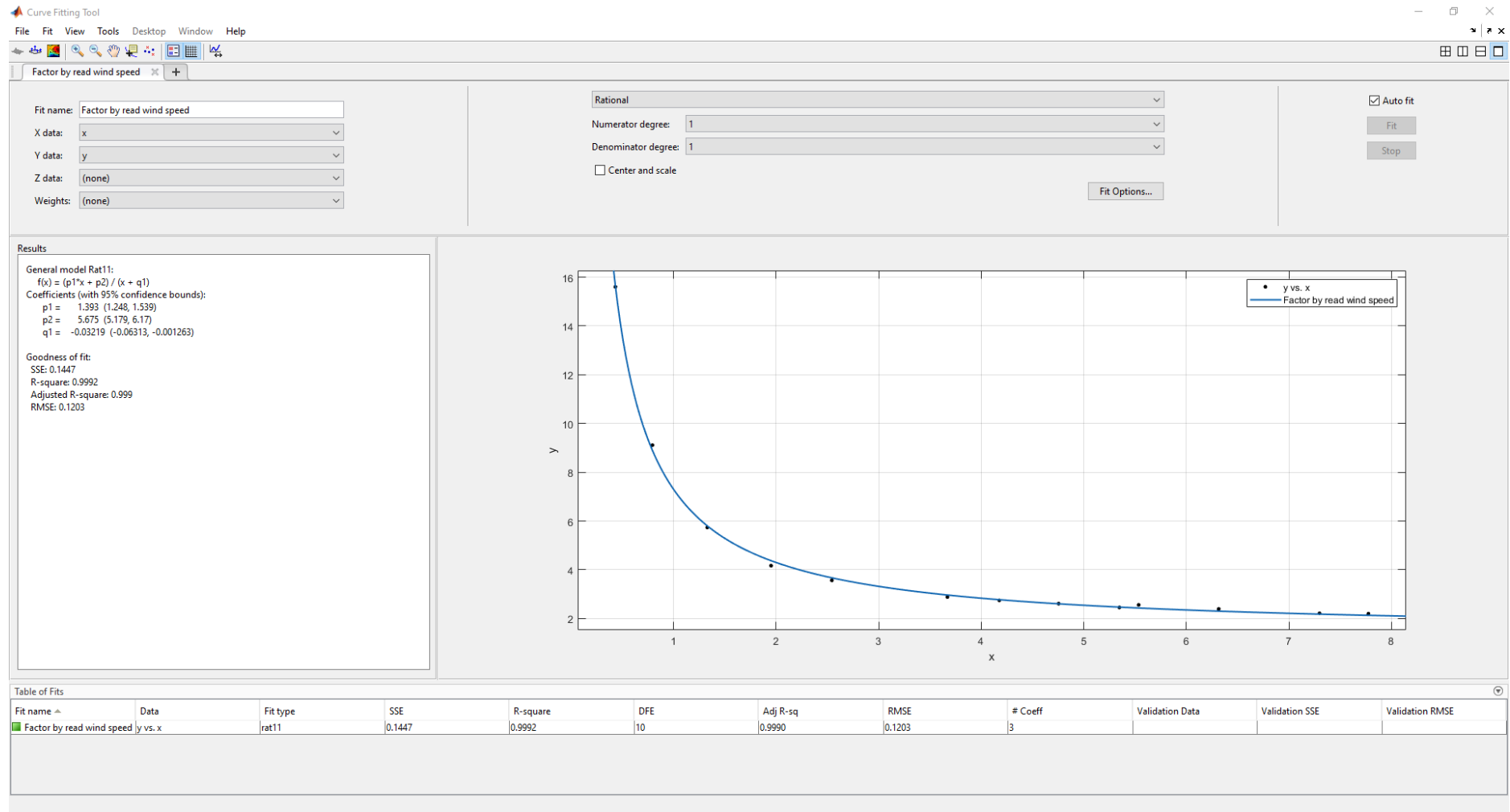


Figure 4-4. Curve Fitting result for N = 1

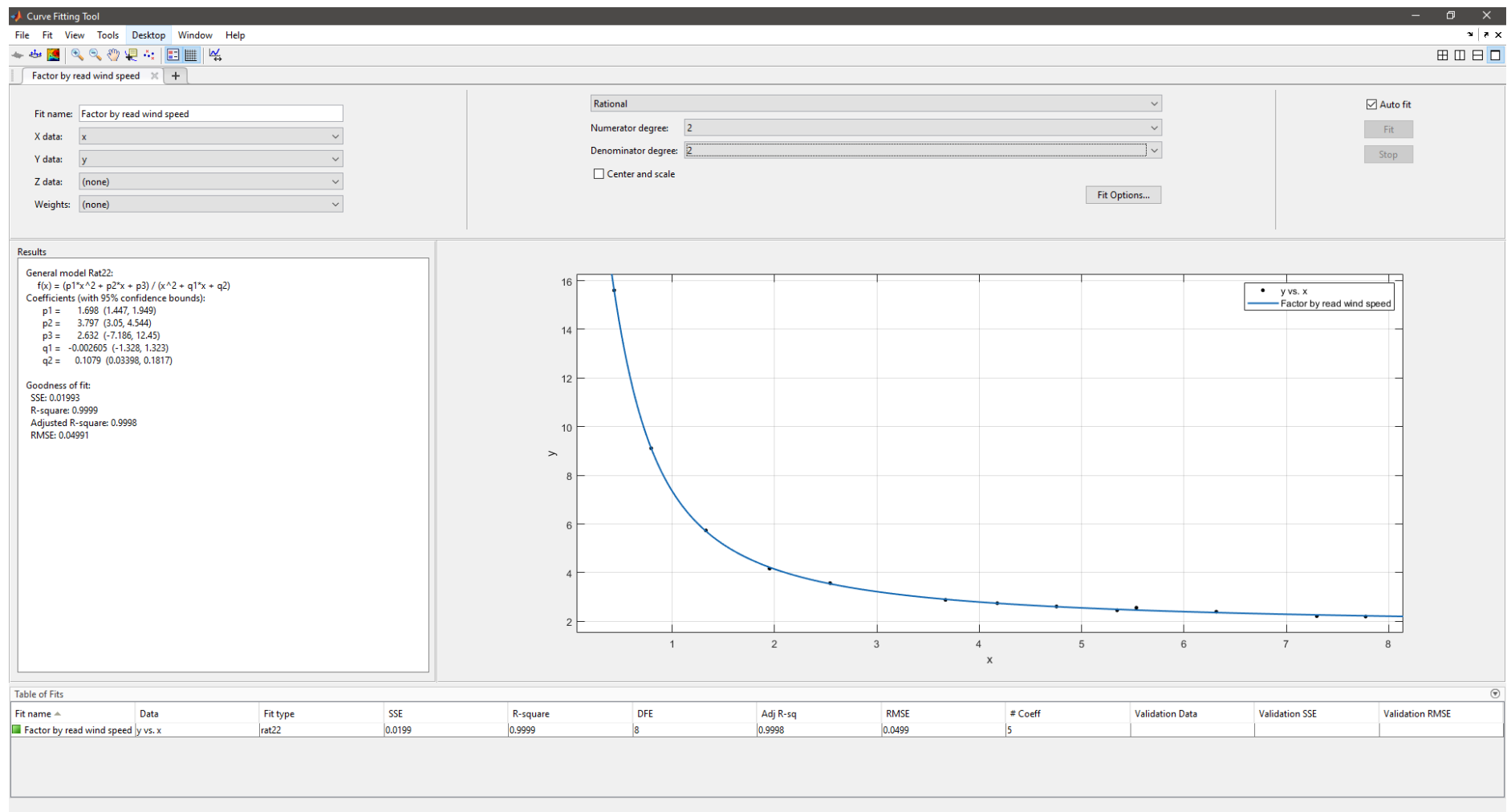


Figure 4-5. Curve Fitting result for N = 2

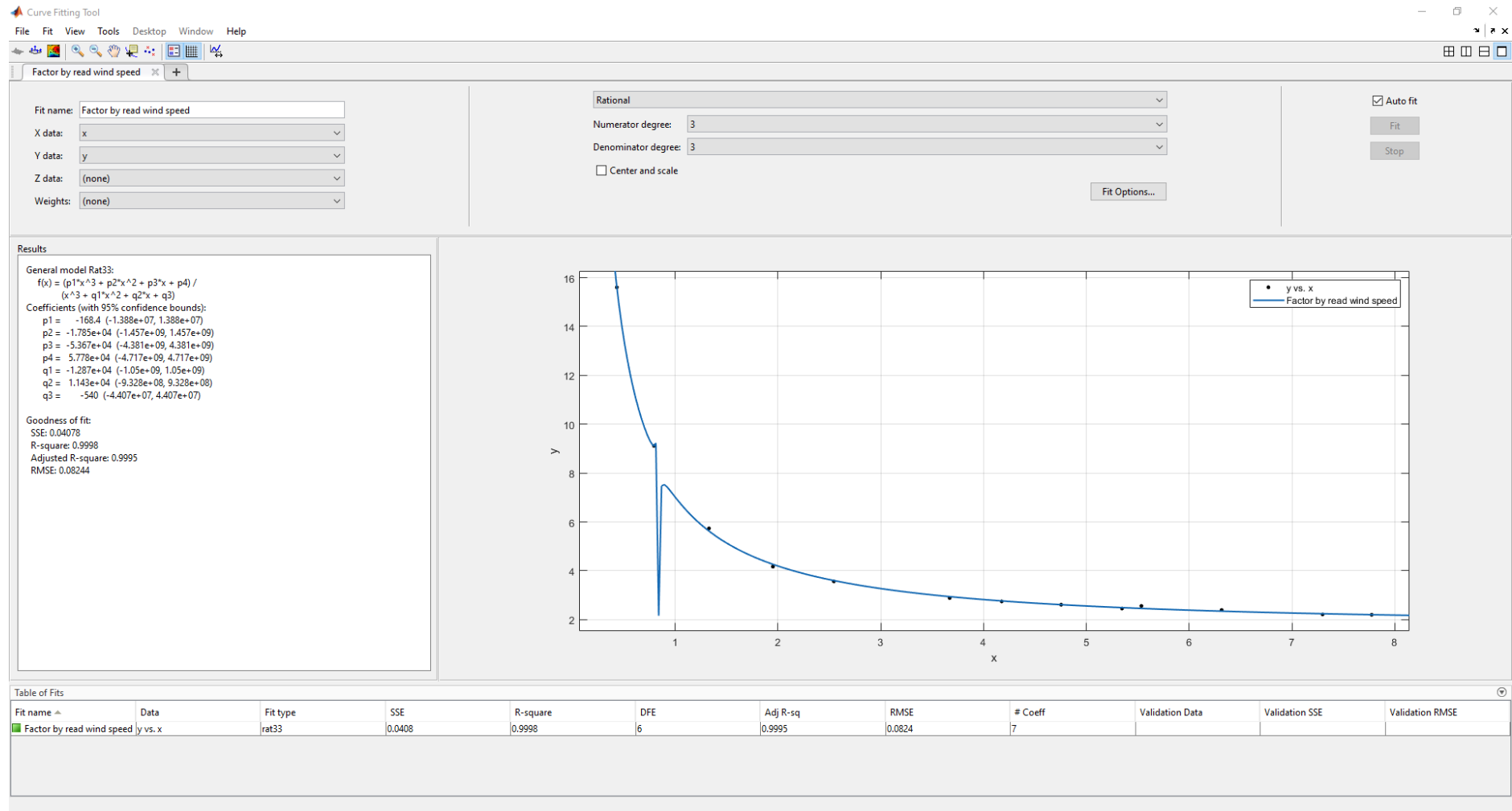


Figure 4-6. Curve Fitting result for N = 3

4.2. Wind Vane

The test for the wind vane is performed mostly on the stage of designing hardware for the microcontroller to read data from the sensor. The wind vane is first integrated with the pull-up resistor to form a voltage divider as described in Section 3.2.2.1. On each stage of the test, the sensor is held and turned manually to every of the 16 directions. Although there are only 4 directions marked on the body of the sensor, a voltmeter is put in use to determine the remaining 12 directions following the voltage outputs shown on the table of Figure 3-13. At each direction, the microcontroller samples 20 ADC values and determine the direction as described in Section 3.2.2.2. The results are written to a CSV file on a microSD card and later processed on Microsoft Excel.

Reading unfiltered signals by the voltage divider

The wind vane test starts with reading the raw signals directly from the voltage regulator. For most of the positions of the rudder blade, the STM32F103C8T6 microcontroller could determine the expected directions. However, there exists bad readings when the microcontroller tries to detect the 0°, 67.5°, 225°, and 337.5° directions, while it completely fails to read the 270°, 292.5°, and 315° directions.

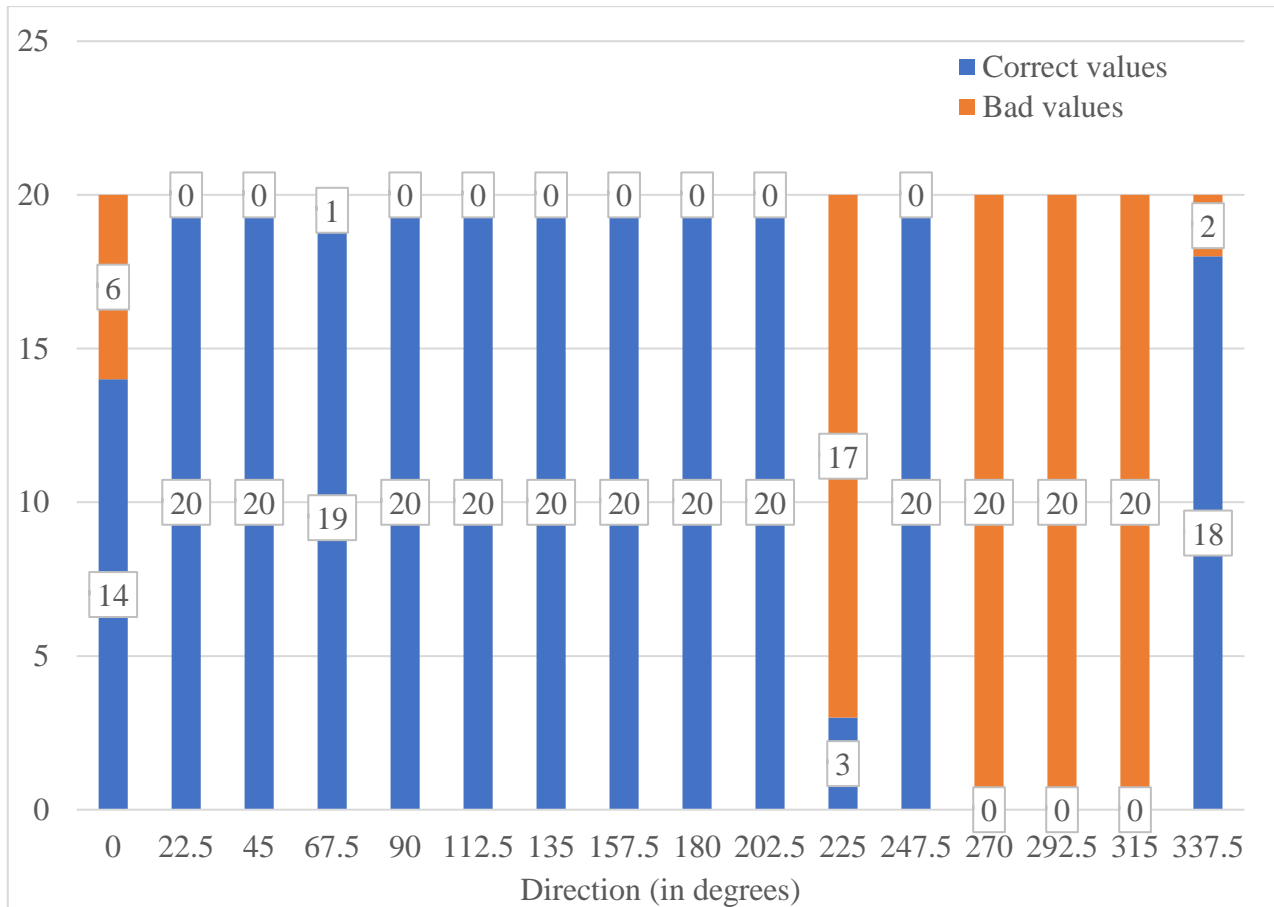


Figure 4-7. Number of correct and bad readings when sampling from the voltage divider

Reading signal outputs by the passive LPF

Upon putting a passive LPF with the cut-off frequency $f_{-3\text{dB}} = 11.587 \text{ kHz}$ between the output of the voltage divider and the ADC input of the microcontroller, the test result greatly improves when the microcontroller only produces 4 erroneous readings on the 270° direction. However, upon inspection

of the incorrect readings, it is discovered that the issue may have been caused by the computational errors of the microcontroller itself, not because of the filtered signal at the input of the ADC module. For example, there are instances (marked with * in Table 4-2) where the same raw ADC value is read (3957), the same V_{in} value is calculated (3.15 V), but the produced R_{read} values are different (95.3 k Ω and 91.9 k Ω), and in turn, the directions. Moreover, the expected R_{read} value for the 270° direction is 120 k Ω (Table 2-1), which means the input signals are too attenuated and all the calculated R_{read} values by the microcontroller are too close to the lower value, 64.9 k Ω of the 315°, to be distinguished properly. The such issue could be resolved by redefining the thresholds between 2 closest resistive values on the software level, but this solution remains open, so that the hardware level is further explored for better results.

Table 4-2. Output by the microcontroller for the 270° direction in the test with the passive LPF

Input direction: 270			
Read direction	Raw ADC	V_{in}	R_{read}
270	3955	3.15	94623.84
270	3955	3.15	93224.98
270	3955	3.15	93224.98
270	3958	3.15	93224.98
270 (*)	3957	3.15	95338.59
270	3955	3.15	94623.84
270	3953	3.15	93224.98
315 (*)	3957	3.15	91865.53
270	3953	3.15	94623.84
315	3956	3.15	91865.53
270	3953	3.15	93919.38
315	3956	3.15	91865.53
270	3953	3.15	93919.38
315	3956	3.15	91865.53
270	3954	3.15	93919.38
270	3956	3.15	92540.44
270	3957	3.15	93919.38
270	3955	3.15	94623.84
270	3956	3.15	93224.98
270	3955	3.15	93919.38

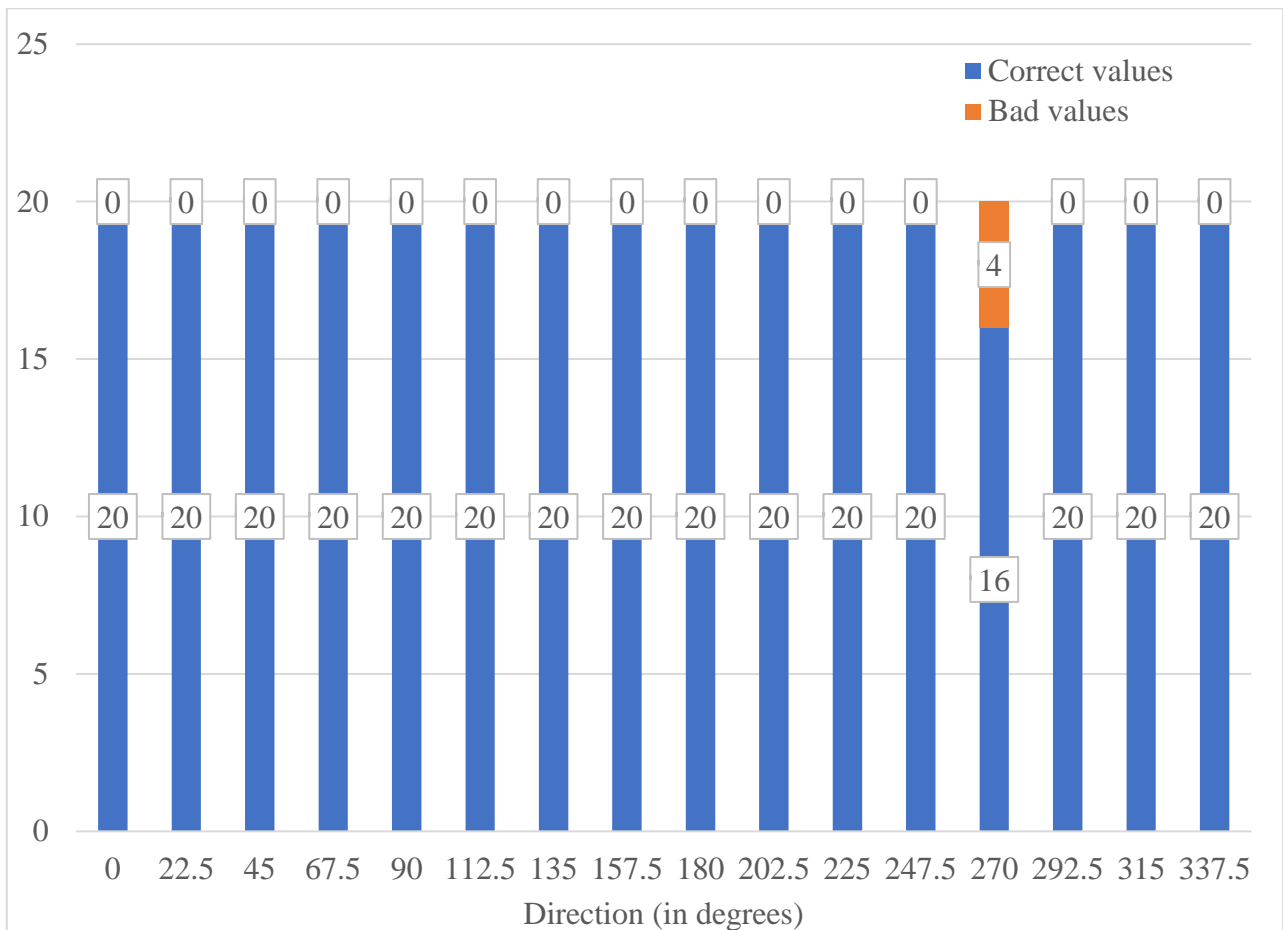


Figure 4-8. Number of correct and bad readings when sampling from the passive 11.587-kHz LPF

Reading signal outputs by an active LPF using CA3149EZ Op-Amp

Following the test stage with the passive LPF, the whole sampling process is redone after a voltage buffer is added between the LPF and the ADC input of the microcontroller, producing an active LPF with the cut-off frequency of $f_{-3\text{dB}} = 11.587 \text{ kHz}$ on this next stage. The Op-Amp in use is a CA3140EZ.

Before the CA3140EZ Op-Amp is added to the wind vane test, it is put through a separate voltage buffer test. The general idea of hardware connections is as illustrated by Figure 4-9. The signal generator in use produces a sine wave at 440 Hz with a 3.3-Vpp amplitude and 1.65-V offset for an input signal between 0 and 3.3 V. The power supply is set manually from 3.3 V, the voltage level of the main system of the Autonomous Wireless Agrometeorology Station. The goal of this mini test is to determine at which power supply VCC the Op-Amp produces the best result as a voltage buffer.

By observing the signals on an oscilloscope (Appendix B), it is determined that the CA3140EZ Op-Amp must be powered at 6 V for the main test with the wind vane. When the supply VCC is under 6V, the outputs of the CA3140EZ as a voltage buffer are either capped (from 3.3 V to 5.41 V) or overshoot (5.9 V). When the power supply reaches 6.3 V, the output waveforms starts having fluctuations. The CA3140EZ Op-Amp is then powered at 6 V and put back to the main test on the wind vane.

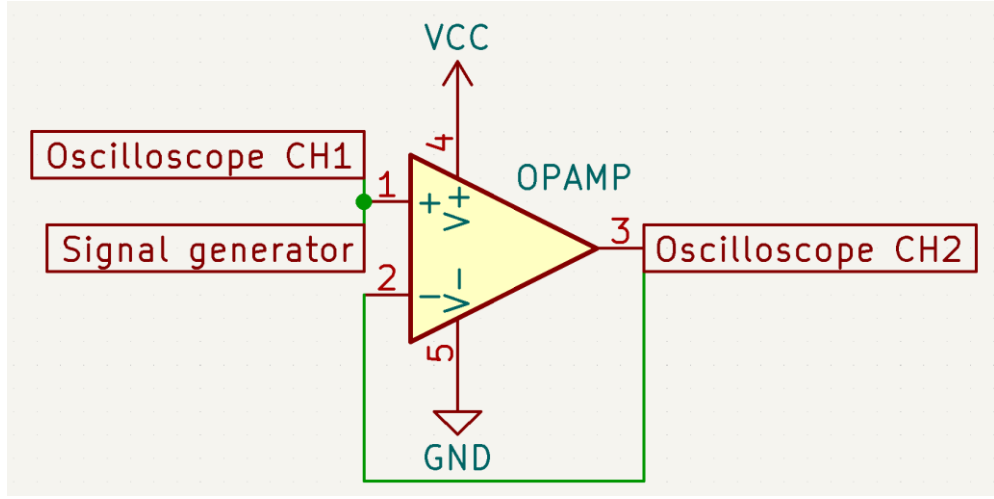


Figure 4-9. Op-Amp setup for the voltage buffer test

It could be said that the result of this test is basically the same as the previous'. The bad readings appear when the microcontroller tries to detect the 67.5° direction, and a single bad value at the 112.5° direction. The difference between the 2 tests is that when the CSV files are checked, the R_{read} values from the active LPF are higher, while the passive LPF produces R_{read} lower than given values by [20] in Table 2-1.

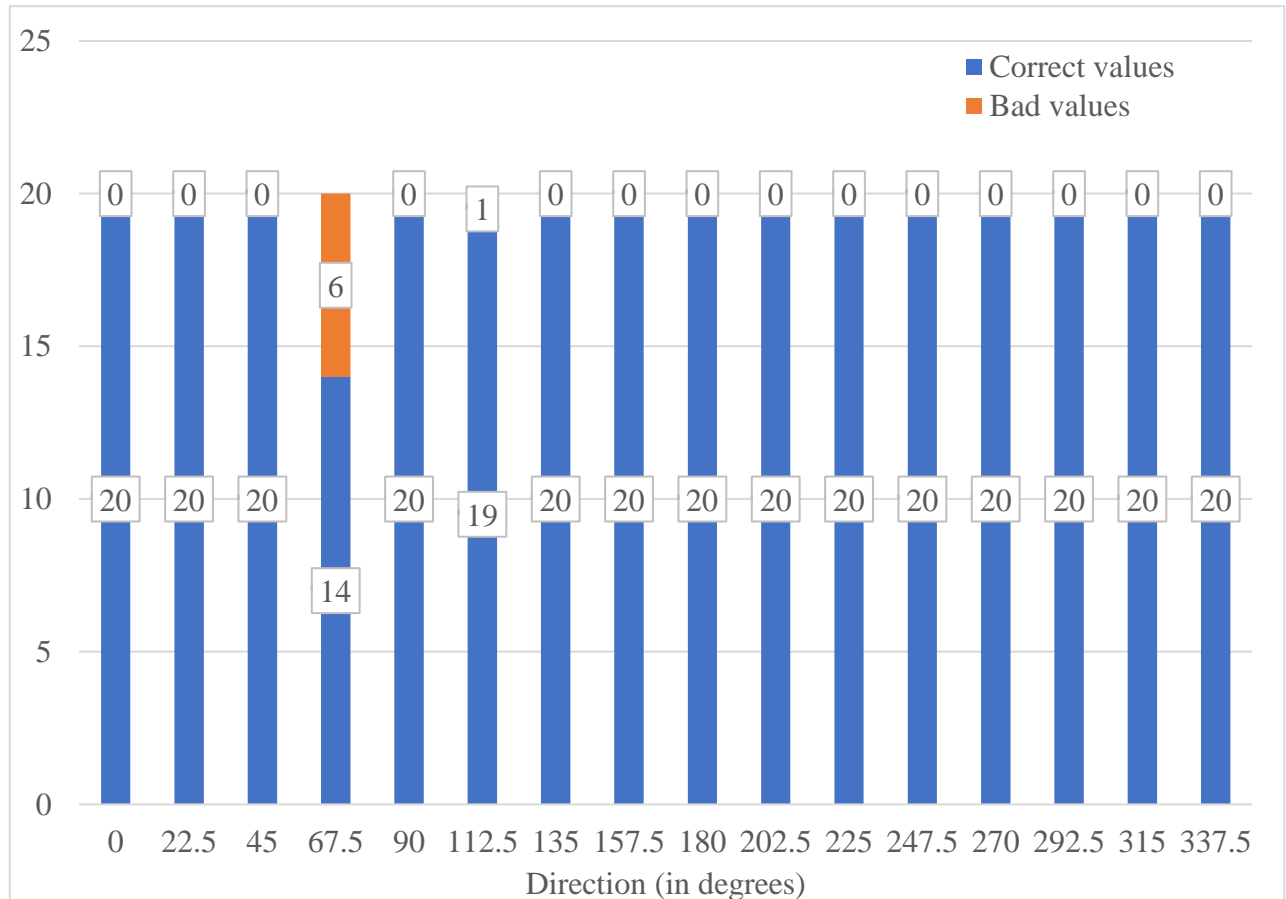


Figure 4-10. Number of correct and bad readings when sampling from an active 11.587-kHz LPF using a CA3140EZ Op-Amp

Reading signal outputs by an active LPF using MCP6002-I/P

Although the active LPF with the CA3140EZ Op-Amp produces decently clean outputs, the supply voltage of 6V for the Op-Amp is not ideal since the main system runs at 3.3V. Therefore, an alternative must be explored. The test is first conducted with the setup like Figure 4-9, but in this case, the VCC is kept at 3.3V and the Op-Amp becomes the variable.

There are a total of 5 Op-Amp options put in test due to their availability: CA3140EZ, LM358P, LM393P, MCP6002-I/P, and UA741CP. In this test, the signal generator is configured to output a triangular waveform because it rises and falls linearly. The frequency of the signal is 250 mHz, the amplitude is 3.3 V, and the offset is 1.65 V for a signal going from 0 V to 3.3 V like the previous test. The results as shown in Appendix C makes MCP6002-I/P the only valid option as the Op-Amp for the voltage buffer part of the active LPF at the 3.3-V power supply. The MCP6002-I/P is a dual Op-Amp device, but only 1 unit is put in use, and the pins of the other are left unconnected.

Upon putting the MCP6002-I/P in test for the wind vane, the result retains the bad entries issue. The 247.5° direction sees 7 bad entries out of 20, while the microcontroller returns the correct direction for only 1 out of 20 readings of the 0° one. All the tests on the wind vane up to this point shows that the STM32F103C8T6 obtains erroneous data from its ADC module, so there arises a question why this happens. Another test attempt then takes place to determine a viable solution.

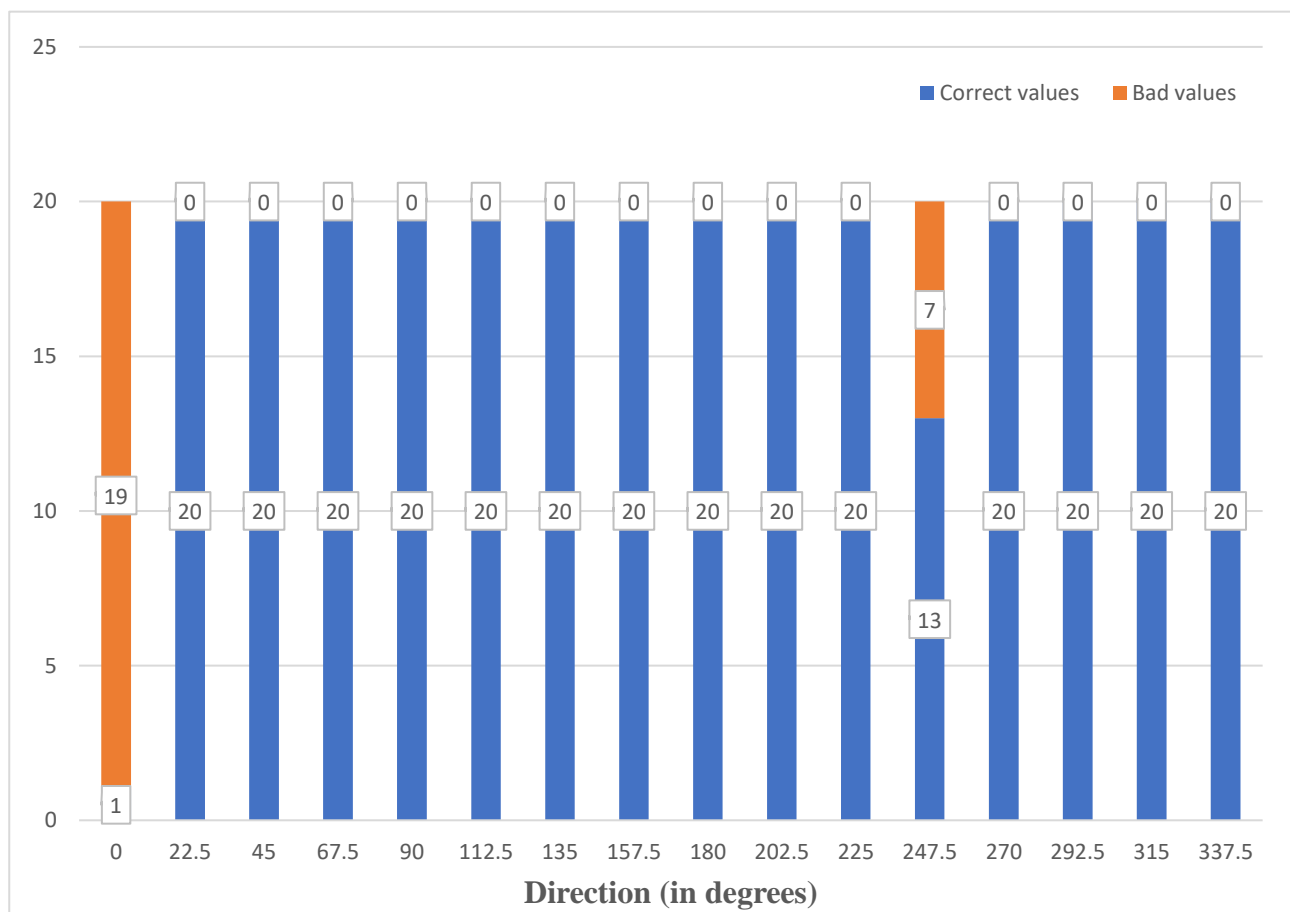


Figure 4-11. Number of correct and bad readings when sampling from an active 11.587-kHz LPF using a MCP6002-I/P Op-Amp

The addition of a pull-down resistor between the latest active LPF design and the microcontroller

On every testing stage, a voltmeter is in use to make sure that the rudder blade of the wind vane is in the correct position to produce expected voltage signals at the ADC input pin of the microcontroller. If the input is closely monitor as such, there potentially is a problem with the ADC, or the hardware design is simply incomplete despite the good separate test results. When reviewed, the CSV files containing test results on the wind vane with both active LPF designs reveal that all entries are higher than their expected values. Therefore, it is determined that all the current of the output signals from the Op-Amp flowing into the ADC input pin of the microcontroller might be the cause. As a result, a pull-down resistor is added as shown in Figure 3-15.

The process of picking a suitable resistor value starts with a 10-k Ω resistor. There is no reason for starting with this value because it is only to observe the behaviours of the microcontroller's outputs for the wind vane direction. Since the result stays the same, the value of the resistor is determined to be lowered to further decrease the current flow into the ADC module. The available resistive values in this test are respectively 8.2k Ω , 6.8k Ω , 5.6k Ω , 4.7k Ω , and 3.3k Ω . The test ends when the pull-down resistor is 3.3-k Ω , and the microcontroller reads the directions as expected.

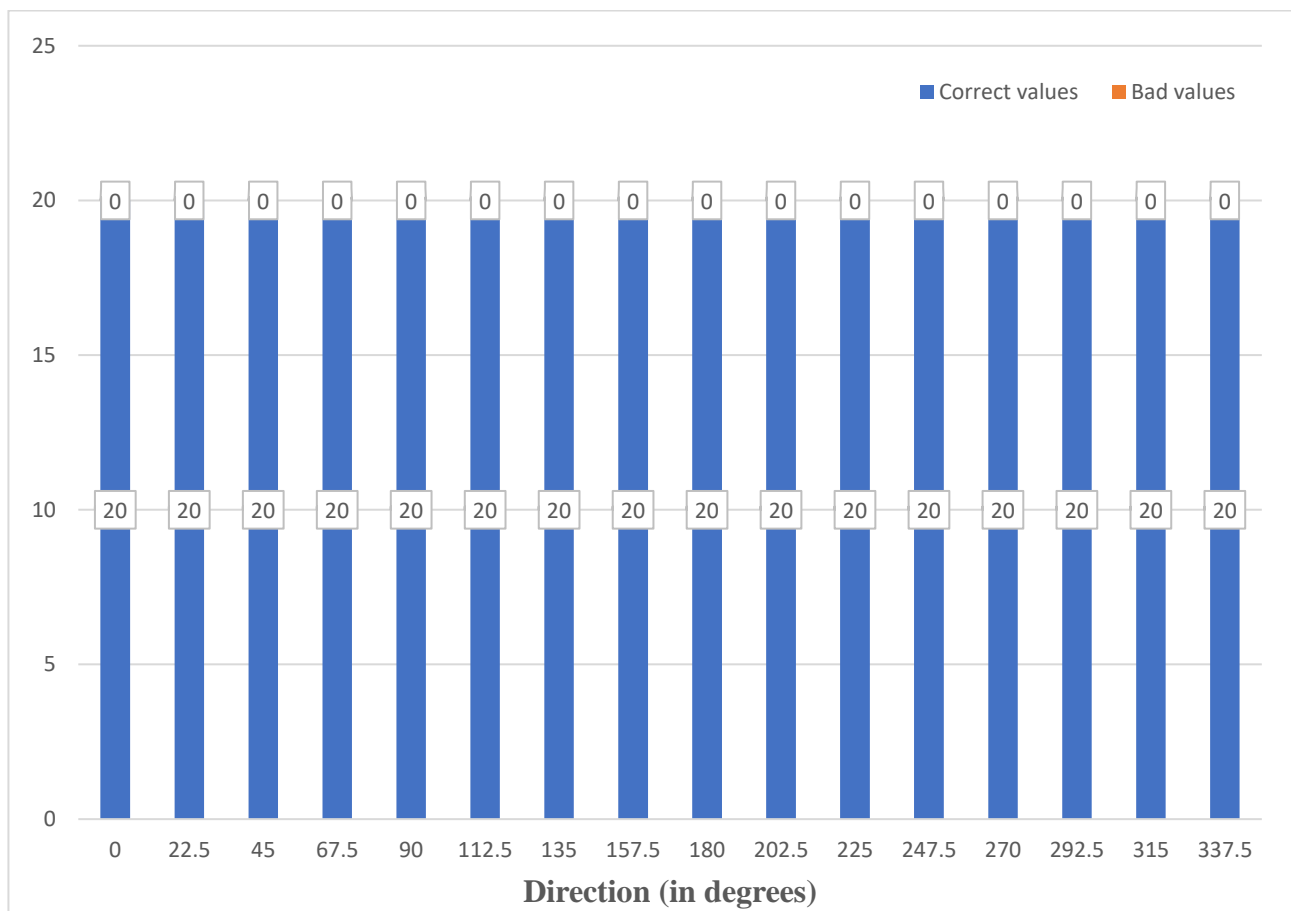


Figure 4-12. Final wind vane test result from the exact circuitry as Figure 3-15

4.3. Rain Gauge

There is no precise measurement tool to use as a reference for testing the rain gauge, so the test is conducted based on the theory that 1 mm of rainfall is equal to 1 litre of water collected by a metre square of a horizontal area [80]. For an area of $S \text{ m}^2$, 1 mm of rainfall then equals S litres of water collected, so if an area of $S \text{ m}^2$ collects A litres of rain water, the amount of rain fall is $\frac{A}{S}$ mm.

Based on the dimensions of the orifice of the rain gauge (Figure 2-10), it is calculated that the device has an area of 5368.54 mm^2 to collect rain water when put in use. For a controlled test, water is poured onto the rain gauge instead. The amount of water is measured by a mini digital scale whose resolution is 0.01 g, then converted from weight to volume by the approximation $1 \text{ kg} \approx 1l$.



Figure 4-13. The mini digital scale used in rain gauge test

The test is conducted twice, once for a fixed amount of water, and once for different amount of water poured onto the rain gauge. The amount of “rainfall” is then calculated on the amount of water and the orifice size of the sensor, and the expected number of pulse counts is then obtained based on the given 0.3 mm of rainfall per tip [22]. The test results are as follows.

Table 4-3. Rain gauge test with a fixed amount of water

Orifice size (mm^2)	5368.54	Supposed rainfall (mm)	Expected pulse counts	Real pulse counts
Amount of water (ml)				
14.80		2.756801663	9	6
14.85		2.766115182	9	6
14.87		2.76984059	9	6
14.82		2.760527071	9	6
14.83		2.762389775	9	6
14.81		2.758664367	9	6
14.83		2.762389775	9	6
14.85		2.766115182	9	6
14.82		2.760527071	9	6
14.82		2.760527071	9	6

Table 4-4. Rain gauge test with different amounts of water

Orifice size (mm²)	5368.54		
Amount of water (ml)	Supposed rainfall (mm)	Expected pulse counts	Real pulse counts
50.38	9.384301877	31	20
104.76	19.51368529	65	39
144.80	26.97195141	90	56
186.16	34.67609443	116	66
233.83	43.55560357	145	81

The first test run shows the consistency in pulse counting by the microcontroller for the approximately same amount of water poured onto the rain gauge, so it could be said that the circuitry of the tipping bucket produces clean signals for the microcontroller to detect (without undesired noise spikes). The number of pulse counts, however, does not match the expected values from the calculation with the product description of the manufacturer.

The second test run confirms that there is a shift in the real pulse counts and the expected values. Without a precise data reference, it is not possible to determine if the rain gauge is faulty, or the rainfall per tip specification is not actually correct. However, the former is assumed, and the software needs modifying accordingly to these findings.

By dividing the amounts of water to the real pulse counts, it is obtained that the buckets tip over once for about every 2.55 ml of water. That converts to $\frac{2.55 \text{ ml}}{5368.54 \text{ mm}^2} = \frac{2.55 \times 10^{-3} \text{ l}}{5368.54 \times 10^{-6} \text{ m}^2} = 0.48 \text{ mm rainfall per tip}$.

4.4. Temperature Sensors – Hygrometer – Barometer

In this test, both the DS18B20 temperature sensor and the BME280 compound sensor have their readings recorded and compared to the data of an Extech 445815 Humidity Alert II Hygro-Thermometer unit due to its precision and availability at Vietnamese – German University. However, the hygro-thermometer unit does not provide a communication interface for data to be extracted directly; instead, this task is done with a USB2.0 UVC Webcam on a Raspberry Pi 4B single board computer. The USB2.0 UVC Webcam is available on icdayroi.com as “Camera USB UVC USB2.0 cho raspberry pi”.

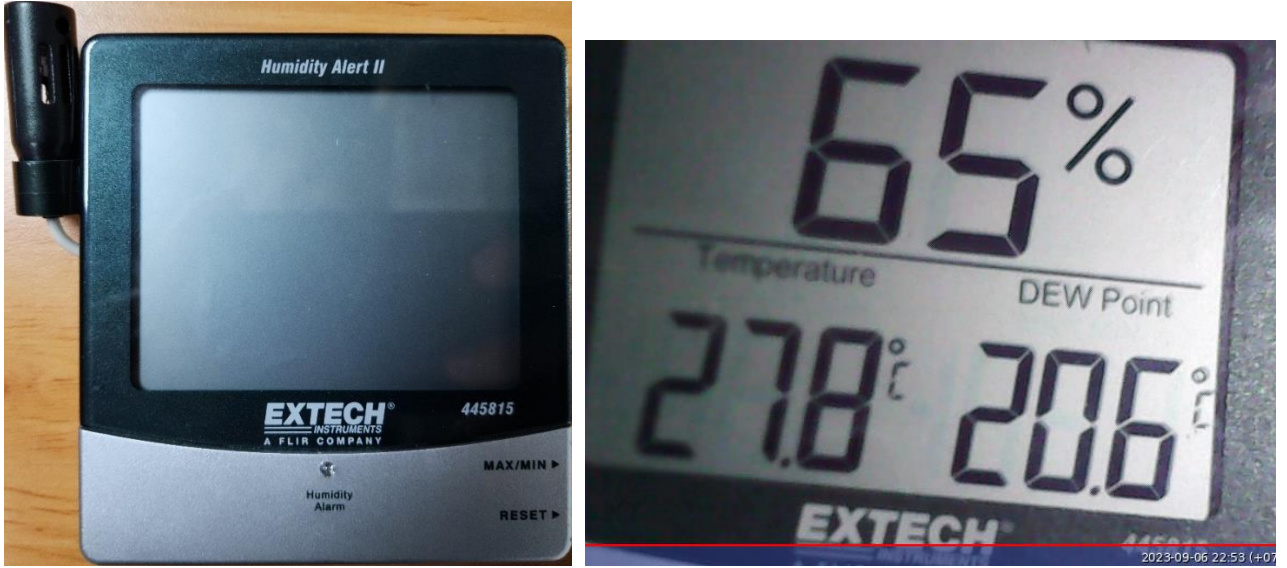


Figure 4-14. Extech 445815 Humidity Alert II Hygro-Thermometer unit used as the reference, and an instance of environment parameters captured during the test

Apart from the sensors, this test also aims at testing the communication interfaces of the STM32F103C8T6 microcontroller when put together, the DS3231 RTC module, and the microSD card module. The STM32F103C8T6 microcontroller is set up with the included sensor units, a DS18B20, a DS3231 RTC module, and a microSD card module as described in the corresponding sections under Chapter 3. It is then powered via a 3.3V pins of the Raspberry Pi 4B, and communicates with the Pi computer via UART; pins PA9 (TX) and PA10 (RX) of the STM32 are wired to pins 10 (UART0 RX) and 8 (UART0 TX) of the Raspberry Pi 4B respectively.

On the Raspberry Pi 4B, the driver for the USB2.0 UVC Webcam needs installing before it could be used. This is done on the Terminal with:

```
sudo apt-get install fswebcam
```

The software on the Raspberry Pi 4B (Appendix E) is written in Python to capture a picture of the hygro-thermometer screen with the USB2.0 UVC Webcam whenever the STM32F103C8T6 sends a data line once every 5 minutes. The picture is first stored locally and then uploaded to Dropbox for remote access while the data via UART is written to a CSV file on the Raspberry Pi. The test is expected to run in 48 hours; however, due to a Internet connection for the Raspberry Pi 4B for a short period, the total run time is extended to 52 hours. Within this window, another CSV file is used to manually log the temperature and humidity from the pictures of the Humidity Alert II screen. At the end of the run period, the 2 CSV files are merged and the comparison of data is performed.

At the beginning, it was found that the microSD card module would halt the STM32F103C8T6 microcontroller when the default SPI was used in the same software with the I²C interface. It was later discovered that the issue fell under a limitation of the STM32F103x8/B medium density devices where I2C1 and remapped SPI1 are in conflict [81]; and the review of the source codes of the STM32duino firmware results in the fact that the SPI1 used for the microSD card is a remapped functionality. The removal of the microSD card module then allowed the test to continue.

The software on the STM32F103C8T6 is firstly built with DS3231 alarm once every minute. When detecting the alarm, the microcontroller clears it and increment a global count variable. When the count variable reaches the value of 5, the microcontroller resets its value to 0, read data and time from the RTC module, and fetch the sensor data, then send to the Raspberry Pi. In fact, if left

untouched, the STM32 microcontroller and the Raspberry Pi would run this test indefinitely since there is no stop condition on the software level. The results of the test are as follows.

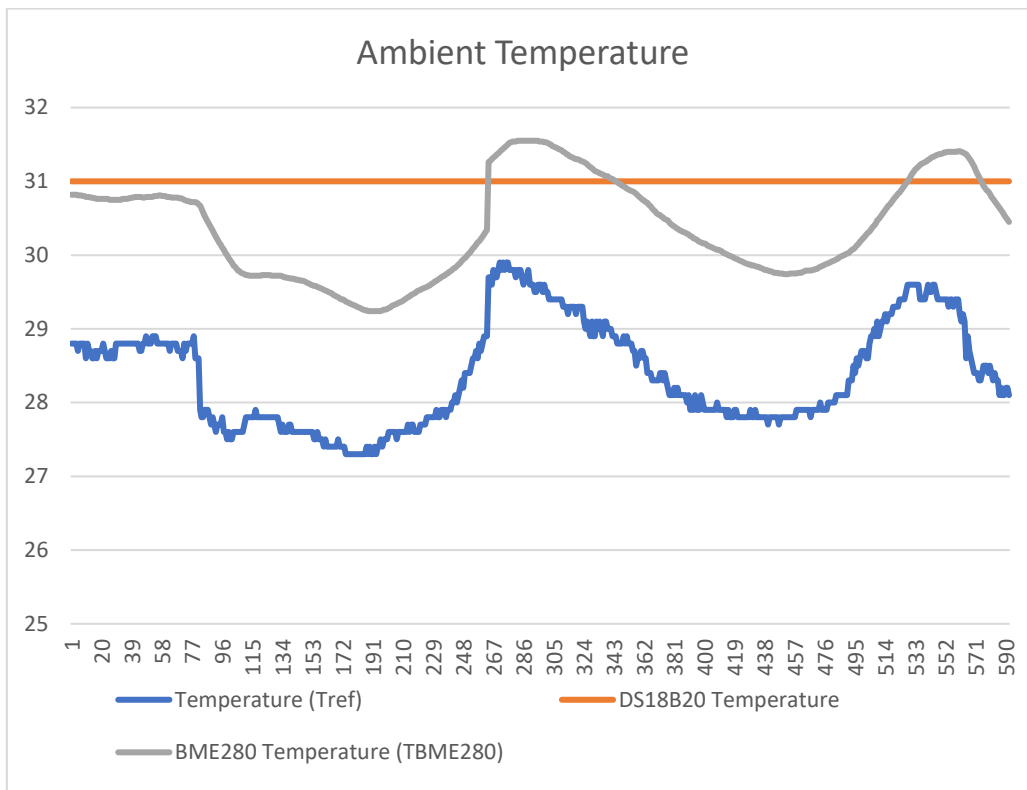


Figure 4-15. Temperature readings from the compound test

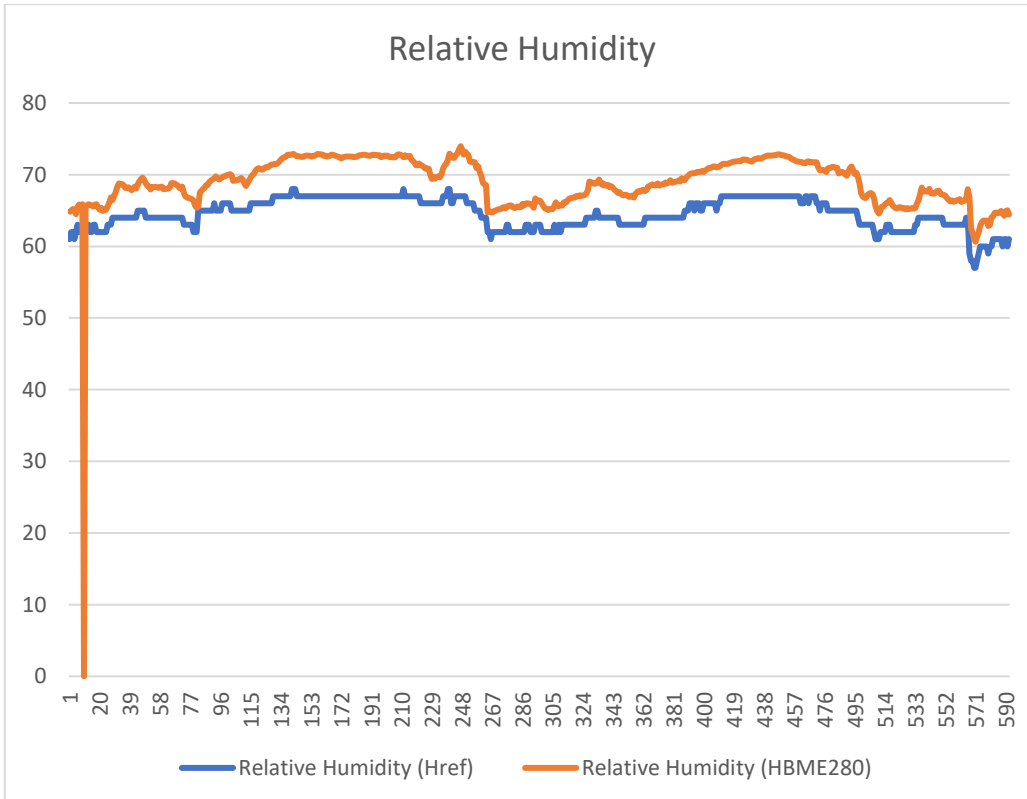


Figure 4-16. Humidity readings from the compound test

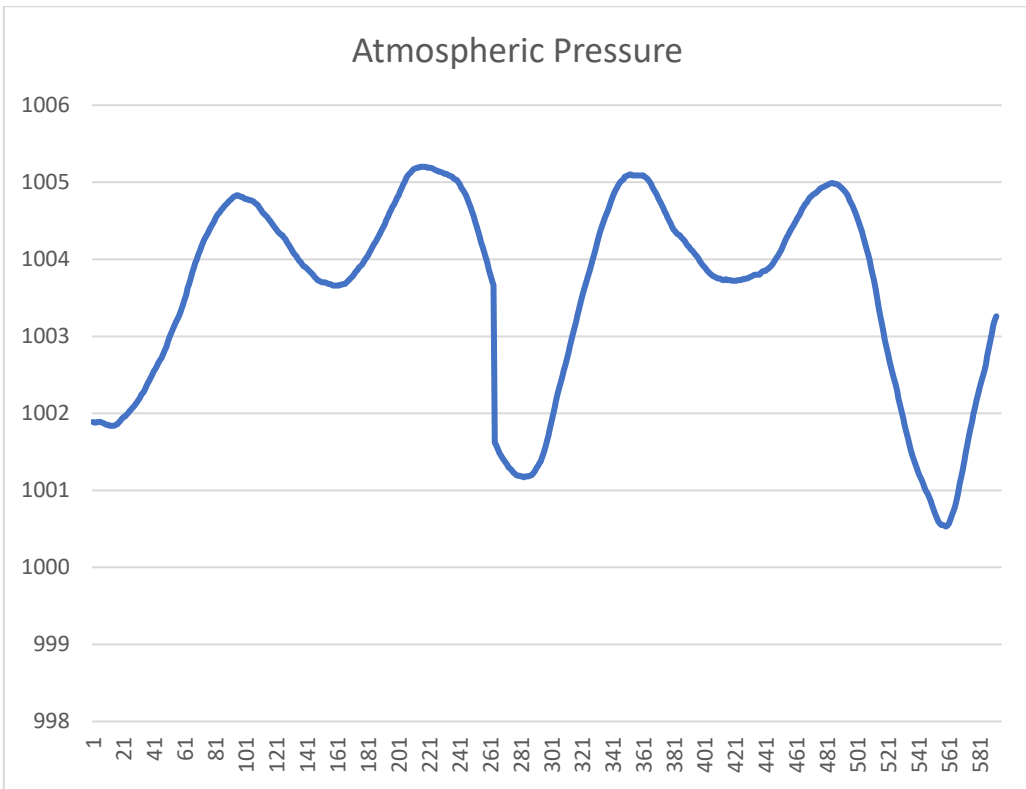


Figure 4-17. Barometric pressure readings from the compound test

For the temperature sensing units, Figure 4-15 shows a smooth temperature line by the BME280, while the DS18B20 returns a constant. It is unclear of the reason why the behaviour of the latter is as such, but that means each DS18B20 device must later be carefully checked before the assembly stage of any design. The BME280, on the other hand, proves to be able to detect changes in ambient temperature much like the reference, the Humidity Alert II device, but there is an offset. Upon checking the final log file, it is found that the difference of temperature readings between the BME280 and the Humidity Alert device ranges from 1.37 °C to 2.83 °C, with a mean value of 1.99 °C. Since the latter is included in this test as a precise reference, it is concluded that the software for the BME280 must introduce a temperature offset value of -1.99 °C. This finding agree with a note from the BME280 datasheet, by which the temperature value “depends on the PCB temperature, sensor element self-heating and ambient temperature and is typically above ambient temperature” [24].

Like temperature, the humidity readings of the BME280 appear to contain an offset, apart from a single value where the sensor returns a “nan” (not a number) entry near the beginning. Since the incident does not repeat throughout the test, it could be assumed that there may have been a single case of data-exchanging error. For the rest of the test result on humidity, the juxtaposition with the reference from the Humidity Alert II device gives that the readings by the BME280 is from 0.5 %RH to 7.89 %RH higher, with an average of 4.46 %RH. As a result, there requires a humidity offset of -4.46 %RH within the software for the BME280.

Finally, there is no reference point to determine if the barometric pressure read by the BME280 is correct or not. However, the chart of Figure 4-17 displays a repeated pattern among over 2 days of test, which means the BME280 does not read random values and could detect changes in atmospheric pressure like it does with ambient temperature and humidity. On the other hand, it could not be ruled out that the barometric readings of the BME280 contain an offset, since [24] specifies that both the humidity and pressure sensing units of the sensor take its read temperature as a parameter for the estimation of the environment sampling results.

4.5. LoRa Connectivity – ThingSpeak

Although this test is on the LoRa connectivity and the communication with ThingSpeak, it roots from the temperature-reading results of the test in Section 4.4, where the DS18B20 in test does not return any values other than 31 °C throughout the 52-hour window.

The test is done with a nodeMCU-ESP8266 as a simple gateway, and an STM32F103C8T6 as a simle node. The communication between the 2 microcontrollers is established via 2 SX1278 LoRa modules. The STM32 microcontroller reads data from a BME280 compound sensor, and 3 DS18B20s with a pre-determined ROM codes on the same 1-wire bus. The data channel on ThingSpeak is set up as follows.

Channel Settings

Percentage complete 30%

Channel ID 2103173

Name	Autonomous Wireless Agrometeorology Station - Server
Description	
Field 1	Temperature <input checked="" type="checkbox"/>
Field 2	Barometric Pressure <input checked="" type="checkbox"/>
Field 3	Relative Humidity <input checked="" type="checkbox"/>
Field 4	DS18B20_1 <input checked="" type="checkbox"/>
Field 5	DS18B20_2 <input checked="" type="checkbox"/>
Field 6	DS18B20_3 <input checked="" type="checkbox"/>
Field 7	
Field 8	

Figure 4-18. Channel settings on ThingSpeak for LoRa connectivity and server test

In this test, the STM32 microcontroller also utilises a 1-minute alarm by a DS3231 RTC module, and it pushes sensor data as soon as there is an alarm. The test is set to run and stopped manually after 7 hours and 33 minutes.

The gateway, apart from handling its LoRa connections and uploading to ThingSpeak server, keeps a log on Serial Monitor, which gives that there exists no failed communication attempts between the LoRa modules and with ThingSpeak. On the webview of the ThingSpeak channel for this test, the results are displayed as follows.

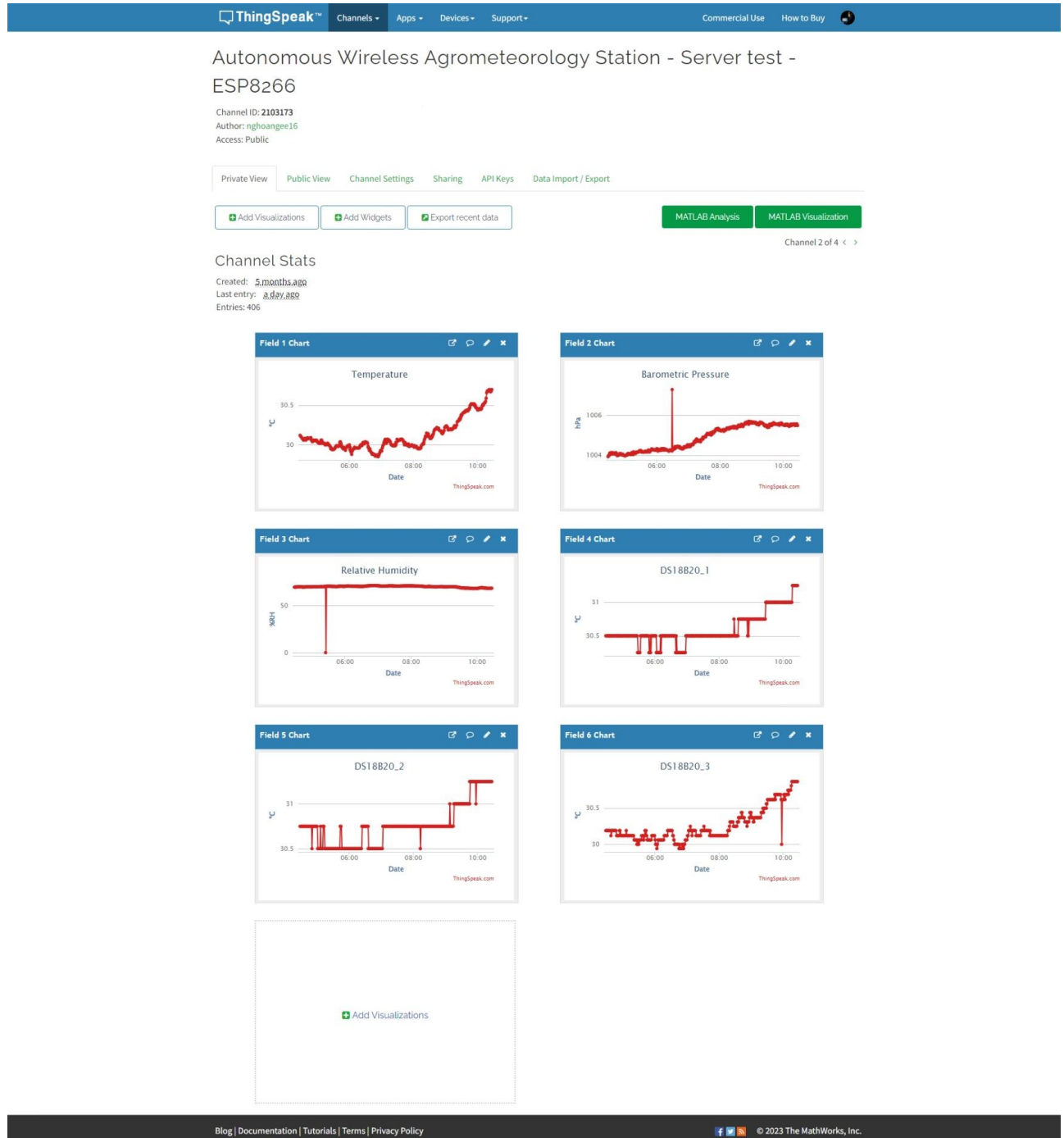


Figure 4-19. Private view of the server test channel on ThingSpeak

It could be seen that ThingSpeak provides a private view and a public view for each data channel. If configured, the public view appears just the same as the private view. Moreover, ThingSpeak allows each chart to be modified to display the data as desired. For example, axes, line colour, background, number of data points in view, etc. of Field 1 Chart could be configured via the Field 1 Chart Option interface as depicted in Figure 4-20.

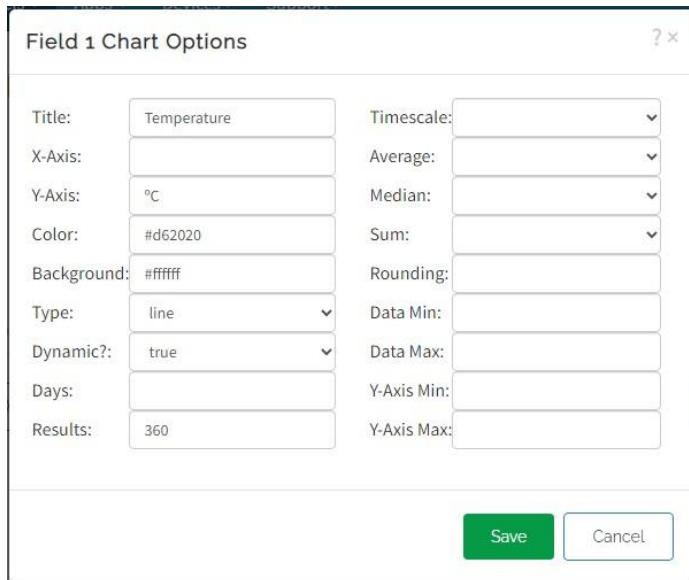


Figure 4-20. Example of Chart Option window on ThingSpeak

On a side note, this test confirms that the DS18B20 device used in the test of Section 4.4 is faulty. The 3 DS18B20 devices used in this test show a capability of detecting changes in temperature much like the BME280 sensor, with the pre-determined resolutions of 0.25 °C for the first 2 DS18B20s and 0.0625 °C for the other. Moreover, the DS18B20 with the 0.0625 °C thermometer resolution reads nearly exactly the same as the BME280, so it could be assumed that the temperature offset error of the 2 sensors are the same, and the calibration value of -1.99 °C could be introduced to the software of the DS18B20.

4.6. LoRa Range Test

The LoRa range test is performed to test the LoRa coverage along with the change of the received signal strength indicator (RSSI), signal-to-noise ratio (SNR), and frequency error of the SX1278 modules when put on the field. The experiment is performed with 2 SX1278 LoRa modules on an open field to ensure they could transfer data on a near line-of-sight. The node is run on an STM32F103C8T6 which receives GPS coordinates via Serial USB Terminal by Kai Morich on a phone; which are then sent uplink to the gateway via LoRa. The gateway is run on a nodeMCU-ESP8266, connected to ThingSpeak via Wi-Fi by another phone to upload the node's GPS coordinates to determine the distances later on, as well as the RSSI, SNR, and frequency error of its received signals. Both the SX1278 modules in test are initialised with the following settings:

- LoRa frequency: 433 MHz
- Spreading factor: 12
- Signal bandwidth: 500 kHz
- Coding rate: 4/5
- Sync word: 0x92

Figure 4-21 displays the locations on the Google Maps where the node transmits data to the server. The start point labelled “Start point – 0” is where the node is put next to the gateway, making the distance near 0 m. By using the distance measurement of Google Maps, the distances between the node and the gateway is determined as depicted in Table 4-5. Although the walking path is a straight line, the markers for each location are not on the same path since GPS modules are rarely able to read the coordinations with a perfect precision.

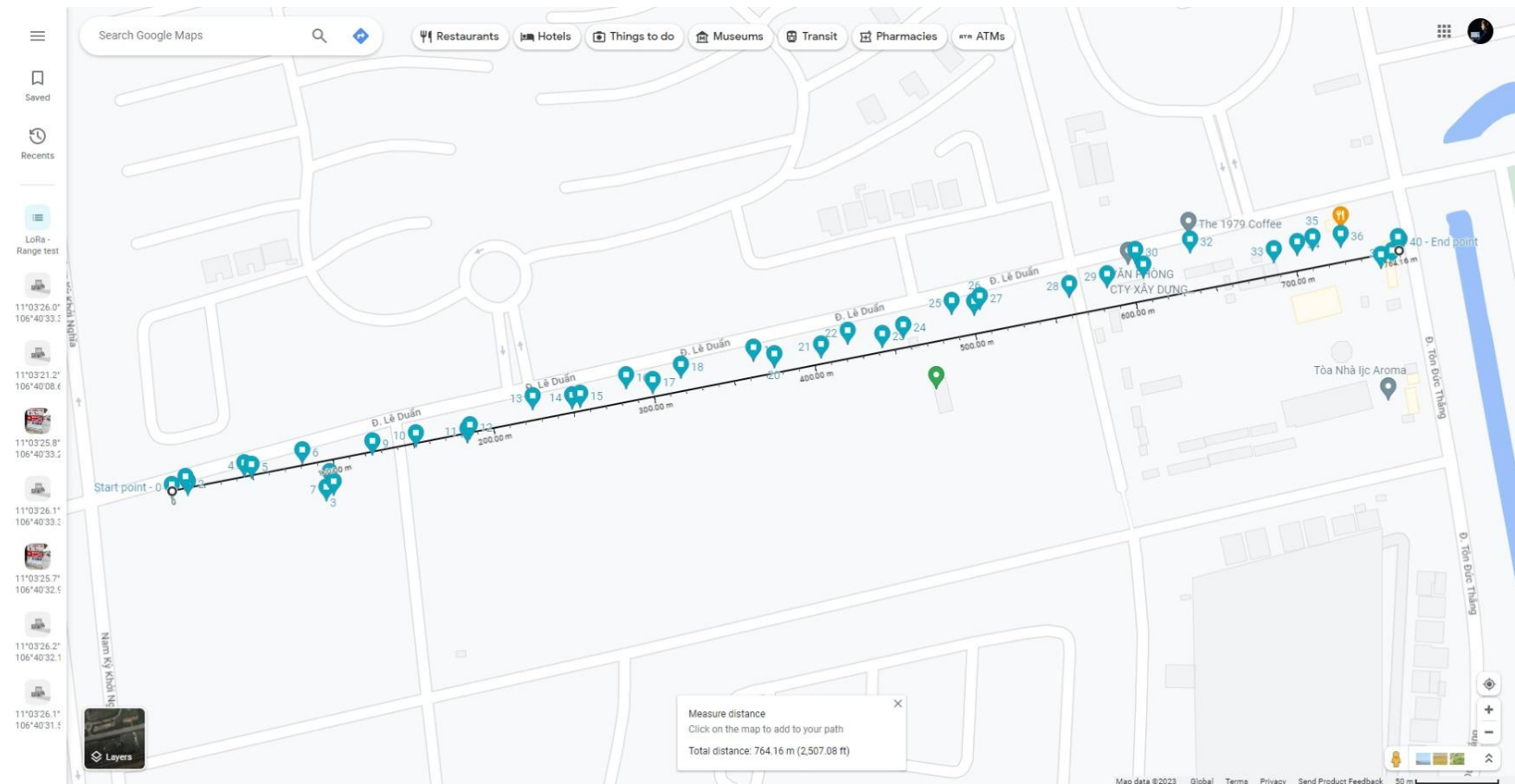


Figure 4-21. LoRa Range Test – logged locations of LoRa transmissions by the node

Table 4-5. LoRa range test result

Index	Latitude	Longitude	Distance (m)	RSSI (dBi)	SNR (dB)	Frequency error (Hz)	Index	Latitude	Longitude	Distance (m)	RSSI (dBi)	SNR (dB)	Frequency error (Hz)
0	11.0559	106.669041	0	-48	6.5	-4669	23	11.0567	106.673019	443.71	-110	-6.75	-4763
1	11.0559	106.669117	9.73	-65	6.5	-4686	24	11.0568	106.673138	457.72	-110	-8.25	-4728
2	11.0559	106.669131	10.42	-76	6.25	-4744	25	11.0569	106.673409	489.78	-111	-11.75	-4776
3	11.0559	106.669946	99.97	-84	7	-4774	26	11.0569	106.673534	502.91	-111	-9	-4742
4	11.056	106.669446	46.6	-89	6.75	-4832	27	11.0569	106.673565	506.99	-111	-15.5	-4780
5	11.056	106.669488	51.1	-107	-1.5	-4851	28	11.057	106.674068	562.19	-112	-15.25	-4734
6	11.0561	106.669772	83.38	-88	6	-4809	29	11.057	106.674277	585.82	-111	-17.75	-4755
7	11.0559	106.669907	95.23	-96	5.75	-4870	30	11.0572	106.674437	606.01	-109	-14.5	-4660
8	11.056	106.669924	97.39	-91	6.25	-4855	31	11.0571	106.674482	608.82	-110	-23.25	-4763
9	11.0561	106.670162	125.93	-99	3.5	-4902	32	11.0572	106.674745	640.18	-111	-12.5	-4612
10	11.0562	106.670407	153.16	-101	4	-4849	33	11.0572	106.675211	688.55	-111	-9	-4579
11	11.0562	106.670696	183.89	-102	3.25	-4782	34	11.0572	106.675343	703.53	-112	-10	-4545
12	11.0562	106.670708	185.61	-104	1.25	-4772	35	11.0572	106.675428	713.37	-111	-20.75	-4545
13	11.0564	106.671063	227.27	-105	1	-4772	36	11.0573	106.675587	730.82	-112	-16.25	-4591
14	11.0564	106.671284	250.92	-109	-3.75	-4772	37	11.0571	106.6758	752.14	-110	-15.25	-4577
15	11.0564	106.671329	255.98	-104	1.25	-4753	38	11.0572	106.6759	764.57	-112	-18	-4579
16	11.0565	106.671586	286.04	-107	-1.5	-4738	39	11.0572	106.6759	759.66	-112	-23.25	-4532
17	11.0565	106.671733	300.79	-108	-3.25	-4711	40	11.0572	106.675914	764.16			
18	11.0565	106.671893	320.1	-108	-3.75	-4656	41	11.0572	106.675914	764.16			
19	11.0566	106.672299	365.68	-110	-13	-4688	42	11.0572	106.675914	764.16			
20	11.0566	106.672413	376.55	-109	-5.75	-4721	43	11.0572	106.675914	764.16			
21	11.0567	106.672675	405.79	-111	-12.5	-4698	44	11.0572	106.675914	764.16			
22	11.0567	106.672825	423.51	-111	-16.5	-4721	45	11.0572	106.675914	764.16			

The RSSI and SNR parameters of the received signals by the gateway are sent and charted on ThingSpeak. It could be observed that from the first to the tenth message by the node, the RSSI at the gateway drops the most drastically, which is -51 dB in total after 125.93 m. Afterwards, it remains between -101 dB and -112 dB. The SNR also shows a generally downward slope as distance between the node and the gateway increases, with an addition of heavy fluctuations when the distance reaches 320.1 m.

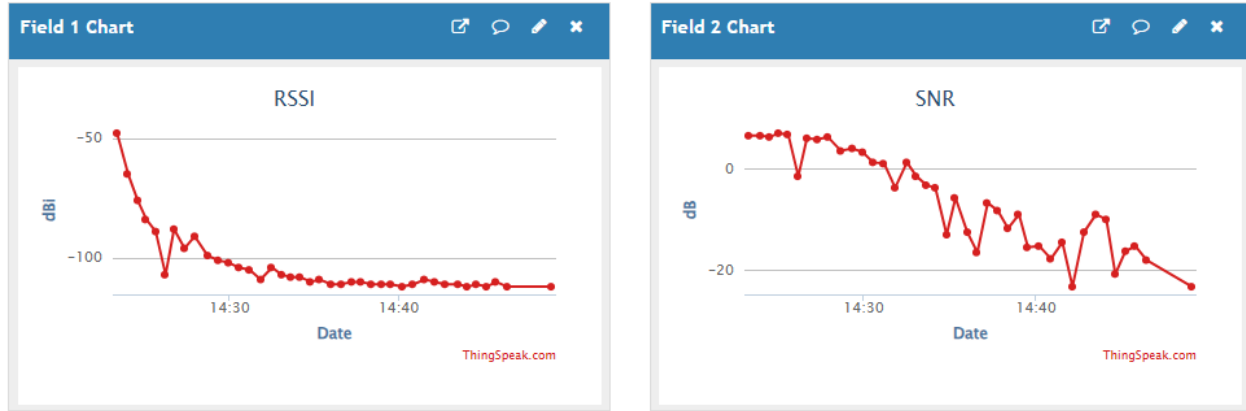


Figure 4-22. RSSI and SNR of the gateway displayed on ThingSpeak

Beyond 759.66 m, the communication between the node and the gateway could no longer be established. It is then determined that the communication range of SX1278 modules at the 500-kHz bandwidth is about 760 m. Since communications via LoRa gain coverage by lowering the signal bandwidth [82], the maximum distance over which the SX1278 modules could communicate is expected to be much higher with proper settings.

Last but not least, this test on LoRa coverage initially aims at testing both uplink and downlink transmissions. However, as the SX1278 modules are put on the field, the downlink transmission (from gateway to node) is severed for unknown reason(s), thus only uplink results available in this experiment. Since the design for the Autonomous Wireless Agrometeorology Station focuses on uploading the data from the station (node) to a server via a gateway, the performance on the downlink connection does not bear heavy weights. Due to the lack of testing equipment and/or methodologies, there does not exist any findings on the data-exchanging rate and transmission success rate either.

5. Conclusion and Further Development

The design of an Autonomous Wireless Agrometeorology Station introduces a new territory toward improvements of agricultural production via monitoring the meteorological factors, including wind parameters, precipitations, temperature, humidity, and atmospheric pressure. The available results suggest that the sensor outputs could become useful after calibrations, and remote data access in real time is possible with LoRa communication and ThingSpeak.

However, the system powering design remains basic and needs improvements, while a data backup solution is missing due to the invalidation of the microSD card in use. Therefore, the further development of the project is suggested as below:

- Design a powering system to make the station truly autonomous. As suggested in section 2.5, a solar panel backed by Lithium-Ion batteries is an option to be considered. In turn, there may require a load-balancing circuit for the energy-harvesting unit (i.e. the solar panel) and the back-up batteries to power the station.
- Add a data backup solution. The microSD card module is suggested to remain, but another microcontroller (i.e. STM8S103F3P6) is to be put between the main one and the microSD card module as a bridge. The bridge is to receive data to be logged via UART then write those data on the microSD card for the main microcontroller.
- Evaluation of the anemometer to complete the wind speed model. Due to the aerodynamic nature of the device, this development may need collaborations with other engineering fields (i.e. Mechanical Engineering faculty at Vietnamese – German University).
- Further evaluation of the rain gauge to determine the fault of the device on top of the product specifications by the manufacturer.
- Further evaluations of the digital sensors.
- Further improvements of communications via LoRa.
- Integration of all modules on a single prototype.

Finally, the conclusion over the applicability of the STM32duino firmware is that it could be used in development and prototyping a project. In a real application, there remains multiple limitations, including the lack of debugging probe, and the compatibility with provided libraries, which is discovered when some research for this thesis is conducted, but not exclusively included.

APPENDIX A. HAL and DMA Configuration Functions for ADC

```
*****  
*** HAL settings generated by STM32CubeMX ***  
*****  
  
/**  
 * @brief ADC MSP Initialization  
 * This function configures the hardware resources used in this example  
 * @param hadc: ADC handle pointer  
 * @retval None  
*/  
extern "C" void HAL_ADC_MspInit(ADC_HandleTypeDef* hadc) {  
    GPIO_InitTypeDef GPIO_InitStruct = {0};  
    if (hadc->Instance == ADC1) {  
        /* Peripheral clock enable */  
        __HAL_RCC_ADC1_CLK_ENABLE();  
  
        __HAL_RCC_GPIOB_CLK_ENABLE();  
        /*ADC1 GPIO Configuration  
        PB1      -----> ADC1_IN9  
        */  
        GPIO_InitStruct.Pin = GPIO_PIN_1;  
        GPIO_InitStruct.Mode = GPIO_MODE_ANALOG;  
        HAL_GPIO_Init(GPIOB, &GPIO_InitStruct);  
  
        /* ADC1 DMA Init */  
        /* ADC1 Init */  
        hdma_adc1.Instance = DMA1_Channel1;  
        hdma_adc1.Init.Direction = DMA_PERIPH_TO_MEMORY;  
        hdma_adc1.InitPeriphInc = DMA_PINC_DISABLE;  
        hdma_adc1.Init.MemInc = DMA_MINC_ENABLE;  
        hdma_adc1.Init.PeriphDataAlignment = DMA_PDATAALIGN_HALFWORD;  
        hdma_adc1.Init.MemDataAlignment = DMA_MDATAALIGN_HALFWORD;  
        hdma_adc1.Init.Mode = DMA_NORMAL;  
        hdma_adc1.Init.Priority = DMA_PRIORITY_HIGH;  
        if (HAL_DMA_Init(&hdma_adc1) != HAL_OK) {  
            while (1);  
        }  
  
        __HAL_LINKDMA(hadc,DMA_Handle,hdma_adc1);  
    }  
}  
  
/**  
 * @brief ADC MSP De-Initialization  
 * This function freeze the hardware resources used in this example  
 * @param hadc: ADC handle pointer  
 * @retval None  
*/
```

```

extern "C" void HAL_ADC_MspDeInit(ADC_HandleTypeDef* hadc) {
  if(hadc->Instance==ADC1) {
    /* Peripheral clock disable */
    __HAL_RCC_ADC1_CLK_DISABLE();

    /**ADC1 GPIO Configuration
    PB1      -----> ADC1_IN9
    */
    HAL_GPIO_DeInit(GPIOB, GPIO_PIN_1);

    /* ADC1 DMA DeInit */
    HAL_DMA_DeInit(hadc->DMA_Handle);
  }
}

/**
 * @brief This function handles DMA1 channel1 global interrupt.
 */
extern "C" void DMA1_Channel1_IRQHandler(void) {
  HAL_DMA_IRQHandler(&hdma_adc1);
}

/**
 * @brief ADC1 Initialization Function
 * @param None
 * @retval None
 */
static void MX_ADC1_Init(ADC_INPUT_TYPE input_type) {
  ADC_ChannelConfTypeDef sConfig = {0};

  /* USER CODE BEGIN ADC1_Init 1 */
  if (!first_run) {
    if (HAL_ADC_DeInit(&hadc1) != HAL_OK)
    {
      while (1);
    }
  }
  else {
    first_run = false;
  }
  /* USER CODE END ADC1_Init 1 */

  /* USER CODE BEGIN ADC1_Init 2 */
  if (INTERNAL_REFERENCE_VOLTAGE == input_type) {
    /** Common config
    */
    hadc1.Instance = ADC1;
    hadc1.Init.ScanConvMode = ADC_SCAN_DISABLE;
    hadc1.Init.ContinuousConvMode = ENABLE;
    hadc1.Init.DiscontinuousConvMode = DISABLE;
  }
}

```

```

hadc1.Init.ExternalTrigConv = ADC_SOFTWARE_START;
hadc1.Init.DataAlign = ADC_DATAALIGN_RIGHT;
hadc1.Init.NbrOfConversion = 1;
if (HAL_ADC_Init(&hadc1) != HAL_OK) {
    while (1);
}

/** Configure Regular Channel
*/
sConfig.Channel = ADC_CHANNEL_VREFINT;
sConfig.Rank = ADC_REGULAR_RANK_1;
sConfig.SamplingTime = ADC_SAMPLETIME_7CYCLES_5;
if (HAL_ADC_ConfigChannel(&hadc1, &sConfig) != HAL_OK) {
    while (1);
}
}

else if (EXTERNAL_INPUT_SIGNAL == input_type) {
    /** Common config
*/
    hadc1.Instance = ADC1;
    hadc1.Init.ScanConvMode = ADC_SCAN_DISABLE;
    hadc1.Init.ContinuousConvMode = ENABLE;
    hadc1.Init.DiscontinuousConvMode = DISABLE;
    hadc1.Init.ExternalTrigConv = ADC_SOFTWARE_START;
    hadc1.Init.DataAlign = ADC_DATAALIGN_RIGHT;
    hadc1.Init.NbrOfConversion = 1;
    if (HAL_ADC_Init(&hadc1) != HAL_OK) {
        while (1);
    }

    /** Configure Regular Channel
*/
    sConfig.Channel = ADC_CHANNEL_9;
    sConfig.Rank = ADC_REGULAR_RANK_1;
    sConfig.SamplingTime = ADC_SAMPLETIME_7CYCLES_5;
    if (HAL_ADC_ConfigChannel(&hadc1, &sConfig) != HAL_OK) {
        while (1);
    }
}
else {
    // Do nothing
}

/* USER CODE END ADC1_Init 2 */
}

/**
 * Enable DMA controller clock
*/
static void MX_DMA_Init(void) {

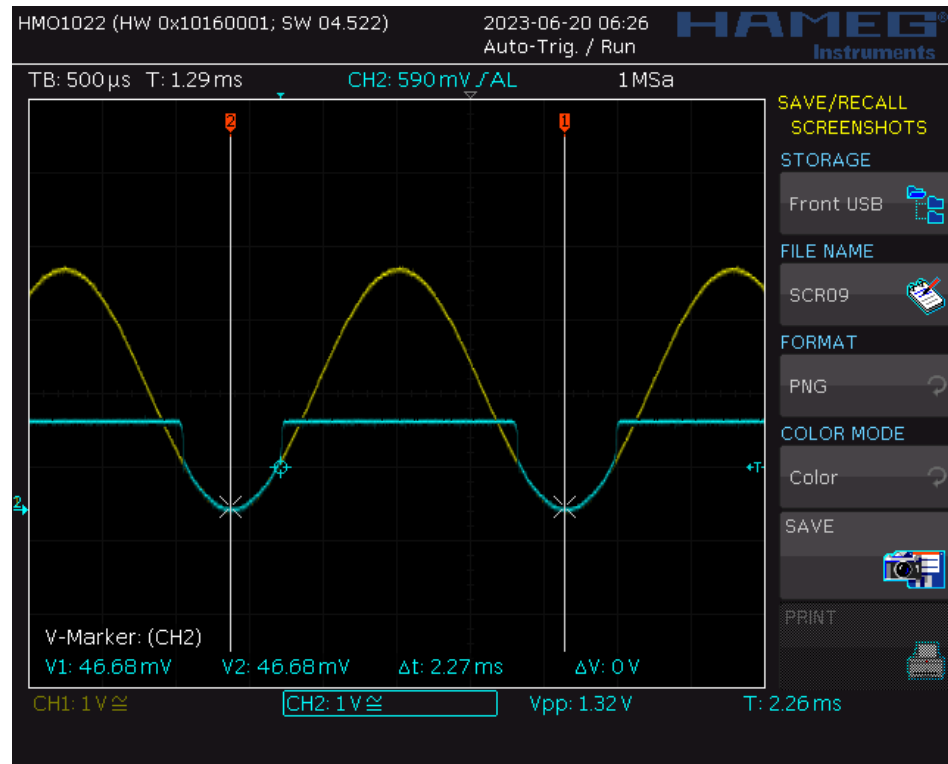
```

```
/* DMA controller clock enable */
__HAL_RCC_DMA1_CLK_ENABLE();

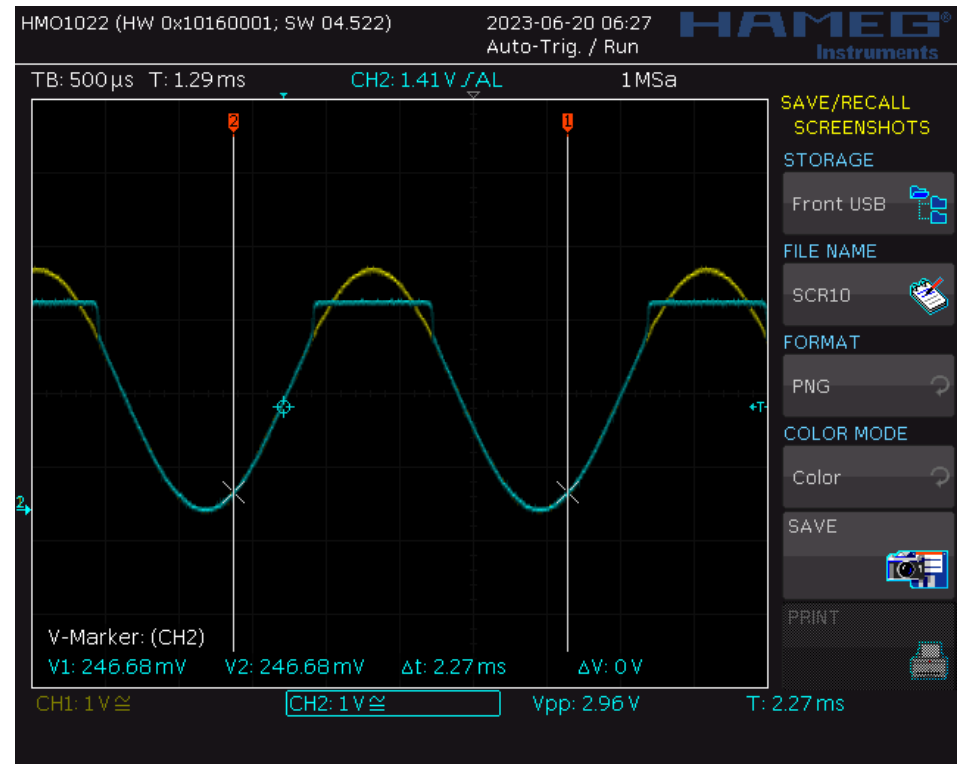
/* DMA interrupt init */
/* DMA1_Channel1_IRQHandler interrupt configuration */
HAL_NVIC_SetPriority(DMA1_Channel1_IRQHandler, 0, 0);
HAL_NVIC_EnableIRQ(DMA1_Channel1_IRQHandler);

}
```

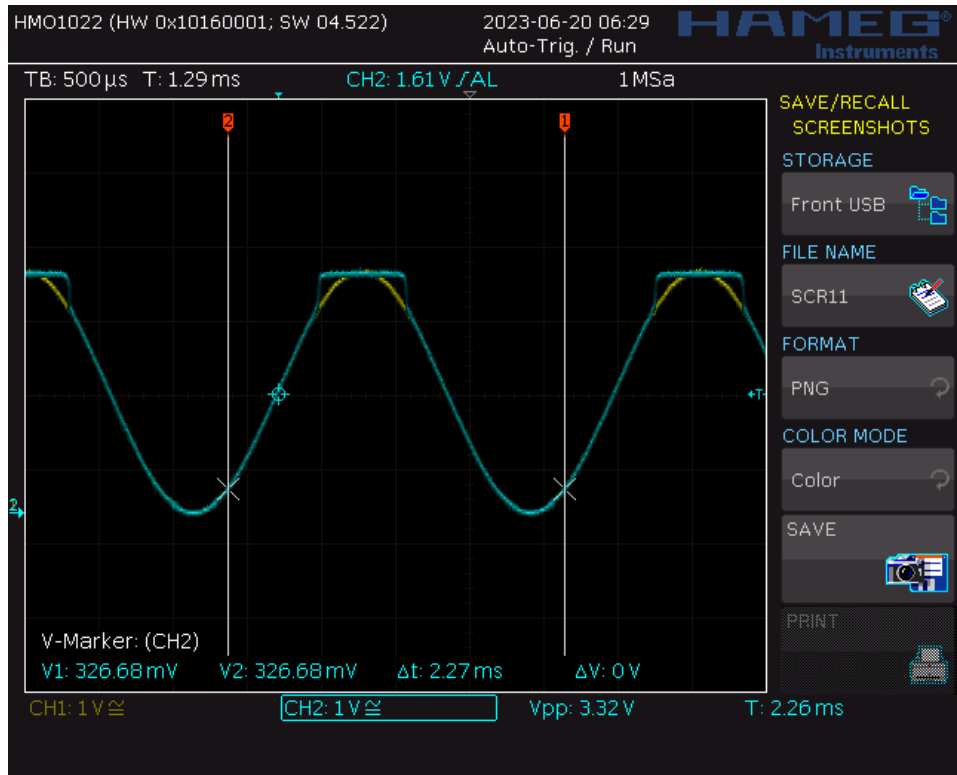
APPENDIX B. CA3140EZ Voltage Buffer Test Result



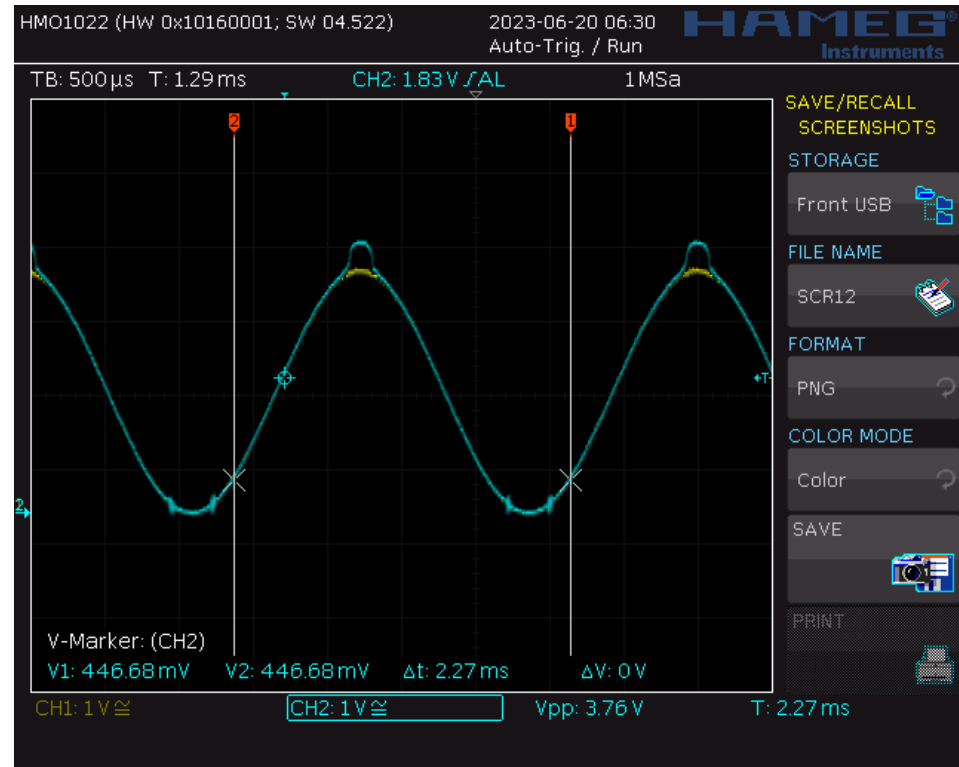
VCC = 3.3 V



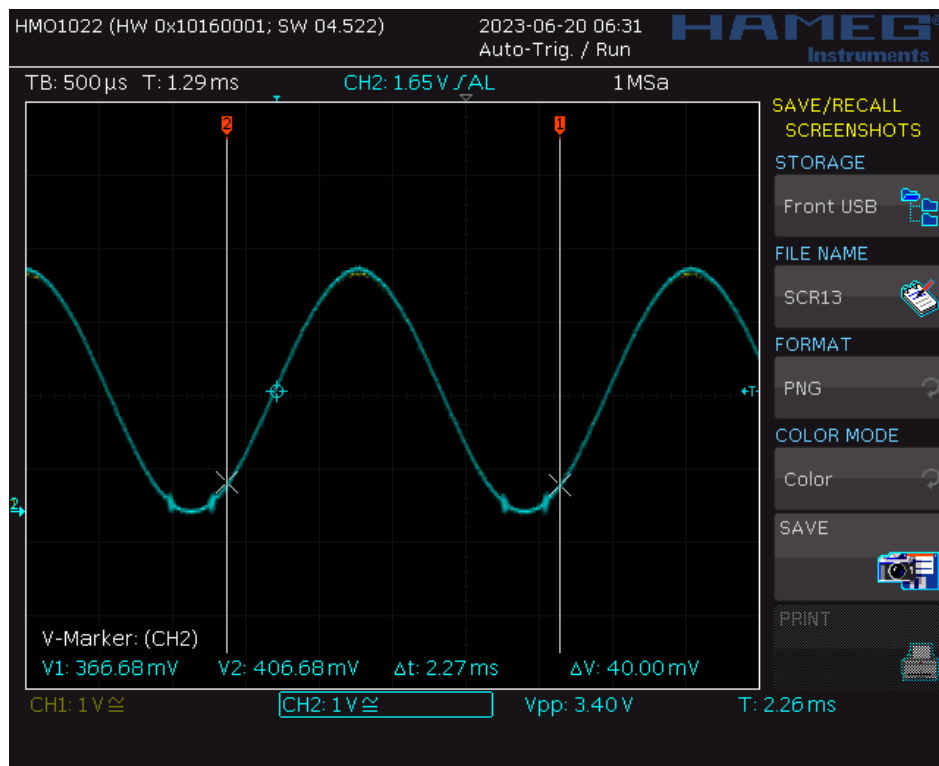
VCC = 5V



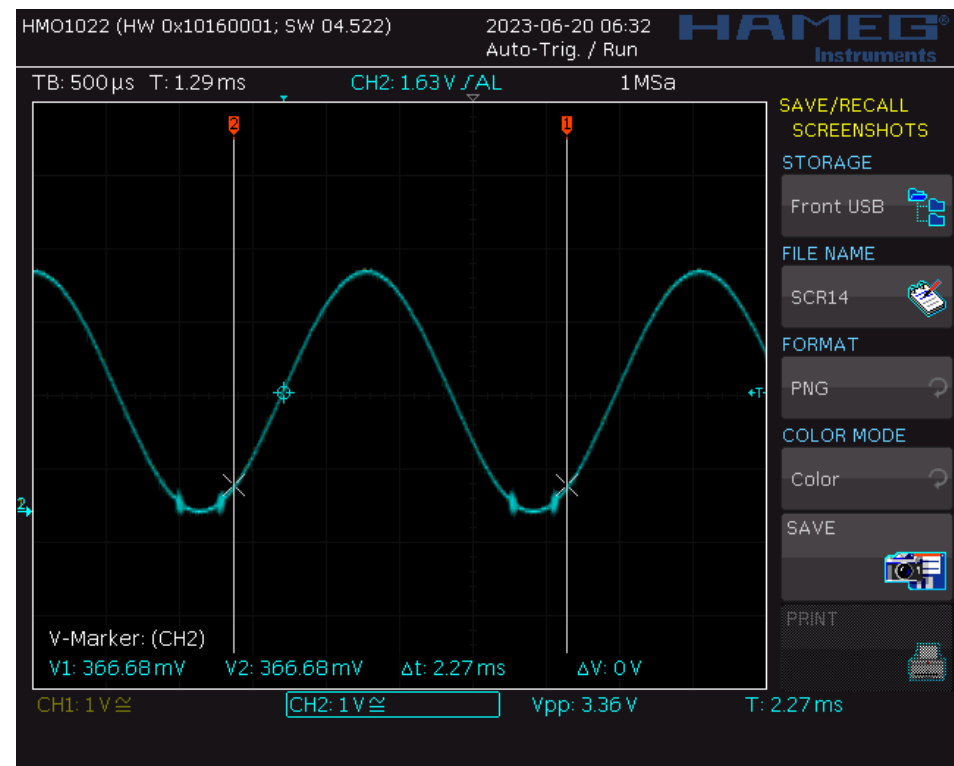
VCC = 5.41 V



VCC = 5.9 V

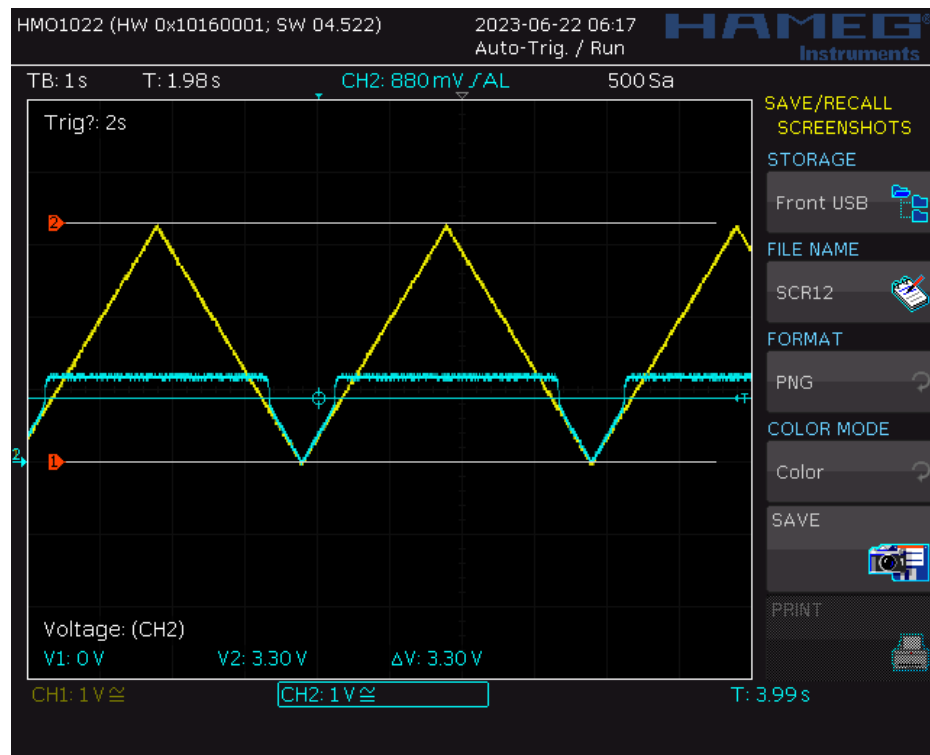


VCC = 6 V

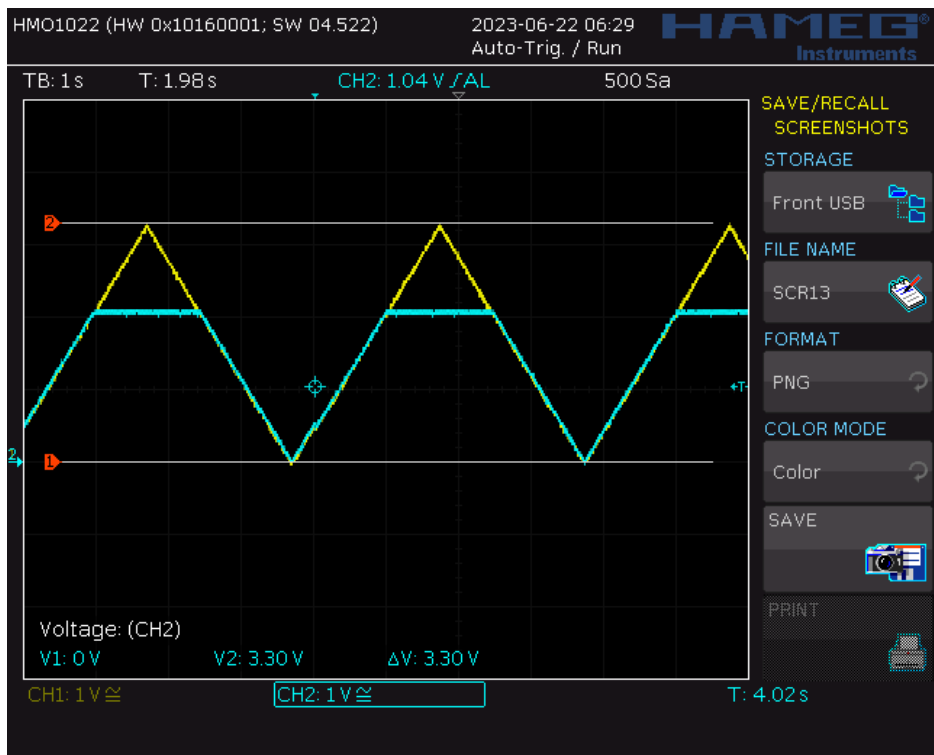


VCC = 6.3 V

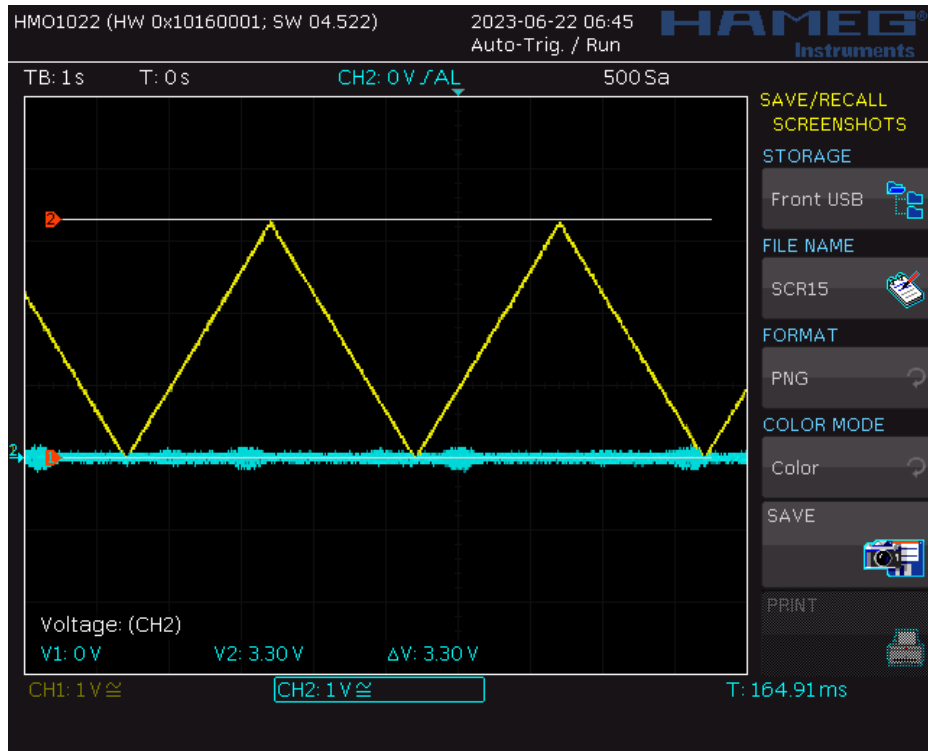
APPENDIX C. Op-Amp Pick-up Test for Voltage Buffer at 3.3-V Power Supply



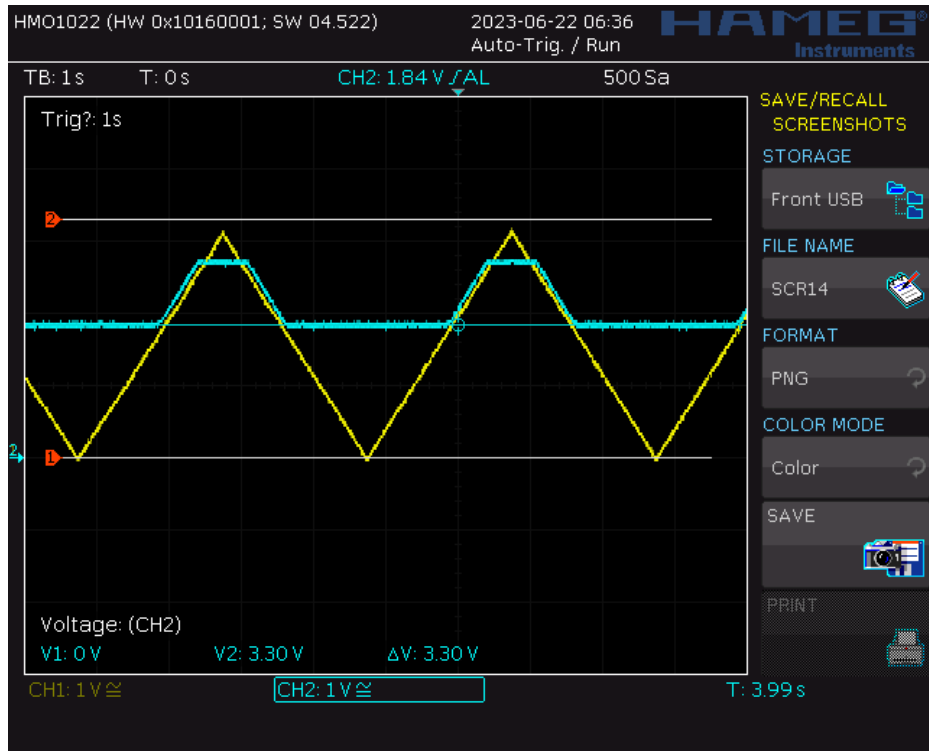
CA3140EZ



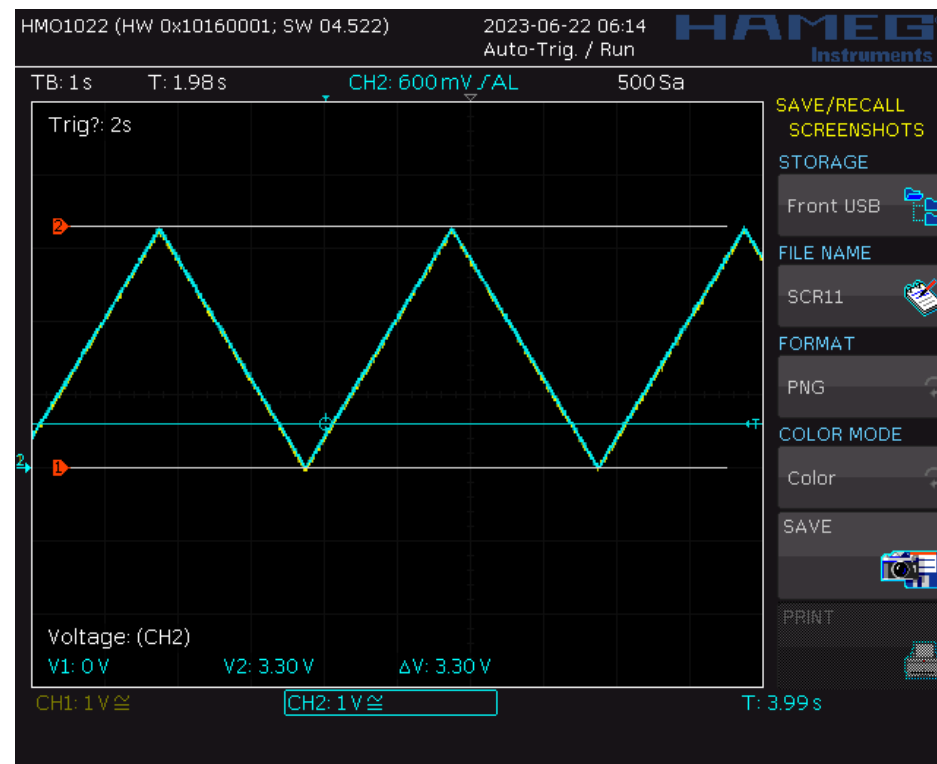
LM358P



LM393P



UA741CP



MCP6002-I/P

APPENDIX D. Wind Vane Test Result for Circuitry of Figure 3-15

Input direction: 0		Voltmeter: 2.9949 V		Input direction: 22.5		Voltmeter: 2.1995 V		Input direction: 45		Voltmeter: 2.3538 V		Input direction: 67.5		Voltmeter: 0.7084 V	
Read direction	Raw ADC	V _{in}	R _{read}	Read direction	Raw ADC	V _{in}	R _{read}	Read direction	Raw ADC	V _{in}	R _{read}	Read direction	Raw ADC	V _{in}	R _{read}
0	3741	2.99	35644	22.5	2740	2.19	6680.4	45	2933	2.34	8339.5	67.5	867	0.69	885.04
0	3738	2.99	34874	22.5	2737	2.19	6673.1	45	2933	2.34	8329.5	67.5	864	0.69	886.34
0	3739	2.98	34553	22.5	2739	2.19	6651	45	2930	2.34	8329.5	67.5	873	0.69	882.45
0	3741	2.99	34659	22.5	2734	2.19	6665.7	45	2929	2.34	8299.6	67.5	863	0.7	894.13
0	3736	2.99	34874	22.5	2735	2.18	6629.1	45	2931	2.34	8289.6	67.5	861	0.69	881.16
0	3734	2.98	34342	22.5	2739	2.18	6636.4	45	2933	2.34	8309.5	67.5	865	0.69	878.57
0	3736	2.98	34134	22.5	2735	2.19	6665.7	45	2934	2.34	8329.5	67.5	863	0.69	883.75
0	3739	2.98	34342	22.5	2738	2.18	6636.4	45	2933	2.34	8339.5	67.5	866	0.69	881.16
0	3741	2.99	34659	22.5	2739	2.19	6658.4	45	2933	2.34	8329.5	67.5	877	0.69	885.04
0	3741	2.99	34874	22.5	2735	2.19	6665.7	45	2929	2.34	8329.5	67.5	863	0.7	899.35
0	3741	2.99	34874	22.5	2745	2.18	6636.4	45	2931	2.34	8289.6	67.5	869	0.69	881.16
0	3736	2.99	34874	22.5	2734	2.19	6710	45	2933	2.34	8309.5	67.5	864	0.69	888.93
0	3738	2.98	34342	22.5	2737	2.18	6629.1	45	2931	2.34	8329.5	67.5	865	0.69	882.45
0	3738	2.98	34553	22.5	2738	2.19	6651	45	2934	2.34	8309.5	67.5	866	0.69	883.75
0	3738	2.98	34553	22.5	2739	2.19	6658.4	45	2934	2.34	8339.5	67.5	867	0.69	885.04
0	3737	2.98	34553	22.5	2726	2.19	6665.7	45	2936	2.34	8339.5	67.5	865	0.69	886.34
0	3739	2.98	34447	22.5	2737	2.18	6571.1	45	2936	2.34	8359.6	67.5	863	0.69	883.75
0	3737	2.99	34659	22.5	2739	2.19	6651	45	2931	2.34	8359.6	67.5	864	0.69	881.16
0	3736	2.98	34447	22.5	2736	2.19	6665.7	45	2930	2.34	8309.5	67.5	865	0.69	882.45
0	3736	2.98	34342	22.5	2739	2.18	6643.7	45	2937	2.34	8299.6	67.5	866	0.69	883.75

Input direction: 90		Voltmeter: 0.7741 V		Input direction: 112.5		Voltmeter: 0.5747 V		Input direction: 135		Voltmeter: 1.3235 V		Input direction: 157.5		Voltmeter: 0.9908 V	
Read direction	Raw ADC	V _{in}	R _{read}	Read direction	Raw ADC	V _{in}	R _{read}	Read direction	Raw ADC	V _{in}	R _{read}	Read direction	Raw ADC	V _{in}	R _{read}
90	947	0.76	1000.9	112.5	694	0.56	676.9	135	1650	1.32	2220.2	157.5	1220	0.98	1408.5
90	957	0.76	992.73	112.5	698	0.55	673.39	135	1644	1.32	2227	157.5	1229	0.97	1400.4
90	950	0.76	1006.4	112.5	691	0.56	678.07	135	1645	1.31	2213.5	157.5	1224	0.98	1415.1
90	953	0.76	996.82	112.5	693	0.55	669.89	135	1645	1.31	2215.7	157.5	1224	0.98	1406.9
90	949	0.76	1000.9	112.5	697	0.55	672.22	135	1646	1.31	2215.7	157.5	1225	0.98	1406.9
90	947	0.76	995.45	112.5	696	0.56	676.9	135	1650	1.31	2218	157.5	1221	0.98	1408.5
90	946	0.76	992.73	112.5	694	0.56	675.73	135	1640	1.32	2227	157.5	1226	0.98	1402
90	947	0.76	991.36	112.5	695	0.55	673.39	135	1646	1.31	2204.5	157.5	1226	0.98	1410.2
90	947	0.76	992.73	112.5	702	0.55	674.56	135	1649	1.31	2218	157.5	1224	0.98	1410.2
90	946	0.76	992.73	112.5	696	0.56	682.76	135	1648	1.32	2224.7	157.5	1232	0.98	1406.9
90	947	0.76	991.36	112.5	694	0.56	675.73	135	1648	1.32	2222.5	157.5	1226	0.98	1420.1
90	948	0.76	992.73	112.5	696	0.55	673.39	135	1647	1.32	2222.5	157.5	1223	0.98	1410.2
90	948	0.76	994.09	112.5	692	0.56	675.73	135	1645	1.32	2220.2	157.5	1226	0.98	1405.3
90	947	0.76	994.09	112.5	712	0.55	671.05	135	1645	1.31	2215.7	157.5	1225	0.98	1410.2
90	947	0.76	992.73	112.5	693	0.57	694.53	135	1644	1.31	2215.7	157.5	1225	0.98	1408.5
90	949	0.76	992.73	112.5	696	0.55	672.22	135	1646	1.31	2213.5	157.5	1225	0.98	1408.5
90	950	0.76	995.45	112.5	695	0.56	675.73	135	1650	1.31	2218	157.5	1225	0.98	1408.5
90	949	0.76	996.82	112.5	696	0.55	674.56	135	1647	1.32	2227	157.5	1222	0.98	1408.5
90	963	0.76	995.45	112.5	699	0.56	675.73	135	1645	1.32	2220.2	157.5	1226	0.98	1403.6
90	948	0.77	1014.7	112.5	696	0.56	679.24	135	1646	1.31	2215.7	157.5	1224	0.98	1410.2

Input direction: 180		Voltmeter: 1.7911 V		Input direction: 202.5		Voltmeter: 1.6124 V		Input direction: 225		Voltmeter: 2.7332 V		Input direction: 247.5		Voltmeter: 2.6726 V	
Read direction	Raw ADC	V _{in}	R _{read}	Read direction	Raw ADC	V _{in}	R _{read}	Read direction	Raw ADC	V _{in}	R _{read}	Read direction	Raw ADC	V _{in}	R _{read}
180	2233	1.79	4012.5	202.5	1988	1.6	3165.8	225	3400	2.72	16228	247.5	3323	2.66	14365
180	2232	1.78	3957.5	202.5	2010	1.59	3113.6	225	3408	2.72	16144	247.5	3324	2.65	14205
180	2228	1.78	3953.6	202.5	2008	1.61	3181.3	225	3400	2.72	16370	247.5	3325	2.65	14227
180	2232	1.78	3938.1	202.5	2008	1.6	3175.1	225	3402	2.72	16144	247.5	3323	2.66	14250
180	2230	1.78	3953.6	202.5	2006	1.6	3175.1	225	3403	2.72	16200	247.5	3323	2.65	14205
180	2227	1.78	3945.8	202.5	2008	1.6	3168.9	225	3400	2.72	16228	247.5	3325	2.65	14205
180	2230	1.78	3934.2	202.5	2008	1.6	3175.1	225	3401	2.72	16144	247.5	3325	2.66	14250
180	2227	1.78	3945.8	202.5	2008	1.6	3175.1	225	3406	2.72	16172	247.5	3327	2.66	14250
180	2230	1.78	3934.2	202.5	2009	1.6	3175.1	225	3397	2.72	16313	247.5	3327	2.66	14296
180	2232	1.78	3945.8	202.5	2005	1.6	3178.2	225	3402	2.71	16060	247.5	3323	2.66	14296
180	2234	1.78	3953.6	202.5	2014	1.6	3165.8	225	3402	2.72	16200	247.5	3326	2.65	14205
180	2229	1.78	3961.4	202.5	2006	1.61	3193.8	225	3402	2.72	16200	247.5	3326	2.66	14273
180	2233	1.78	3942	202.5	2008	1.6	3168.9	225	3400	2.72	16200	247.5	3327	2.66	14273
180	2228	1.78	3957.5	202.5	2009	1.6	3175.1	225	3400	2.72	16144	247.5	3325	2.66	14296
180	2230	1.78	3938.1	202.5	2006	1.6	3178.2	225	3402	2.72	16144	247.5	3328	2.66	14250
180	2226	1.78	3945.8	202.5	2006	1.6	3168.9	225	3402	2.72	16200	247.5	3326	2.66	14319
180	2229	1.78	3930.3	202.5	2006	1.6	3168.9	225	3400	2.72	16200	247.5	3328	2.66	14273
180	2229	1.78	3942	202.5	2004	1.6	3168.9	225	3402	2.72	16144	247.5	3320	2.66	14319
180	2229	1.78	3942	202.5	2007	1.6	3162.7	225	3400	2.72	16200	247.5	3343	2.65	14137
180	2228	1.78	3942	202.5	2004	1.6	3172	225	3400	2.72	16144	247.5	3325	2.67	14670

Input direction: 270		Voltmeter: 3.2039 V		Input direction: 292.5		Voltmeter: 3.0544 V		Input direction: 315		Voltmeter: 3.1338 V		Input direction: 337.5		Voltmeter: 2.8647 V	
Read direction	Raw ADC	V _{in}	R _{read}	Read direction	Raw ADC	V _{in}	R _{read}	Read direction	Raw ADC	V _{in}	R _{read}	Read direction	Raw ADC	V _{in}	R _{read}
270	3987	3.19	131835	292.5	3813	3.05	45135	315	3904	3.12	68580	337.5	3571	2.85	22294
270	3987	3.18	121825	292.5	3808	3.04	44620	315	3906	3.12	67451	337.5	3563	2.85	22489
270	3992	3.18	121825	292.5	3811	3.04	43785	315	3899	3.12	68200	337.5	3568	2.85	22101
270	3988	3.19	127899	292.5	3811	3.04	44283	315	3909	3.11	65646	337.5	3566	2.85	22342
270	3987	3.18	122994	292.5	3811	3.04	44283	315	3904	3.12	69353	337.5	3571	2.85	22245
270	3990	3.18	121825	292.5	3811	3.04	44283	315	3906	3.12	67451	337.5	3568	2.85	22489
270	3987	3.19	125400	292.5	3813	3.04	44283	315	3904	3.12	68200	337.5	3566	2.85	22342
270	3994	3.18	121825	292.5	3811	3.04	44620	315	3906	3.12	67451	337.5	3567	2.85	22245
270	3990	3.19	130497	292.5	3811	3.04	44283	315	3905	3.12	68200	337.5	3566	2.85	22294
270	3992	3.19	125400	292.5	3802	3.04	44283	315	3907	3.12	67824	337.5	3568	2.85	22245
270	3993	3.19	127899	292.5	3813	3.04	42821	315	3907	3.12	68580	337.5	3557	2.85	22342
270	3987	3.19	129185	292.5	3816	3.04	44620	315	3907	3.12	68580	337.5	3567	2.84	21818
270	3994	3.18	121825	292.5	3810	3.05	45135	315	3904	3.12	68580	337.5	3565	2.85	22294
270	3987	3.19	130497	292.5	3811	3.04	44116	315	3906	3.12	67451	337.5	3566	2.85	22197
270	3987	3.18	121825	292.5	3811	3.04	44283	315	3906	3.12	68200	337.5	3563	2.85	22245
270	3984	3.18	121825	292.5	3803	3.04	44283	315	3906	3.12	68200	337.5	3563	2.85	22101
270	3989	3.18	118443	292.5	3817	3.04	42979	315	3907	3.12	68200	337.5	3565	2.85	22101
270	3990	3.19	124186	292.5	3811	3.05	45310	315	3906	3.12	68580	337.5	3568	2.85	22197
270	3990	3.19	125400	292.5	3811	3.04	44283	315	3906	3.12	68200	337.5	3563	2.85	22342
270	3987	3.19	125400	292.5	3811	3.04	44283	315	3904	3.12	68200	337.5	3563	2.85	22101

APPENDIX E. Python Program on Raspberry Pi 4B

```
import os
import time

import serial

import dropbox
import dropbox.files

# Serial handler(s)
ser = serial.Serial("/dev/ttyS0", 9600)
serial_input_available = False
received_string = ''

# Camera handler(s)
webcamBaseCommand = "fswebcam -r 640x480 "

fileDirectory = "/home/pi/Desktop/WebcamLogger/entries"
fileNameIndex = 0
fileNameExtension = ".jpg"

# Dropbox handler(s)
fileForDropbox = ''
fileOnDropbox = ''

APP_KEY = 'c4zjrcgqwz9ym02'
APP_SECRET = '9oy93mpg5gre7tz'
REFRESH_TOKEN = '3RoiSnQVa4wAAAAAAAAAAZaNqTksHYuLQ6dxacvw4kBB3JFZ2ujUH-zwENNDmaG_'

dbc = dropbox.Dropbox(
    app_key=APP_KEY,
    app_secret=APP_SECRET,
    oauth2_refresh_token=REFRESH_TOKEN
)

# Taking a picture with a designated name
def webcamCapture():
    global fileForDropbox, fileNameIndex

    if fileNameIndex < 10:
        fileOnDropbox = "/000"
    elif fileNameIndex < 100:
        fileOnDropbox = "/00"
    elif fileNameIndex < 1000:
        fileOnDropbox = "/0"
    else:
        fileOnDropbox = "/"
```

```

fileOnDropbox += f"{fileNameIndex}"
fileOnDropbox += fileNameExtension
fileForDropbox = fileDirectory + fileOnDropbox

webcamCaptureCommand = webcamBaseCommand + fileForDropbox

try:
    os.system(webcamCaptureCommand)
except:
    webcamCapture()

# Upload to Dropbox
def dropbox_captureUpload():
    global fileForDropbox, fileOnDropbox
    with open(fileForDropbox, 'rb') as f:
        data = f.read()
        dbc.files_upload(data, fileOnDropbox,
mode=dropbox.files.WriteMode('overwrite'))

# Monitor and handle serial events
def UART_watch():
    global received_string, serial_input_available, fileNameIndex

    rx_data = ser.readline()
    rx_data = rx_data.strip()
    received_string = rx_data.decode("utf-8")

    dataPoint_Index = received_string.split(',')[0]

    if dataPoint_Index.isnumeric():
        fileNameIndex = int(dataPoint_Index)
        serial_input_available = True
    else:
        with open('logger.csv', 'a') as f:
            f.write(received_string)
            f.write('\n')
            f.close()

def main():
    global serial_input_available

    while True:
        UART_watch()
        if serial_input_available:
            webcamCapture()
            try:
                dropbox_captureUpload()
            except:
                print("Network issue.")

```

```
with open('logger.csv', 'a') as f:  
    f.write(received_string)  
    f.write(',') + fileOnDropbox[1:])  
    f.write('\n')  
    f.close()  
  
if __name__ == '__main__':  
    main()
```

APPENDIX F. LoRa Range Test – Node's Log

14:20:12.848 USB device detected
14:20:22.573 Connected to CP210x device
14:23:19.989 Input: 11.055887,106.669041
14:23:20.017 Index: 0
14:23:20.026 Latitude = 11.055887; Longtitude = 106.669041
14:23:20.448 Coordinations sent.
14:23:59.072 Input: 11.055929,106.669117
14:23:59.100 Index: 1
14:23:59.109 Latitude = 11.055929; Longtitude = 106.669117
14:23:59.531 Coordinations sent.
14:24:33.659 Input: 11.055904,106.669131
14:24:33.688 Index: 2
14:24:33.696 Latitude = 11.055904; Longtitude = 106.669131
14:24:34.119 Coordinations sent.
14:25:03.464 Input: 11.055904,106.669946
14:25:03.491 Index: 3
14:25:03.501 Latitude = 11.055904; Longtitude = 106.669946
14:25:03.924 Coordinations sent.
14:25:37.438 Input: 11.056005,106.669446
14:25:37.466 Index: 4
14:25:37.475 Latitude = 11.056005; Longtitude = 106.669446
14:25:37.898 Coordinations sent.
14:26:11.659 Input: 11.055999,106.669488
14:26:11.688 Index: 5
14:26:11.696 Latitude = 11.055999; Longtitude = 106.669488
14:26:12.118 Coordinations sent.
14:26:42.179 Input: 11.056077,106.669772
14:26:42.208 Index: 6
14:26:42.216 Latitude = 11.056077; Longtitude = 106.669772
14:26:42.638 Coordinations sent.
14:27:19.506 Input: 11.055875,106.669907
14:27:19.534 Index: 7
14:27:19.542 Latitude = 11.055875; Longtitude = 106.669907
14:27:19.965 Coordinations sent.
14:27:54.840 Input: 11.055959,106.669924
14:27:54.868 Index: 8
14:27:54.877 Latitude = 11.055959; Longtitude = 106.669924
14:27:55.300 Coordinations sent.
14:28:41.034 Input: 11.056128,106.670162
14:28:41.062 Index: 9
14:28:41.071 Latitude = 11.056128; Longtitude = 106.670162
14:28:41.493 Coordinations sent.
14:29:19.124 Input: 11.056172,106.670407
14:29:19.151 Index: 10
14:29:19.160 Latitude = 11.056172; Longtitude = 106.670407
14:29:19.583 Coordinations sent.
14:29:56.104 Input: 11.056193,106.670696
14:29:56.132 Index: 11
14:29:56.142 Latitude = 11.056193; Longtitude = 106.670696

14:29:56.564 Coordinations sent.
14:30:31.986 Input: 11.056214,106.670708
14:30:32.014 Index: 12
14:30:32.023 Latitude = 11.056214; Longtitude = 106.67070
14:30:32.445 Coordinations sent.
14:31:11.523 Input: 11.056376,106.671063
14:31:11.551 Index: 13
14:31:11.560 Latitude = 11.056376; Longtitude = 106.671063
14:31:11.982 Coordinations sent.
14:31:49.314 Input: 11.05638,106.671284
14:31:49.341 Index: 14
14:31:49.350 Latitude = 11.05638; Longitude = 106.671284
14:31:49.706 Coordinations sent.
14:32:29.950 Input: 11.056388,106.671329
14:32:29.978 Index: 15
14:32:29.987 Latitude = 11.056388; Longitude = 106.671329
14:32:30.409 Coordinations sent.
14:33:02.989 Input: 11.056491,106.671586
14:33:03.017 Index: 16
14:33:03.025 Latitude = 11.056491; Longitude = 106.671586
14:33:03.448 Coordinations sent.
14:33:39.486 Input: 11.056461,106.671733
14:33:39.514 Index: 17
14:33:39.522 Latitude = 11.056461; Longitude = 106.671733
14:33:39.945 Coordinations sent.
14:34:09.441 Input: 11.056548,106.671893
14:34:09.468 Index: 18
14:34:09.477 Latitude = 11.056548; Longitude = 106.671893
14:34:09.900 Coordinations sent.
14:34:48.494 Input: 11.056641,106.672299
14:34:48.521 Index: 19
14:34:48.530 Latitude = 11.056641; Longitude = 106.672299
14:34:48.953 Coordinations sent.
14:35:19.346 Input: 11.056602,106.672413
14:35:19.374 Index: 20
14:35:19.383 Latitude = 11.056602; Longitude = 106.672413
14:35:19.805 Coordinations sent.
14:35:59.694 Input: 11.056656,106.672675
14:35:59.723 Index: 21
14:35:59.731 Latitude = 11.056656; Longitude = 106.672675
14:36:00.154 Coordinations sent.
14:36:35.079 Input: 11.056731,106.672825
14:36:35.108 Index: 22
14:36:35.117 Latitude = 11.056731; Longitude = 106.672825
14:36:35.539 Coordinations sent.
14:37:10.961 Input: 11.056715,106.673019
14:37:10.989 Index: 23
14:37:10.999 Latitude = 11.056715; Longitude = 106.673019
14:37:11.421 Coordinations sent.
14:37:45.747 Input: 11.056764,106.673138
14:37:45.775 Index: 24
14:37:45.784 Latitude = 11.056764; Longitude = 106.673138

14:37:46.206 Coordinations sent.
14:38:22.112 Input: 11.056897,106.673409
14:38:22.141 Index: 25
14:38:22.151 Latitude = 11.056897; Longtitude = 106.673409
14:38:22.572 Coordinations sent.
14:39:00.236 Input: 11.056891,106.673534
14:39:00.264 Index: 26
14:39:00.273 Latitude = 11.056891; Longtitude = 106.673534
14:39:00.695 Coordinations sent.
14:39:30.772 Input: 11.056922,106.673565
14:39:30.801 Index: 27
14:39:30.810 Latitude = 11.056922; Longtitude = 106.673565
14:39:31.232 Coordinations sent.
14:40:10.938 Input: 11.056991,106.674068
14:40:10.967 Index: 28
14:40:10.975 Latitude = 11.056991; Longtitude = 106.674068
14:40:11.398 Coordinations sent.
14:40:50.857 Input: 11.057044,106.674277
14:40:50.884 Index: 29
14:40:50.893 Latitude = 11.057044; Longtitude = 106.674277
14:40:51.316 Coordinations sent.
14:41:30.659 Input: 11.057174,106.674437
14:41:30.687 Index: 30
14:41:30.695 Latitude = 11.057174; Longtitude = 106.674437
14:41:31.118 Coordinations sent.
14:42:06.691 Input: 11.057097,106.674482
14:42:06.719 Index: 31
14:42:06.728 Latitude = 11.057097; Longtitude = 106.674482
14:42:07.150 Coordinations sent.
14:42:46.277 Input: 11.057232,106.674745
14:42:46.305 Index: 32
14:42:46.314 Latitude = 11.057232; Longtitude = 106.674745
14:42:46.736 Coordinations sent.
14:43:27.521 Input: 11.057179,106.675211
14:43:27.550 Index: 33
14:43:27.559 Latitude = 11.057179; Longtitude = 106.675211
14:43:27.982 Coordinations sent.
14:44:03.636 Input: 11.057219,106.675343
14:44:03.664 Index: 34
14:44:03.673 Latitude = 11.057219; Longtitude = 106.675343
14:44:04.094 Coordinations sent.
14:44:35.186 Input: 11.057246,106.675428
14:44:35.214 Index: 35
14:44:35.223 Latitude = 11.057246; Longtitude = 106.675428
14:44:35.645 Coordinations sent.
14:45:09.276 Input: 11.057264,106.675587
14:45:09.303 Index: 36
14:45:09.312 Latitude = 11.057264; Longtitude = 106.675587
14:45:09.735 Coordinations sent.
14:45:42.666 Input: 11.057148,106.675811
14:45:42.693 Index: 37
14:45:42.703 Latitude = 11.057148; Longtitude = 106.675811

14:45:43.125 Coordinations sent.
14:46:24.195 Input: 11.057244,106.675908
14:46:24.223 Index: 38
14:46:24.232 Latitude = 11.057244; Longtitude = 106.675908
14:46:24.654 Coordinations sent.
14:47:08.745 Input: 11.057171,106.675876
14:47:08.773 Index: 39
14:47:08.783 Latitude = 11.057171; Longtitude = 106.675876
14:47:09.205 Coordinations sent.
14:47:57.281 Input: 11.057233,106.675914
14:47:57.309 Index: 40
14:47:57.318 Latitude = 11.057233; Longtitude = 106.675914
14:47:57.740 Coordinations sent.
14:48:16.773 Input: 11.057233,106.675914
14:48:16.802 Index: 41
14:48:16.810 Latitude = 11.057233; Longtitude = 106.675914
14:48:17.233 Coordinations sent.
14:48:26.918 Input: 11.057233,106.675914
14:48:26.946 Index: 42
14:48:26.956 Latitude = 11.057233; Longtitude = 106.675914
14:48:27.378 Coordinations sent.
14:48:41.547 Input: 11.057233,106.675914
14:48:41.575 Index: 43
14:48:41.583 Latitude = 11.057233; Longtitude = 106.675914
14:48:42.006 Coordinations sent.
14:48:55.262 Input: 11.057233,106.675914
14:48:55.289 Index: 44
14:48:55.299 Latitude = 11.057233; Longtitude = 106.675914
14:48:55.722 Coordinations sent.
14:49:01.740 Input: 11.057233,106.675914
14:49:01.768 Index: 45
14:49:01.778 Latitude = 11.057233; Longtitude = 106.675914
14:49:02.200 Coordinations sent.
14:49:52.150 Input: 11.057233,106.675914
14:49:52.178 Index: 46
14:49:52.187 Latitude = 11.057233; Longtitude = 106.675914
14:49:52.609 Coordinations sent.
14:50:51.511 Disconnected

APPENDIX G. LoRa Range Test – Gateway's Log

14:20:48.097 LoRa init succeeded.
14:21:37.660 Attempting to connect
14:21:47.645 Connected.
14:21:47.645
14:23:19.484 (Latitude, Longitude) = (11.055887,106.669041)
14:23:19.516 RSSI = -48 dB
14:23:19.550 SNR = 6.50 dB
14:23:19.550 Frequency error = -4669 Hz
14:23:21.245 TxDone
14:23:21.245
14:23:58.566 (Latitude, Longitude) = (11.055929,106.669117)
14:23:58.599 RSSI = -65 dB
14:23:58.632 SNR = 6.50 dB
14:23:58.632 Frequency error = -4686 Hz
14:24:00.186 TxDone
14:24:00.186
14:24:33.154 (Latitude, Longitude) = (11.055904,106.669131)
14:24:33.188 RSSI = -76 dB
14:24:33.221 SNR = 6.25 dB
14:24:33.221 Frequency error = -4744 Hz
14:24:34.768 TxDone
14:24:34.768
14:25:02.958 (Latitude, Longitude) = (11.055904,106.669946)
14:25:02.991 RSSI = -84 dB
14:25:03.025 SNR = 7.00 dB
14:25:03.025 Frequency error = -4774 Hz
14:25:04.566 TxDone
14:25:04.566
14:25:36.932 (Latitude, Longitude) = (11.056005,106.669446)
14:25:36.965 RSSI = -89 dB
14:25:36.999 SNR = 6.75 dB
14:25:36.999 Frequency error = -4832 Hz
14:25:38.357 TxDone
14:25:38.357
14:26:11.153 (Latitude, Longitude) = (11.055999,106.669488)
14:26:11.187 RSSI = -107 dB
14:26:11.220 SNR = -1.50 dB
14:26:11.220 Frequency error = -4851 Hz
14:26:12.664 TxDone
14:26:12.664
14:26:41.674 (Latitude, Longitude) = (11.056077,106.669772)
14:26:41.707 RSSI = -88 dB
14:26:41.740 SNR = 6.00 dB
14:26:41.740 Frequency error = -4809 Hz
14:26:43.382 TxDone
14:26:43.382
14:27:19.000 (Latitude, Longitude) = (11.055875,106.669907)
14:27:19.033 RSSI = -96 dB
14:27:19.067 SNR = 5.75 dB
14:27:19.067 Frequency error = -4870 Hz

14:27:20.499 TxDone
14:27:20.499
14:27:54.334 (Latitude, Longitude) = (11.055959,106.669924)
14:27:54.368 RSSI = -91 dB
14:27:54.401 SNR = 6.25 dB
14:27:54.401 Frequency error = -4855 Hz
14:27:55.696 TxDone
14:27:55.696
14:28:40.528 (Latitude, Longitude) = (11.056128,106.670162)
14:28:40.562 RSSI = -99 dB
14:28:40.595 SNR = 3.50 dB
14:28:40.595 Frequency error = -4902 Hz
14:28:42.413 TxDone
14:28:42.413
14:29:18.618 (Latitude, Longitude) = (11.056172,106.670407)
14:29:18.651 RSSI = -101 dB
14:29:18.685 SNR = 4.00 dB
14:29:18.685 Frequency error = -4849 Hz
14:29:20.256 TxDone
14:29:20.256
14:29:55.599 (Latitude, Longitude) = (11.056193,106.670696)
14:29:55.632 RSSI = -102 dB
14:29:55.665 SNR = 3.25 dB
14:29:55.665 Frequency error = -4782 Hz
14:29:57.324 TxDone
14:29:57.324
14:30:31.480 (Latitude, Longitude) = (11.056214,106.670708)
14:30:31.514 RSSI = -104 dB
14:30:31.547 SNR = 1.25 dB
14:30:31.547 Frequency error = -4772 Hz
14:30:33.164 TxDone
14:30:33.164
14:31:11.017 (Latitude, Longitude) = (11.056376,106.671063)
14:31:11.051 RSSI = -105 dB
14:31:11.084 SNR = 1.00 dB
14:31:11.084 Frequency error = -4772 Hz
14:31:12.588 TxDone
14:31:12.588
14:31:48.741 (Latitude, Longitude) = (11.05638,106.671284)
14:31:48.775 RSSI = -109 dB
14:31:48.808 SNR = -3.75 dB
14:31:48.808 Frequency error = -4772 Hz
14:31:50.066 TxDone
14:31:50.066
14:32:29.444 (Latitude, Longitude) = (11.056388,106.671329)
14:32:29.478 RSSI = -104 dB
14:32:29.511 SNR = 1.25 dB
14:32:29.511 Frequency error = -4753 Hz
14:32:30.923 TxDone
14:32:30.923
14:33:02.484 (Latitude, Longitude) = (11.056491,106.671586)
14:33:02.516 RSSI = -107 dB

14:33:02.549 SNR = -1.50 dB
14:33:02.549 Frequency error = -4738 Hz
14:33:03.998 TxDone
14:33:03.998
14:33:38.981 (Latitude, Longitude) = (11.056461,106.671733)
14:33:39.013 RSSI = -108 dBi
14:33:39.046 SNR = -3.25 dB
14:33:39.046 Frequency error = -4711 Hz
14:33:40.656 TxDone
14:33:40.656
14:34:08.934 (Latitude, Longitude) = (11.056548,106.671893)
14:34:08.968 RSSI = -108 dBi
14:34:09.001 SNR = -3.75 dB
14:34:09.001 Frequency error = -4656 Hz
14:34:10.454 TxDone
14:34:10.454
14:34:47.989 (Latitude, Longitude) = (11.056641,106.672299)
14:34:48.021 RSSI = -110 dBi
14:34:48.054 SNR = -13.00 dB
14:34:48.054 Frequency error = -4688 Hz
14:34:49.570 TxDone
14:34:49.570
14:35:18.841 (Latitude, Longitude) = (11.056602,106.672413)
14:35:18.873 RSSI = -109 dBi
14:35:18.907 SNR = -5.75 dB
14:35:18.907 Frequency error = -4721 Hz
14:35:20.290 TxDone
14:35:20.290
14:35:59.189 (Latitude, Longitude) = (11.056656,106.672675)
14:35:59.222 RSSI = -111 dBi
14:35:59.255 SNR = -12.50 dB
14:35:59.255 Frequency error = -4698 Hz
14:36:00.636 TxDone
14:36:00.636
14:36:34.574 (Latitude, Longitude) = (11.056731,106.672825)
14:36:34.607 RSSI = -111 dBi
14:36:34.640 SNR = -16.50 dB
14:36:34.640 Frequency error = -4721 Hz
14:36:36.064 TxDone
14:36:36.064
14:37:10.455 (Latitude, Longitude) = (11.056715,106.673019)
14:37:10.489 RSSI = -110 dBi
14:37:10.522 SNR = -6.75 dB
14:37:10.522 Frequency error = -4763 Hz
14:37:11.835 TxDone
14:37:11.835
14:37:45.241 (Latitude, Longitude) = (11.056764,106.673138)
14:37:45.274 RSSI = -110 dBi
14:37:45.308 SNR = -8.25 dB
14:37:45.308 Frequency error = -4728 Hz
14:37:47.035 TxDone
14:37:47.035

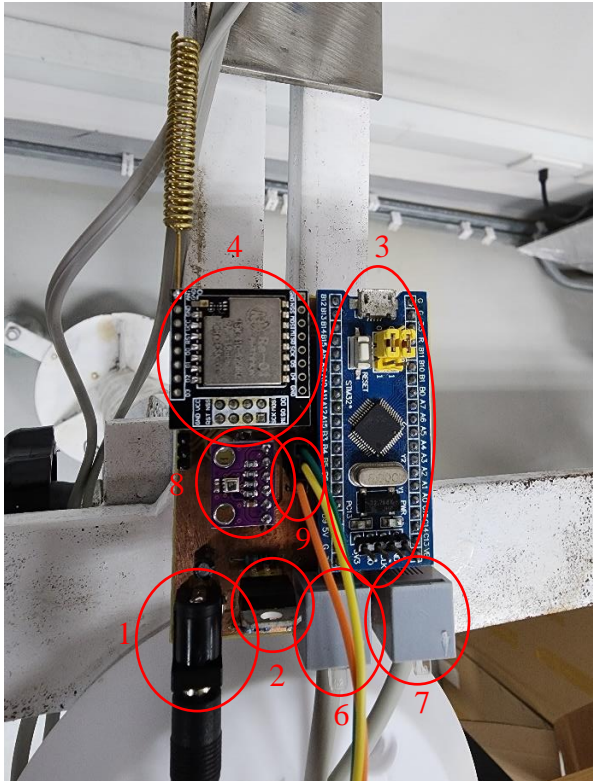
14:38:21.607 (Latitude, Longitude) = (11.056897,106.673409)
14:38:21.641 RSSI = -111 dB
14:38:21.674 SNR = -11.75 dB
14:38:21.674 Frequency error = -4776 Hz
14:38:22.903 TxDone
14:38:22.903
14:38:59.730 (Latitude, Longitude) = (11.056891,106.673534)
14:38:59.763 RSSI = -111 dB
14:38:59.797 SNR = -9.00 dB
14:38:59.797 Frequency error = -4742 Hz
14:39:01.370 TxDone
14:39:01.370
14:39:30.267 (Latitude, Longitude) = (11.056922,106.673565)
14:39:30.301 RSSI = -111 dB
14:39:30.334 SNR = -15.50 dB
14:39:30.334 Frequency error = -4780 Hz
14:39:31.783 TxDone
14:39:31.783
14:40:10.433 (Latitude, Longitude) = (11.056991,106.674068)
14:40:10.466 RSSI = -112 dB
14:40:10.500 SNR = -15.25 dB
14:40:10.500 Frequency error = -4734 Hz
14:40:11.706 TxDone
14:40:11.706
14:40:50.351 (Latitude, Longitude) = (11.057044,106.674277)
14:40:50.384 RSSI = -111 dB
14:40:50.418 SNR = -17.75 dB
14:40:50.418 Frequency error = -4755 Hz
14:40:51.988 TxDone
14:40:51.988
14:41:30.154 (Latitude, Longitude) = (11.057174,106.674437)
14:41:30.187 RSSI = -109 dB
14:41:30.220 SNR = -14.50 dB
14:41:30.220 Frequency error = -4660 Hz
14:41:31.692 TxDone
14:41:31.692
14:42:06.186 (Latitude, Longitude) = (11.057097,106.674482)
14:42:06.218 RSSI = -110 dB
14:42:06.251 SNR = -23.25 dB
14:42:06.251 Frequency error = -4763 Hz
14:42:07.532 TxDone
14:42:07.532
14:42:45.772 (Latitude, Longitude) = (11.057232,106.674745)
14:42:45.805 RSSI = -111 dB
14:42:45.839 SNR = -12.50 dB
14:42:45.839 Frequency error = -4612 Hz
14:42:47.263 TxDone
14:42:47.263
14:43:27.017 (Latitude, Longitude) = (11.057179,106.675211)
14:43:27.050 RSSI = -111 dB
14:43:27.083 SNR = -9.00 dB
14:43:27.083 Frequency error = -4579 Hz

14:43:28.835 TxDone
14:43:28.835
14:44:03.131 (Latitude, Longitude) = (11.057219,106.675343)
14:44:03.164 RSSI = -112 dB
14:44:03.197 SNR = -10.00 dB
14:44:03.197 Frequency error = -4545 Hz
14:44:04.675 TxDone
14:44:04.675
14:44:34.681 (Latitude, Longitude) = (11.057246,106.676428)
14:44:34.713 RSSI = -111 dB
14:44:34.747 SNR = -20.75 dB
14:44:34.747 Frequency error = -4545 Hz
14:44:36.009 TxDone
14:44:36.009
14:45:08.770 (Latitude, Longitude) = (11.057264,106.675587)
14:45:08.803 RSSI = -112 dB
14:45:08.836 SNR = -16.25 dB
14:45:08.836 Frequency error = -4591 Hz
14:45:11.235 TxDone
14:45:11.235
14:45:42.161 (Latitude, Longitude) = (11.057148,106.675811)
14:45:42.194 RSSI = -110 dB
14:45:42.227 SNR = -15.25 dB
14:45:42.227 Frequency error = -4577 Hz
14:45:46.153 TxDone
14:45:46.153
14:46:23.689 (Latitude, Longitude) = (11.057244,106.675908)
14:46:23.722 RSSI = -112 dB
14:46:23.756 SNR = -18.00 dB
14:46:23.756 Frequency error = -4579 Hz
14:46:25.425 TxDone
14:46:25.425
14:49:01.235 (Latitude, Longitude) = (11.057171,106.675876)
14:49:01.268 RSSI = -112 dB
14:49:01.302 SNR = -23.25 dB
14:49:01.302 Frequency error = -4532 Hz
14:49:02.555 TxDone
14:49:02.555

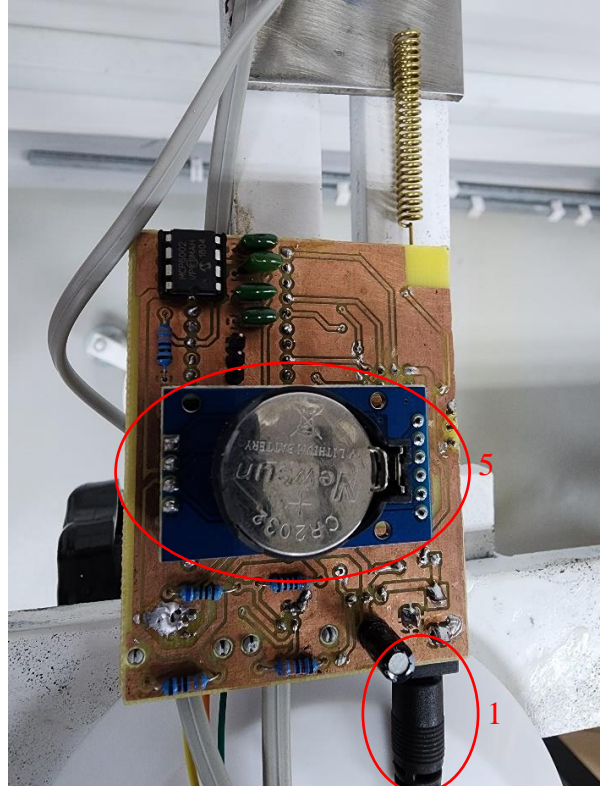
APPENDIX H. Deployed Prototype



APPENDIX I. Encased Units – Printed Circuit Board



Top view



Bottom view

1. Power input via a 5.5-mm barrel jack
2. Voltage regulator using LM317
3. Microcontroller unit: STM32F103C8T6 Blue Pill board
4. LoRa module: SX1278
5. RTC module: DS3231SN
6. RJ11 port: Combined input from anemometer and wind vane
7. RJ11 port: Input from rain gauge
8. BME280: Ambient Temperature – Relative Humidity – Barometric Pressure Sensor
9. 3-pin header for Temperature Sensor DS18B20

APPENDIX J. Turnitin Similarity Checking Report

Autonomous Wireless Agrometeorology Station

ORIGINALITY REPORT

6% SIMILARITY INDEX **5%** INTERNET SOURCES **2%** PUBLICATIONS **3%** STUDENT PAPERS

PRIMARY SOURCES

1	riull.ull.es Internet Source	1%
2	git.etud.insa-toulouse.fr Internet Source	<1%
3	git.trustie.net Internet Source	<1%
4	Submitted to Vietnamese-German University Student Paper	<1%
5	Xiangguo Fan, haoming Fan, Shuang Dong. "The coupling of hillslope- and gully-erosion increases their controlling efforts: A case study in Liaoning Province, China", Soil and Water Research, 2022 Publication	<1%
6	forum.arduino.cc Internet Source	<1%
7	mikroavr.com Internet Source	<1%
8	Submitted to University of Wolverhampton Student Paper	<1%

9	Submitted to Cranfield University Student Paper	<1%
10	Hollister, . "The Difference Amplifier", Wideband Amplifier Design, 2007. Publication	<1%
11	Submitted to Universitas Brawijaya Student Paper	<1%
12	Submitted to University of Pretoria Student Paper	<1%
13	www.tube-amp.de Internet Source	<1%
14	randomnerdtutorials.com Internet Source	<1%
15	Jiri Petrzela. "Fractional-Order Chaotic Memory with Wideband Constant Phase Elements", Entropy, 2020 Publication	<1%
16	blog.bessereau.eu Internet Source	<1%
17	electronics.stackexchange.com Internet Source	<1%
18	learn.sparkfun.com Internet Source	<1%

19	os.mbed.com	<1 %	Publication
Internet Source			
20	pliki.elektroda.pl	<1 %	<1 %
Internet Source			
21	robu.in	<1 %	
Internet Source			
22	oa.upm.es	<1 %	
Internet Source			
23	Santiago Pindado, Javier Cubas, Félix Sorribes-Palmer. "On the harmonic analysis of cup anemometer rotation speed: A principle to monitor performance and maintenance status of rotating meteorological sensors", <i>Measurement</i> , 2015	<1 %	
Publication			
24	www.bosch-sensortec.com	<1 %	
Internet Source			
25	www.infineon.com	<1 %	
Internet Source			
26	Jorge Tuesta, Demetrio Albornoz, Guillermo Kemper, Carlos A. Almenara. "A Sociometric Sensor Based on Proximity, Movement and Verbal Interaction Detection", 2019 International Conference on Information Systems and Computer Science (INCISCOS), 2019	<1 %	
27	Sedra, Adel. "Microelectronic Circuits 7th Edition, International Edition", Oxford University Press	<1 %	
Publication			
28	github.com	<1 %	
Internet Source			
29	lists.xen.org	<1 %	
Internet Source			
30	www.ti.com	<1 %	
Internet Source			
31	Submitted to Consorcio CIXUG	<1 %	
Student Paper			
32	Steven F. Barrett. "Arduino I", Springer Science and Business Media LLC, 2020	<1 %	
Publication			
33	Submitted to University Politehnica of Bucharest	<1 %	
Student Paper			
34	digilib.tugraz.at	<1 %	
Internet Source			
35	link.springer.com	<1 %	
Internet Source			
36	ucexperiment.wordpress.com	<1 %	
Internet Source			

37	www.mdpi.com Internet Source	<1 %
38	www.st.com Internet Source	<1 %
39	eprints.kingston.ac.uk Internet Source	<1 %
40	upcommons.upc.edu Internet Source	<1 %
41	Submitted to University of York Student Paper	<1 %
42	1library.net Internet Source	<1 %
43	Submitted to CSU, Bakersfield Student Paper	<1 %
44	Submitted to University of Stirling Student Paper	<1 %
45	www.mkcr.cz Internet Source	<1 %
46	www.research-collection.ethz.ch Internet Source	<1 %
47	Submitted to University of Greenwich Student Paper	<1 %
48	dspace.cc.tut.fi Internet Source	<1 %
49	www.diva-portal.se Internet Source	<1 %
50	www.meteomex.com Internet Source	<1 %
51	ptelectronics.ru Internet Source	<1 %
52	www.sony.net Internet Source	<1 %
53	cc.oulu.fi Internet Source	<1 %
54	git.m-labs.hk Internet Source	<1 %
55	ia801301.us.archive.org Internet Source	<1 %
56	www.siliconchip.com.au Internet Source	<1 %
57	Carlos A. Trasviña-Moreno, Rubén Blasco, Roberto Casas, Ángel Asensio. "Chapter 21 A Network Performance Analysis of LoRa Modulation for LPWAN Sensor Devices", Springer Nature, 2016 Publication	<1 %
58	Du Guangyue, Liu Meili, Yin Feng'e, Wang Xiaohong, Du Xiaomeng, Shen Benlan. "Study on synchronous method of multi-sensor data	<1 %

	acquisition in space based on Single-bus digital temperature sensor", 2022 International Conference on Advanced Mechatronic Systems (ICAMechS), 2022 Publication	<1 %
59	Steven F. Barrett. "Arduino III", Springer Science and Business Media LLC, 2021 Publication	<1 %
60	community.simplefoc.com Internet Source	<1 %
61	docplayer.net Internet Source	<1 %
62	gist.github.com Internet Source	<1 %
63	hrcak.srce.hr Internet Source	<1 %
64	ir.lib.uwo.ca Internet Source	<1 %
65	particle.hackster.io Internet Source	<1 %
66	www.hackster.io Internet Source	<1 %
67	www.mathworks.com Internet Source	<1 %
68	www.stm32duino.com Internet Source	<1 %
69	Andrew M. Bierer. "Development of an open-source soil water potential management system for horticultural applications, "Open_Irr""", HardwareX, 2023 Publication	<1 %
70	Nikša Tadić, Gojko Ratković, Milena Erceg, Alija Dervić. " -to-Digital Converter Using Single-Slope Integration with Bisection of the Reference Voltage ", IEEE Transactions on Instrumentation and Measurement, 2023 Publication	<1 %
71	d82c9452-4eac-4e1a-b539-b508e9e25c03.filesusr.com Internet Source	<1 %
72	eecs.oregonstate.edu Internet Source	<1 %
73	estudogeral.sib.uc.pt Internet Source	<1 %
74	etheses.bham.ac.uk Internet Source	<1 %
75	hdl.handle.net Internet Source	<1 %
76	infocenter.nordicsemi.com Internet Source	<1 %

77	kipdf.com Internet Source	<1 %	
78	mechatronicsblog.com Internet Source	<1 %	
79	patents.justia.com Internet Source	<1 %	
80	qdoc.tips Internet Source	<1 %	
81	repository.sdum.uminho.pt Internet Source	<1 %	
82	scholar.sun.ac.za Internet Source	<1 %	
83	trepo.tuni.fi Internet Source	<1 %	
84	tu-dresden.de Internet Source	<1 %	
85	www.ele.auckland.ac.nz Internet Source	<1 %	
86	www.ideals.illinois.edu Internet Source	<1 %	
87	www.intechopen.com Internet Source	<1 %	
88	www.scribd.com Internet Source	<1 %	
89	Jiri Petrzela. "Accurate Constant Phase Elements Dedicated for Audio Signal Processing", <i>Applied Sciences</i> , 2019 Publication		<1 %
90	Xiaobing Yan, Jianhui Zhao, Yunfeng Ran, Yifei Pei et al. "Memristors based in NdNiO ₃ nanocrystals film as sensory neurons for neuromorphic computing", <i>Materials Horizons</i> , 2023 Publication		<1 %
91	avesis.gazi.edu.tr Internet Source		<1 %

Exclude quotes

Off

Exclude bibliography

On

Exclude matches

Off

REFERENCES

- [1] J. Buttinger *et al.*, "Agriculture, forestry, and fishing," *Encyclopaedia Britannica*.
- [2] Trading Economics, "Vietnam - Agriculture, Value Added (% Of GDP)," *Trading Economics*. <https://tradingeconomics.com/vietnam/agriculture-value-added-percent-of-gdp-wb-data.html>.
- [3] U. Nguyen, "Vietnam's Agricultural Sector: Rising Star in Food Production," *Vietnam Briefing*, 2023.
- [4] Ministry of Natural Resources and Environment Vietnam, "Hiện trạng mạng lưới quan trắc khí tượng còn nhiều khó khăn, hạn chế," *Ministry of Natural Resources and Environment Vietnam*, 2019. <https://www.monre.gov.vn/Pages/hien-trang-mang-luoi-quan-trac-khi-tuong-con-nhieu-kho-khan,-han-che..aspx>.
- [5] "Trung tâm Ứng dụng công nghệ Khí tượng Thuỷ văn tiếp tục rà soát báo cáo về Đề án khí tượng nông nghiệp," *Vietnam Meteorological and Hydrological Administration*, 2022.
- [6] H. N. Do, "Conceptual Design of an Autonomous Wireless Agrometeorology Station," 2023.
- [7] E. Fahad, "Microcontroller Selection Criteria for your project, 8 bit Vs 16 bit Microcontroller," *Electronic Clinic*, 2021. <https://www.electronicclinic.com/microcontroller-selection-criteria-for-your-project-8-bit-vs-16-bit-microcontroller/>.
- [8] J. Koon, "Key factors to consider when choosing a microcontroller," *Microcontroller Tips*, 2019. <https://www.microcontrollertips.com/key-factors-consider-choosing-microcontroller/>.
- [9] EntcEngg Team, "Criteria for Choosing a Microcontroller." 2017, [Online]. Available: <https://www.etcengg.com/criteria-choosing-microcontroller/>.
- [10] Robocraze, "How to choose a microcontroller," *Robocraze*, 2021. <https://robocraze.com/blogs/post/selecting-a-microcontroller-for-your-projects>.
- [11] Texas Instruments, "Benefits and Issues on Migration of 5-V and 3.3-V Logic to Lower-Voltage Supplies," 1999. [Online]. Available: <https://www.ti.com/lit/an/sdaa011a/sdaa011a.pdf>.
- [12] STM32-base, "Blue Pill," *STM32-base*. <https://stm32-base.org/boards/STM32F103C8T6-Blue-Pill.html>.
- [13] STMicroelectronics, "STM32F101xx, STM32F102xx, STM32F103xx, STM32F105xx and STM32F107xx advanced Arm®-based 32-bit MCUs," no. February 2021. 2021.
- [14] STMicroelectronics, "STM32F103x8, STM32F103xB." pp. 1–116, 2022.
- [15] M. Cardinali, "The importance of weather data in agriculture," *Agricolus*, 2022. <https://www.agricolus.com/en/the-importance-of-weather-data-in-agriculture/>.
- [16] B. Gardiner, P. Berry, and B. Moulia, "Review: Wind impacts on plant growth, mechanics and damage," *Plant Sci.*, vol. 245, pp. 94–118, Apr. 2016, doi: 10.1016/j.plantsci.2016.01.006.

- [17] E. de Langre, "Effects of Wind on Plants," *Annu. Rev. Fluid Mech.*, vol. 40, no. 1, pp. 141–168, Jan. 2008, doi: 10.1146/annurev.fluid.40.111406.102135.
- [18] Misol Electronics, "misol SP-WS02 Spare part (outdoor unit) for Professional Wireless Weather Station." <http://www.misolweather.com/index.php?m=home&c=View&a=index&aid=60>.
- [19] S. Pindado, J. Cubas, and F. Sorribes-Palmer, "The Cup Anemometer, a Fundamental Meteorological Instrument for the Wind Energy Industry. Research at the IDR/UPM Institute," *Sensors*, vol. 14, no. 11, pp. 21418–21452, Nov. 2014, doi: 10.3390/s141121418.
- [20] Argent Data System, "Weather Sensor Assembly p / n 80422." 2014, [Online]. Available: https://www.argentdata.com/files/80422_datasheet.pdf.
- [21] T. Reed, "Multimeter Measurements Explained," *Electronic Design*, 2020.
- [22] Misol Electronics, "Professional Weather Station (Wind and Air Pressure) - Operational Manual." pp. 1–24.
- [23] Bosch Sensortec GmbH, "Humidity sensor BME280," *Bosch Sensortec GmbH*. <https://www.bosch-sensortec.com/products/environmental-sensors/humidity-sensors-bme280/#description>.
- [24] Bosch Sensortec GmbH, "BME280 Environmental Sensor," *Bosch Sensortec GmbH*. Jan. 2022.
- [25] Linh Kiện 888, "Cảm Biến Áp Suất BME280 3.3V." <https://linhkien888.vn/cam-bien-ap-suat-bme280-3-3v>.
- [26] C. Petrich, N. P. Dang, I. Sæther, Ø. Kleven, and M. O'Sadnick, "A Note on Remote Temperature Measurements with DS18B20 Digital," 2020, [Online]. Available: <https://hdl.handle.net/11250/2716073>.
- [27] Maxim Integrated, "DS18B20." 2019, [Online]. Available: <https://datasheets.maximintegrated.com/en/ds/DS18B20.pdf>.
- [28] M. Fezari and A. Al Dahoud, *Exploring One-wire Temperature sensor "DS18B20" with Microcontrollers*. 2019.
- [29] S. Budijono and Felita, "Smart Temperature Monitoring System Using ESP32 and DS18B20," *IOP Conf. Ser. Earth Environ. Sci.*, vol. 794, no. 1, p. 012125, Jul. 2021, doi: 10.1088/1755-1315/794/1/012125.
- [30] Widodo and E. A. Stiyawan, "Design of Total Dissolve Solid (Tds) Measuring Using Conductivity Sensor and Temperature Sensor Ds18B20," *BEST J. Appl. Electr. Sci. Technol.*, vol. 2, no. 1, pp. 25–29, 2020, doi: 10.36456/best.vol2.no1.2583.
- [31] Process Parameters Ltd, "HOW TO CALIBRATE PT100 TEMPERATURE SENSOR," *Process Parameters Ltd*. <https://www.processparameters.co.uk/how-to-calibrate-pt100/>.
- [32] Thegioiic, "DS18B20-1M Digital Temperature Sensor." <https://www.thegioiic.com/ds18b20-day-cam-bien-nhiet-do-1m>.
- [33] Thegioiic, "AM2315 Temperature And Humidity Module." <https://www.thegioiic.com/am2315-cam-bien-nhiet-do-do-am>.
- [34] B. Linke, "Reading and Writing 1-Wire® Devices Through Serial Interfaces," 2009.

- [35] Texas Instruments, “Implementing 1-Wire Enumeration for TMP1826 With TM4C129x Microcontrollers.” 2018, [Online]. Available: <https://www.ti.com/lit/an/spma057d/spma057d.pdf>.
- [36] Speedtest® by Ookla®, “Speedtest Global Index,” *Speedtest® by Ookla®*. <https://www.speedtest.net/global-index/vietnam>.
- [37] B. Mitchell, “What is the Range of a Typical Wi-Fi Network?,” *Lifewire*. 2020, [Online]. Available: <https://www.lifewire.com/range-of-typical-wifi-network-816564%0Ahttp://comnetworking.about.com/cs/wirelessproducts/f/wifirange.htm>.
- [38] J. G. Sponås, “Things You Should Know About Bluetooth Range,” *Get Connected Blog*, 2023. <https://blog.nordicsemi.com/getconnected/things-you-should-know-about-bluetooth-range>.
- [39] A. Lavric and V. Popa, “Performance Evaluation of LoRaWAN Communication Scalability in Large-Scale Wireless Sensor Networks,” *Wirel. Commun. Mob. Comput.*, vol. 2018, pp. 1–9, Jun. 2018, doi: 10.1155/2018/6730719.
- [40] A. Ambanloc, “What Communication Protocol to Use and When,” *NeuronicWorks*. <https://neuronicworks.com/blog/wireless-communication-protocols/>.
- [41] Voler Systems, “Wireless Communication Choices for IoT Designs,” *Voler Systems*. <https://www.volersystems.com/blog/wireless-communication-choices-for-iot-designs>.
- [42] EPB, “How Far Will Your Wi-Fi Signal Reach?,” *EPB.com*. <https://epb.com/get-connected/gig-internet/how-far-will-your-wi-fi-signal-reach/>.
- [43] Tessie, “HC-06 vs. HC-05 Bluetooth Module: What is the difference between HC-06 and HC-05?,” *Utmel Electronics*, 2021. <https://www.utmel.com/components/hc-06-vs-hc-05-bluetooth-module-what-is-the-difference-between-hc-06-and-hc-05?id=889>.
- [44] A. Wang, “Comparison between LoRa and other wireless technologies,” *MOKOLoRa*, 2021. <https://www.mokolora.com/lora-and-wireless-technologies/>.
- [45] Thegioiic, “Zigbee Modules.” <https://www.thegioiic.com/product/mach-zigbee>.
- [46] Thegioiic, “RF Transceivers.” <https://www.thegioiic.com/product/mach-thu-phat-rf>.
- [47] Semtech, “Semtech SX1276,” *Wirel. Sens. Prod.*, no. May, 2020, [Online]. Available: <https://www.semtech.com/products/wireless-rf/lora-core/sx1276>.
- [48] HeyPete, “Major differences between the DS3231 and DS3231M RTC chips.” 2017, [Online]. Available: <https://blog.heypete.com/2017/09/05/major-differences-between-the-ds3231-and-ds3231m-rtc-chips/>.
- [49] HeyPete, “DS3231 Drift Results (5 months).” 2018, [Online]. Available: <https://blog.heypete.com/2018/02/04/ds3231-drift-results-5-months/>.
- [50] Maxim Integrated, “DS3231.” 2015.
- [51] Thegioiic, “Mạch Đọc Thẻ Nhớ MicroSD Mini Giao Tiếp SPI.” <https://www.thegioiic.com/mach-doc-the-nho-microsd-mini-giao-tiep-spi>.
- [52] Omega Engineering, “Sources of Noise and Some Typical Solutions,” *Omega Engineering*. <https://www.omega.co.uk/techref/das/noise.html>.

- [53] J. Heath, "Electrical noise can come from anywhere," *Analog IC Tips*, 2021. <https://www.analogictips.com/electrical-noise-can-come-from-anywhere/>.
- [54] V. Muthukrishnan, "Cutoff Frequency: What is it? Formula And How To Find it," *Electrical4U*, 2022. <https://www.electrical4u.com/cutoff-frequency/>.
- [55] STMicroelectronics, "Arduino_Core_STM32." [Online]. Available: https://github.com/stm32duino/Arduino_Core_STM32.
- [56] SparkFun, "Pull-up Resistors," *SparkFun*. <https://learn.sparkfun.com/tutorials/pull-up-resistors/all> (accessed Jul. 26, 2023).
- [57] J. Christoffersen, "Switch Bounce and How to Deal with It," *All About Circuits*, 2015. <https://www.allaboutcircuits.com/technical-articles/switch-bounce-how-to-deal-with-it/>.
- [58] Texas Instruments, "Debounce a Switch." 2020.
- [59] Raspberry Pi Foundation, "Build your own weather station." <https://projects.raspberrypi.org/en/projects/build-your-own-weather-station/0>.
- [60] Windy.app, "Where wind gusts come from," *Windy.app Meteorological Textbook*. <https://windy.app/textbook/where-wind-gusts-come-from.html>.
- [61] J. W. Nilsson and S. A. Riedel, "The Step Response of RL and RC Circuits," in *Electric Circuits*, 10th ed., Pearson Education, Inc., 2015, pp. 224–231.
- [62] Electronics Tutorials Team, "RC Charging Circuit." https://www.electronics-tutorials.ws/rc/rc_1.html.
- [63] Z. Peterson, "ADC Sampling Rate and Layout for Mixed Signal Boards," *Altium Limited*, 2020. <https://resources.altium.com/p/adc-sampling-rate-and-layout-mixed-signal-boards>.
- [64] N. Abbas, "SPI vs I2C vs UART: In-Depth Comparison," *Wevolver*, 2023. <https://www.wevolver.com/article/spi-vs-i2c-vs-uart-in-depth-comparison>.
- [65] L. Fried, "Adafruit_BME280_Library." [Online]. Available: https://github.com/adafruit/Adafruit_BME280_Library.
- [66] I. Analog Devices, "How to Power the Extended Features of 1-Wire® Devices," *Analog Devices, Inc.* <https://www.analog.com/en/technical-articles/how-to-power-the-extended-features-of-1wire-devices.html>.
- [67] M. Centenaro, L. Vangelista, A. Zanella, and M. Zorzi, "Long-range communications in unlicensed bands: the rising stars in the IoT and smart city scenarios," *IEEE Wirel. Commun.*, vol. 23, no. 5, pp. 60–67, Oct. 2016, doi: 10.1109/MWC.2016.7721743.
- [68] The Things Network, "What are LoRa and LoRaWAN?," *The Things Network*. <https://www.thethingsnetwork.org/docs/lorawan/what-is-lorawan/>.
- [69] V. Q. Tran, "Evaluate The Effectiveness Of Lora Network For Data Collection," 2022.
- [70] R. P. Centelles, F. Freitag, R. Meseguer, and L. Navarro, "Beyond the Star of Stars: An Introduction to Multihop and Mesh for LoRa and LoRaWAN," *IEEE Pervasive Comput.*, vol. 20, no. 2, pp. 63–72, Apr. 2021, doi: 10.1109/MPRV.2021.3063443.
- [71] D. Kjendal, "LoRa-Alliance Regional Parameters Overview," *J. ICT Stand.*, vol. 9, no. 1, pp. 35–46, Apr. 2021, doi: 10.13052/jicts2245-800X.914.

- [72] The Things Network, “Frequency Plans by Country,” *The Things Network*. <https://www.thethingsnetwork.org/docs/lorawan/frequencies-by-country/>.
- [73] LORIOT, “LoRaWAN Network Server v7.x (Osprey) - Global Frequency Plans,” *LORIOT*. <https://docs.loriot.io/display/LNS/Global+Frequency+Plans>.
- [74] Heltec Automation, “LoRaWAN Frequency Plans,” *Heltec Automation*. https://docs.heltec.org/general/lorawan_frequency_plans.html.
- [75] S. Mistry, “Arduino LoRa.” GitHub, [Online]. Available: <https://github.com/sandeepmistry/arduino-LoRa>.
- [76] Texas Instruments, “LM317 3-Terminal Adjustable Regulator,” 2020.
- [77] S. Santos, “ESP8266 Pinout Reference: Which GPIO pins should you use?,” *Random Nerd Tutorials*, 2019. <https://randomnerdtutorials.com/esp8266-pinout-reference-gpios/>.
- [78] ESP8266 Community, “Arduino core for ESP8266 WiFi chip.” <https://github.com/esp8266/Arduino#readme>.
- [79] AYVA Educational Solutions, “TecQuipment Axial Fan Module – MFP107,” *AYVA Educational Solutions*. <https://www.tecquipment.com/axial-fan-module>.
- [80] S. Bhattacharjee, “Explained: What exactly is 1 mm of rainfall?,” *CNBC TV18*, Jul. 23, 2021.
- [81] STMicroelectronics, “STM32F101x8/B, STM32F102x8/B and STM32F103x8/B medium-density device limitations.” 2015.
- [82] M. Zachmann, “The Best LoRa Settings for Range and Reliability,” *Medium.com*, 2018. <https://medium.com/home-wireless/testing-lora-radios-with-the-limesdr-mini-part-2-37fa481217ff>.